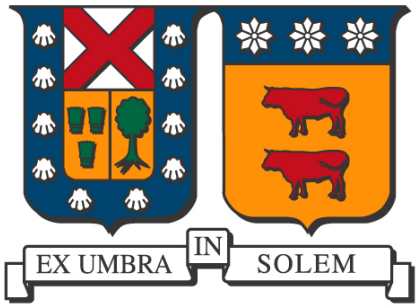

UNIVERSIDAD TECNICA
FEDERICO SANTA MARIA

Application of the Principle of Maximum Conformality in perturbative Quantum Chromodynamics

A thesis submitted in fulfillment of the requirements for the degree of Doctor in Physical Sciences.

Departamento de Física
Universidad Técnica Federico Santa María

Author:
Daniel Salinas-Arizmendi

Supervisors:
Dr. Iván Schmidt Andrade
Dr. Claudio Dib Venturelli

Valparaíso, Chile

March 30, 2025

CONSTANCIA DE VALIDACIÓN Y CONFIDENCIALIDAD DE MONOGRAFÍA A REPOSITORIO ACADÉMICO

1.- IDENTIFICACIÓN DEL TRABAJO ACADÉMICO

Tipo de monografía (marcar una opción): ☐ Memoria o trabajo de título; ☒ Tesis de Postgrado;

Título del trabajo: Application of the Principle of Maximum Conformality in perturbative Quantum Chromodynamics

Nombre del candidato(a): Daniel Esteban Salinas Arizmendi

Carrera / Grado: Doctorado en Ciencias mención Física / Grado de Doctor

Campus: Casa Central Valparaiso **;** **Departamento**: Física

2.- VALIDACIÓN DEL PROFESOR GUÍA/DIRECTOR DE TESIS

Yo, Claudio Dib Venturelli, en mi calidad de profesor(a) guía/director(a) del trabajo académico mencionado anteriormente **DEJO CONSTANCIA** que:

- He revisado esta versión del documento y corresponde a la versión final aprobada del trabajo.
- El trabajo cumple con los requisitos académicos y de formato establecidos por la institución

3.- EVALUACIÓN DE CONFIDENCIALIDAD POR PROPIEDAD INDUSTRIAL

☒ El trabajo **NO contiene información que amerite confidencialidad** y puede ser publicado de inmediato en repositorio con acceso abierto.

☐ El trabajo **CONTIENE** información con potenciales implicancias de propiedad industrial o intelectual y requiere un periodo de confidencialidad (embargo) por:

☐ 6 meses; ☐ 12 meses; ☐ 2 años; ☐ 3 años; ☐ 5 años; ☐ 10 años

Fundamentación de la necesidad de confidencialidad (obligatorio si se solicita embargo):

4.- FIRMAS

Profesor(a) guía o director(a) de memoria o tesis:

Fecha: 30/03/2025 ; **Firma:** 

Estudiante o Candidato(a):

Fecha: 30/03/2025 ; **Firma:** 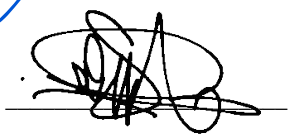

Este formulario debe ser insertado como página 2 de la memoria o tesis, completado y firmado por estudiante y profesor(a) antes de la entrega en portal PRISMA de Biblioteca USM.

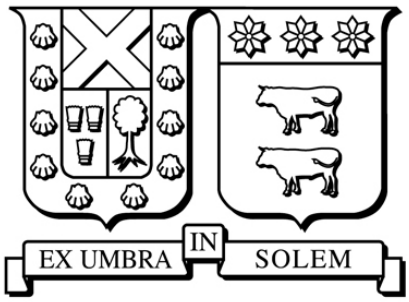

UNIVERSIDAD TECNICA
FEDERICO SANTA MARIA

Application of the Principle of Maximum Conformality in perturbative Quantum Chromodynamics

A thesis submitted in fulfillment of the requirements for the degree of Doctor in Physical Sciences.

Departamento de Física
Universidad Técnica Federico Santa María, Casilla 110-V, Valparaíso, Chile

Supervisors:
Dr. Iván Schmidt Andrade
Dr Claudio Dib Venturelli
claudio.dib@usm.cl

Author:
Daniel Salinas-Arizmendi
daniel.salinas@usm.cl

Internal Referee:
Dr. Marat Siddikov
marat.siddikov@usm.cl

External Referee:
Dr. Iván González
ivan.gonzalez@uv.cl
Universidad de Valparaíso

Valparaíso, Chile

March 30, 2025

Abstract

The thesis addresses the problem of ambiguity in the choice of the renormalization scale in perturbative QCD. These ambiguities, along with the dependence on the renormalization scheme, represent a significant source of uncertainty in theoretical predictions for fundamental processes. The research presents and compares two methods for setting the renormalization scale: the Conventional Scale Setting (CSS) and the Principle of Maximum Conformality (PMC).

The PMC method is introduced as a solution to suppress the dependence on the renormalization scale by systematically absorbing the non-conformal terms into the strong running coupling. In this way, an effective coupling is obtained, and an optimal effective scale (PMC scale) is determined as the result of the adjustment. The PMC method provides a completely conformal perturbative observable. Based on the standard invariance of the renormalization group, this method eliminates unnecessary systematic errors in high-precision perturbative QCD predictions. Finally, the PMC method is applied to improve the relation between heavy quark masses in the On-shell and $\overline{\text{MS}}$ schemes, the electroweak parameter ρ, and the determination of the hadronic decay width of the W boson.

This thesis is based on the following work:

D. Salinas-Arizmendi and I. Schmidt, *Relation Between Pole and Running Masses of Heavy Quarks Using the Principle of Maximum Conformality*, PTEP **2024**, no.3, 033B02 (2024) doi:10.1093/ptep/ptae020, arXiv:2209.06881 [hep-ph].

D. Salinas-Arizmendi, C. Dib and I. Schmidt, *Improvement of W Boson Hadronic Decay Width up to $\mathcal{O}(\alpha_s^4)$-order*, arXiv:2210.01851 [hep-ph]. (**Send**)

This dissertation includes work that was presented at the following conferences:

XXIV Chilean Physics Symposium, *On the Principle of Maximum Conformality*, Universidad de la Frontera, Chile (**Noviembre 2024**).

8th International Conference on High Energy Physics in the LHC Era, *The Renormalization Scale Setting Problem in QCD*, Universidad Técnica Federico Santa María, Chile (**Enero 2023**).

XXIII Chilean Physics Symposium, *Research the renormalization scale-setting problem in QCD* Universidad Técnica Federico Santa María, Chile (**Diciembre 2022**).
Daniel Salinas-Arizmendi and Iván Schmidt, *Investigation of the renormalization scale setting problem in QCD*, **Proceedings-SOCHIFI 2022**,
https://repositorio.usm.cl/handle/11673/56510.

Contents

List of Figures

List of Tables

Abbreviations

PMC	The Principle of Maximum Conformality
QCD	Quantum Chromodynamics
pQCD	perturbative Quantum Chromodynamics
RG	Renormalization Group
RGE	Renormalization Group Equations
QFT	Quantum Field Theory
UV	Ultraviolet
IR	Infrared
$\overline{\textbf{MS}}$	Minimal subtraction modified
QED	Quantum Electrodynamics
BLM	Brodsky-Lepage-Mackenzie
CSS	Convencional Scale Setting
LO	Leading Order
NLO	Next to Leading Order
$\mathbf{N^2LO}$	Next to Next to Leading Order
$\mathbf{N^3LO}$	Next to Next to Next to Leading Order
CKM	Cabibbo–Kobayashi–Maskawa
EW	Electroweak
PDG	Particle Data Group

Acknowledgments

I would like to express my deepest gratitude to Professor Claudio Dib V. for accepting me as a thesis student after the sudden and sad passing of Professor Iván Schmidt. I am immensely grateful for his valuable advice, suggestions, and the time he dedicated both during and outside of working hours, starting in February 2024 (a vacation period in our institution). His guidance has been fundamental to the completion of this research.

I would also like to thank the members of my evaluation committee, Professors Marat Siddikov and Iván González, for dedicating their time to reviewing, correcting, and suggesting changes that have significantly improved this work. Similarly, I want to express my gratitude to Professors Alfonso Zerwekh, Antonio Cárcamo, and Gorazd Cvetic for their classes, meetings, and insightful discussions. Additionally, I thank Professor Stanley Brodsky for suggesting the topic of this thesis.

I am grateful for the financial support provided by the grants FONDECYT 1210131, 1210378, 1230391, ANID PIA/APOYO AFB180002 and AFB120003, the Project PIIC No. 026/2019 DPP-USM, and the Internal Scholarship from the Office of Graduate Studies.

I would like to express my gratitude to my family: Matilda, Scarlett, Ivonne and my friends for their understanding and unconditional support.

Finally, I wish to pay a special tribute to Professor Iván Schmidt, whose infinite patience, challenges, and steadfast teaching style motivated me not to give up, even during the most difficult moments of recent years. Thank you, Professor. I hope that, wherever you are, you continue discussing the fundamental ideas of nature. Your dedication to science and teaching has been a constant source of inspiration for me, and this achievement would not have been possible without your invaluable support.

Chapter 1

Introduction

La teoria cuántica de campos se dispone efectivamente a esconder el comportamiento de la naturaleza a nuestros sofisticados experimentos, es por aquella razón que el profesor Iván en nuestra primera reunión me señala ingenuamente y con un leve sonrrisa: "renormalizar es simplemente conectar el parámetro de la predición teórica con su medición", como si no fuerse ya complejo deteminar por ejemplo el acoplamiento, ahora hay que ver como medir, fue lo primero que pense.

The Principle of Maximum Conformality (PMC) represents a significant advancement in addressing the ambiguities associated with the renormalization scale and scheme in perturbative Quantum Chromodynamics (pQCD). In high-energy calculations, the arbitrary choice of these scales has been a major source of uncertainty in theoretical predictions. The PMC method tackles this challenge by systematically absorbing non-conformal terms into the running coupling, achieving a fully conformal expansion and eliminating artificial dependencies on renormalization parameters.

This thesis aims to explore and apply the PMC method in various pQCD contexts, highlighting its ability to improve theoretical precision and scheme independence for key observables. In particular, processes such as the relation between heavy quark masses, the hadronic decay width of the W boson, and the electroweak parameter ρ are analyzed, providing concrete examples where optimal scale setting overcomes the limitations of conventional approaches.

The structure of this thesis is organized as follows: Chapter 1 introduces the fundamentals of QCD and the Renormalization Group. Chapter 2 presents a review of how to optimize renormalization scale setting at the leading order of perturbation theory. Chapter 3 develops the PMC framework, including Type I and Type II approaches (multi-scale and single-scale). Chapters 4, 5, and 6 are dedicated to the detailed analysis of PMC applications in the heavy quark mass relations, the electroweak parameter ρ, and the hadronic decay of the W boson, respectively.

Finally, conclusions and future perspectives are presented, emphasizing this work's contribution to establishing more reliable and precise theoretical predictions in QCD. This approach not only reinforces the validity of the Standard Model but also provides essential tools to explore potential deviations attributable to new physics.

Chapter 2

Elements of Quantum Chromodynamics

The aim of this chapter is to provide a concise overview of key aspects and tools of Quantum Chromodynamics (QCD) and the Renormalization Group (RG), which will be utilized throughout this work. In particular, the phenomena of confinement and asymptotic freedom are discussed. Scattering processes involving hadrons are also analyzed, as well as the origin and cancellation of infrared divergences in matrix elements [2–8].

2.1 Quark Model

In the early 1960s, Gell-Mann and Zweig [9, 10] introduced the `quark model` to explain the classification of hadrons into multiplets of the $SU(3)$ flavor symmetry group (see Appendix A). According to this model, mesons are composed of a quark and an antiquark, while baryons (and their corresponding antibaryons) consist of three quarks (or antiquarks). To accurately describe the known hadron spectrum at the time, it was necessary to assume the existence of three quark flavors: up (u), down (d), and strange (s). Currently, it is known that there are three additional quark flavors: charm (c), top (t), and bottom (b).

Quarks are fermions that interact strongly, have spin-1/2, and, by convention, positive parity. Antiquarks have negative parity. Quarks carry an additive baryon number of 1/3, while antiquarks have a baryon number of $-1/3$. Table 2.1 shows the other additive quantum numbers (flavors) for the three generations of quarks. These are related to the electric charge Q_e (in units of the elementary charge e) through the generalized Gell-Mann–Nishijima formula:

$$Q_e = \mathrm{I}_z + \frac{\mathcal{B} + S + C + B + T}{2}, \tag{2.1}$$

where $\mathcal{B}$ is the baryon number. By convention, a quark's flavor (I_z, S, C, B, or T) has the same sign as its charge Q_e. The values are presented in Table 2.1.

While the quark model successfully described the observed particles and resonances, it presented three fundamental problems. First, it did not explain why free quarks are not observed in nature. Second, it failed to account for antisymmetric spin-flavor combinations in the baryon sector, contradicting theoretical expectations. Finally, the existence of baryons with fully symmetric wavefunctions was inconsistent with the Pauli exclusion principle, since

	d	u	s	c	b	t
Q - electric charge	$-\frac{1}{3}$	$+\frac{2}{3}$	$-\frac{1}{3}$	$+\frac{2}{3}$	$-\frac{1}{3}$	$+\frac{2}{3}$
I - isospin	$\frac{1}{2}$	$\frac{1}{2}$	0	0	0	0
I_z - isospin z-component	$-\frac{1}{2}$	$+\frac{1}{2}$	0	0	0	0
S− strangeness	0	0	-1	0	0	0
C - charm	0	0	0	+1	0	0
B - bottomness	0	0	0	0	-1	0
T - topness	0	0	0	0	0	+1

Table 2.1: Quantum numbers associated with the six quarks: d (down), u (up), s (strange), c (charm), b (bottom), and t (top). The table includes their electric charge Q, isospin I, z-component of isospin I_z, and their corresponding quantum numbers for strangeness (S), charm (C), bottomness (B), and topness (T).

quarks are fermions and must obey Fermi-Dirac statistics, which require fully antisymmetric wavefunctions.

To resolve the latter issue, Han and Nambu [11, 12], along with Greenberg and Gell-Mann, proposed introducing a new quantum number for quarks: color. This additional quantum number allowed baryon wavefunctions to be antisymmetric under color transformations, ensuring that the total wavefunction was fully antisymmetric, as required by fermionic quantum statistics. To achieve this, three distinct colors were introduced: red, green, and blue. For a given quark flavor, such as u, there exist three types: u_r, u_g, and u_b. Antiquarks, on the other hand, are associated with the corresponding anticolors. Experimental evidence for exactly three quark colors comes from processes such as the decay rate $\Gamma(\pi^0 \to \gamma\gamma)$ [13] and the ratio of cross sections $\sigma(e^+e^- \to \text{hadrons})/\sigma(e^+e^- \to \mu^+\mu^-)$ [14, 15].

This insight led to the postulation of a new internal symmetry that rotates the color degrees of freedom. Since there are three colors, this symmetry is described by the $SU(3)$ color symmetry group, denoted as $SU(3)_c$ [16, 17]. Furthermore, hadrons must be color singlets under $SU(3)_c$ transformations, meaning they are invariant under rotations in color space.

Another key development in understanding hadron structure and strong interactions came in 1968 from a deep-inelastic scattering experiment involving electrons and protons at Stanford (SLAC) [18–20]. This experiment investigated the electromagnetic charge distribution of the proton at high momentum transfer squared. The measured proton form factors showed negligible dependence on this primary interaction scale, leading to the phenomenon known as `Bjorken scaling` [21]. This behavior indicates that the constituents of hadrons, which are strongly bound at low energy scales, behave almost like free particles when the energy scale is sufficiently high.

Subsequently, a quantum field theory was developed to describe the strong interactions between the hadron constituents, based on a `non-Abelian gauge theory` for the interactions between quarks and gluons. The exact color symmetry in strong interactions, already preexisting, naturally allowed for the introduction of renormalizable interactions between quarks, applying this color symmetry as a local gauge symmetry, inspired by the success of the electroweak gauge theory. Moreover, perturbative analysis [22–24] of non-Abelian gauge theories demonstrated that the `renormalized coupling constants`, characterizing the interaction

strength, decrease logarithmically as the energy scale increases. This phenomenon, known as `asymptotic freedom`, is exclusive to non-Abelian gauge theories [25], in contrast to Abelian theories like Quantum Electrodynamics (QED), where the coupling constant increases with energy.

When this global symmetry is promoted to a local symmetry, it becomes necessary to introduce a vector boson whose dynamics are governed by a Yang-Mills Lagrangian. This boson is the gluon, the mediator of the strong interaction. As discussed in the following section, a theory of strong interactions based on the Yang-Mills group $SU(3)_c$, known as Quantum Chromodynamics (QCD), predicts the phenomenon of confinement. Confinement explains why quarks cannot be observed freely and must always remain confined within hadrons.

2.2 Quantum Chromodynamics

QCD is the quantum field theory that describes the strong interactions responsible for binding quarks within hadrons. Building on the quark model developed by Gell-Mann and Zweig and the subsequent introduction of the quantum number of color by Han, Nambu, Greenberg, and Gell-Mann, it became necessary to construct a theory explaining not only the existence of the three quark colors but also why these quarks are never observed in isolation. In this framework, QCD emerges as a non-Abelian gauge theory based on the local symmetry group $SU(3)$, which governs the interactions between quarks and gluons, the mediators of the strong force. A key feature of QCD is confinement, which ensures that quarks cannot exist in isolation and are always confined within hadrons. Moreover, QCD exhibits a unique property called asymptotic freedom, implying that at high energies, quarks interact weakly and behave almost as free particles, whereas at low energies, strong interactions become increasingly intense, keeping the quarks bound within hadrons.

The Lagrangian describing the interactions between quarks and gluons through a non-Abelian gauge field (Yang-Mills theory Lagrangian) [2, 3] is given by:

$$\mathcal{L}_{\rm YM} = -\frac{1}{4}F^a_{\mu\nu}F^{\mu\nu}_a + \sum_f \overline{\psi}^f_i(x)\left[i\gamma^\mu D_\mu - m_f\right]_{ij}\psi^f_i(x), \tag{2.2}$$

where $F^a_{\mu\nu}$ is the gluon field strength tensor defined as

$$F_{\mu\nu} = t^a F^a_{\mu\nu} = \frac{i}{g}\left[D_\mu, D_\nu\right], \tag{2.3}$$

with D_μ as the covariant derivative:

$$D_\mu = \partial_\mu - ig_s A_\mu = \partial_\mu - ig_s T^a A^a_\mu. \tag{2.4}$$

Here, g_s is the coupling constant, T^a are the generators of SU(3) in the fundamental representation ($T^a = \lambda^a/2$), and λ^a are the Gell-Mann matrices presented in Appendix A. The field $A^a_\mu(x)$ describes the gluon, a massless spin-1 particle with color index a ($a = 1, \ldots, 8$), in the adjoint representation of the SU(3) gauge group. Using Eq. (2.4), the gluon field strength tensor can be expressed as:

$$F^a_{\mu\nu} = \partial_\mu A^a_\nu - \partial_\nu A^a_\mu + g_s f^{abc} A^b_\mu A^c_\nu, \tag{2.5}$$

where f^{abc} are the structure constants of the SU(3) color group. The fields $\psi^f_i(x)$ and $\overline{\psi}^f_i(x)$ are the Dirac spin-1/2 fields corresponding to the quarks and antiquarks of color i, flavor f,

and mass m_f, with $\overline{\psi} = \psi^\dagger\gamma^0$. Summation over repeated color indices a and Lorentz indices is assumed, where $i, j = 1, 2, 3$.

The Lagrangian $\mathcal{L}_{\rm QCD}$ is invariant under the transformations:

$$A_\mu(x) \rightarrow A'_\mu = \omega(x)\left(A_\mu(x) + \frac{i}{g_s}\partial_\mu\right)\omega^{-1}(x), \tag{2.6}$$

$$\psi(x) \rightarrow \psi'(x) = \omega(x)\psi(x), \tag{2.7}$$

$$\overline{\psi}(x) \rightarrow \overline{\psi}'(x) = \overline{\psi}(x)\omega^{-1}(x), \tag{2.8}$$

where $\omega(x)$ is the finite group transformation operator given by:

$$\omega(x) = e^{-i\Theta^a(x)T_a}, \tag{2.9}$$

with $\Theta^a(x)$ being coordinate-dependent local group parameters.

The gauge invariance of the Lagrangian $\mathcal{L}_{\rm YM}$, while fundamental to the formulation of gauge theories, introduces complications in the quantization process. These difficulties can be overcome by adding specific terms to the Lagrangian: a gauge-fixing term, $\mathcal{L}_{\rm gauge}$, and a Faddeev-Popov term or ghost terms, $\mathcal{L}_{\rm ghost}$.

The gauge-fixing term $\mathcal{L}_{\rm gauge}$ acts as a Lagrange multiplier, allowing the selection of a specific gauge condition to eliminate redundant degrees of freedom associated with gauge invariance. It can be written as:

$$\mathcal{L}_{\rm gauge} = -\frac{1}{2\xi}\left[G(A)\right]^2, \tag{2.10}$$

where $G(A) = \partial^\mu A^a_\mu$. Practical calculations often require parametrizing equivalent configurations by choosing unique representatives within each class, typically by imposing a gauge condition. Common gauges include:

$$G(A)_L \equiv \partial_\mu A^\mu = 0 \quad \text{(Lorenz gauge)}, \tag{2.11}$$

$$G(A)_C \equiv \partial_k A^k = 0 \quad \text{(Coulomb gauge)}, \tag{2.12}$$

$$G(A)_H \equiv A_0 = 0 \quad \text{(Hamilton gauge)}, \tag{2.13}$$

$$G(A)_A \equiv A_3 = 0 \quad \text{(axial gauge)}. \tag{2.14}$$

Generally, gauges that preserve Lorentz invariance, such as the covariant Lorenz gauge, are preferred as they simplify calculations by maintaining relativistic symmetry explicitly.

Additionally, the Faddeev-Popov terms (which cancel non-physical polarizations) are given by:

$$\mathcal{L}_{\rm ghost} = -\frac{1}{2\xi}\left(\partial^\mu A^a_\mu\right)^2 + \left(\partial^\mu c^{a*}\right)\left(\delta^{ac}\partial^\mu + g_s f^{abc}A^b_\mu\right)c^c, \tag{2.15}$$

where c_a are scalar fields associated with ghosts.

Thus, the inclusion of these terms ensures that the quantization of the gauge theory is consistent, eliminating redundancies associated with gauge symmetry and enabling the application of quantum field theory methods. Consequently, the complete Lagrangian of the theory is given by:

$$\mathcal{L}_{\rm QCD} = \mathcal{L}_{\rm YM} + \mathcal{L}_{\rm gauge} + \mathcal{L}_{\rm ghost}\,. \tag{2.16}$$

QCD Feynman rules

Quark propagator: 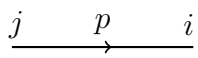

$$= \frac{i\,(\not{p} + m_f)}{p^2 - m_f^2 + i\epsilon}\delta^{ij},$$

Ghost propagator: 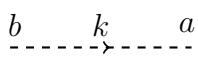

$$= \frac{i}{k^2 + i\epsilon}\delta^{ab},$$

Gluon propagator: 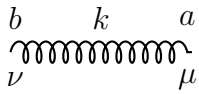

$$= \tfrac{-iD_{\mu\nu}(k)}{k^2+i\epsilon}\delta^{ab},,$$

Quark–gluon vertex: 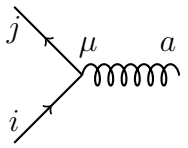

$$= ig_s\gamma^\mu\,(t^a)_{ji}\,,$$

Ghost–gluon vertex 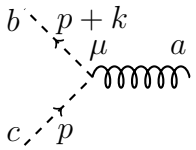

$$= g_s(p+k)^\mu f^{abc},$$

Three-gluon vertex: 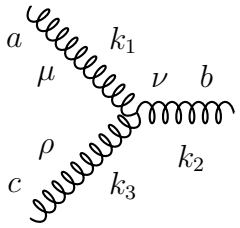

$$= \begin{array}{l} -\,g_s f^{abc}\Big[(k_1-k_3)^\nu g^{\mu\rho} + (k_2-k_1)^\rho g^{\mu\nu} \\ \quad + (k_3-k_2)^\mu g^{\nu\rho}\Big], \end{array}$$

Four-gluon vertex: 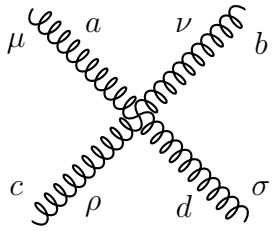

$$= \begin{array}{l} -ig_s^2[f^{abe}f^{cde}\,(g^{\mu\rho}g^{\nu\sigma} - g^{\mu\sigma}g^{\nu\rho}) \\ \quad + f^{\rm ace}\,f^{bde}\,(g^{\mu\nu}g^{\rho\sigma} - g^{\mu\sigma}g^{\nu\rho}) \\ \quad + f^{\rm ade}\,f^{bce}\,(g^{\mu\nu}g^{\rho\sigma} - g^{\mu\rho}g^{\nu\sigma})\big]\,, \end{array}$$

where in the rules Ghost-gluon vertex is in Lorentz gauge only, and three-gluon vertex all momenta flow into the vertex. And in the Lorenz gauge ($\partial \cdot A^a = 0$) we have:

$$D_{\mu\nu}(k) = g_{\mu\nu} - (1-\xi)\frac{k_\mu k_\nu}{k^2}, \tag{2.17}$$

the choice $\xi = 0$ is referred to as the Landau gauge and the choice $\xi = 1$ is called the Feynman gauge. In the light cone gauge $\eta \cdot A^a = 0$ with $\xi \to 0$ one has

$$D_{\mu\nu}(k) = g_{\mu\nu} - \frac{\eta_\mu k_\nu + \eta_\nu k_\mu}{\eta \cdot k}. \tag{2.18}$$

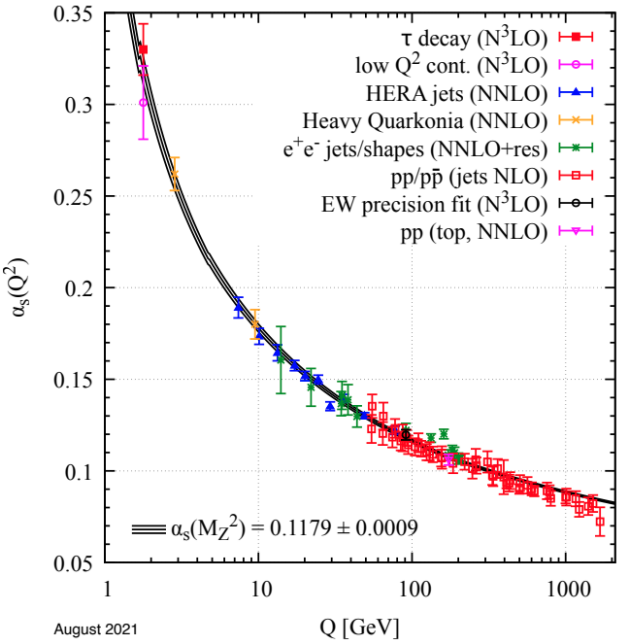

Figure 2.1: Summary of α_s measurements as a function of the energy scale Q. The respective order of perturbative QCD theory used in the extraction of α_s is indicated in parentheses. Image adapted from [1].

The Feynman rules that are standard for all field theories, such as the conservation of four-momentum in the vertices and the inclusion of a factor -1 for each fermion loop or of proper symmetry factor, applu to QCD as wll and will not be explicitly spelled out here.

2.3 Running Coupling and Quantum Corrections

La constante de acoplamiento QCD (running coupling constant) se define por

$$\alpha_s = \frac{g_s^2}{4\pi}. \tag{2.19}$$

The ability to predict both asymptotic freedom at high energies and confinement at low energies is essential for a theory of the strong interaction. These phenomena are determined by the dependence of the effective coupling, α_s. At lower orders, the QCD interaction potential includes contributions from gluon self-interactions and ghost loops, which are absent in QED due to the non-Abelian nature of the $SU(3)_C$ gauge group. These one-loop corrections introduce a logarithmic dependence on α_s, requiring renormalization by introducing an arbitrary energy scale μ_r. The variation of the coupling constant with energy scale, as predicted by QCD, fully agrees with experimental results obtained over a broad range of energy scales [1]. This consistency, illustrated in Figure 2.1, establishes QCD as the fundamental theory that accurately describes the strong interaction.

On the other hand, QCD quantum corrections capture the internal dynamics of nucleons, reflecting the fact that they are not static states but rather exhibit a rich dynamical structure driven by strong interactions. At first order in the strong coupling constant, α_s, QCD corrections are divided into two main classes. First, there are the virtual one-loop corrections, which involve the emission and reabsorption of a gluon by the quarks. These

corrections provide additional contributions to the process amplitudes, similar to those appearing in the evolution of α_s. Second, the real corrections entail the emission of additional particles, such as gluons, in the final state of the process. The diagrams corresponding to both types of corrections are shown in Figure 2.2. Panel (a) represents the Born-level (or tree-level) process, whereas the corrections in panels (b,c) are quantum corrections. Note that the loop correction is proportional to $g_s^2 \sim \alpha_s$. These corrections are essential to account for QCD effects in deep inelastic scattering (DIS) and other high-energy phenomena.

Both types of contributions introduce divergences into the calculations. Virtual corrections display ultraviolet (UV) and infrared (IR) divergences. The UV divergences are associated with large momenta ($p \to \infty$) in the loops and reflect the incompleteness of the theory's definition at arbitrarily high energy scales. These divergences are managed through a renormalization procedure. On the other hand, IR divergences arise when the internal gluon momentum tends to zero ($p \to 0$), reflecting a degeneracy in the phase space.

In the case of real corrections, IR divergences arise in two scenarios: the *soft* limit, when the emitted gluon carries very small momentum, and the collinear limit, when the gluon is parallel to the quark that emits it. Although these singularities diverge individually, their combination between real and virtual corrections leads to exact cancellation, as stated by the Kinoshita–Lee–Nauenberg theorem. However, this cancellation is only possible if the contributions are calculated separately and by using an appropriate regularization method.

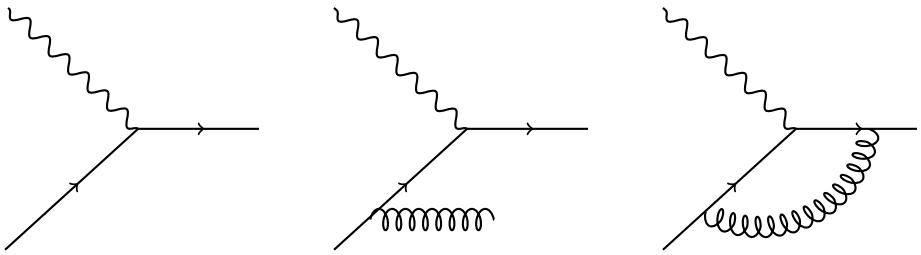

Figure 2.2: Examples of the corresponding diagrams: (a) Born-level process, (b) real correction, and (c) virtual QCD corrections.

2.4 Renormalization

As is common in Quantum Field Theory (QFT), we encounter UV divergences when computing quantum corrections. In a renormalizable theory, these can be absorbed into renormalized parameters and the normalizations of the fields.

In a renormalizable theory, these divergences can be absorbed into local counterterms that redefine the parameters and the field normalizations in the original Lagrangian. The counterterms introduce additional diagrams that cancel the ultraviolet divergences. The peculiarity of this procedure, as described by the Bogoliubov–Parasiuk theorem, lies in the fact that the singularities are local in coordinate space—they are functions of a single point and can contain only a finite number of derivatives. In theories of the renormalizable class, where the number of divergent structures is finite, the number of types of counterterms is also finite, and these replicate the terms of the original Lagrangian. This implies that introducing such counterterms is effectively equivalent to modifying the coefficients of various terms, i.e., changing their normalization. Hence, this procedure is referred to as renormalization.

In principle, the renormalization procedures in QED and QCD are similar, but the schemes used differ. In QED, one typically selects physical quantities, such as the mass, and absorbs the divergences into these quantities. In QCD, the low-energy dynamics is more involved, as there is no physical mass for the quarks nor is there a physical coupling analogous to $\alpha = \alpha(q^2 = 0)$ in QED. Thus, in QCD, the divergences are absorbed directly into parameters defined in the Lagrangian, which allows one to obtain finite Green's functions.

First, to control divergences, it is necessary to regularize the theory. This regularization may break some of the theory's symmetries; for instance, placing a cutoff in the momentum integral spoils both Lorentz invariance and gauge invariance. Restoring these symmetries by hand after renormalization can be quite tedious. Instead, a suitable way to handle the UV divergences in a **physical quantity** is dimensional regularization[1] (DR), which discretizes spacetime to $D = 4 - 2\epsilon$ [26, 27] while introducing a kinematic scale μ. In this scheme, the divergences manifest as $1/\epsilon$ poles, which can be absorbed into the renormalization of parameters such as the strong coupling a_s: the bare strong coupling, $a_s^{(0)} \equiv {g_s^{(0)}}^2/16\pi^2$, is defined in terms of the renormalized gauge coupling a_s^R as

$$a_s^{(0)} = \mu^{2\epsilon} Z_a a_s^R, \tag{2.20}$$

where the scale μ is introduced to keep a_s^R dimensionless, and Z_a is the renormalization factor obtained from the generating functional of the bare Green's function. In our case, it can be written as:

$$\begin{aligned} Z_a - 1 = \delta_a =& \sum_{i=1}^{4} \sum_{j=-i}^{0} a_s^i \frac{c_i^{[j]}}{\epsilon^{-j}} \\ =& -\frac{\beta_0}{\epsilon} a_s + \left(\frac{\beta_0^2}{\epsilon^2} - \frac{\beta_1}{2\epsilon}\right) a_s^2 - \left(\frac{\beta_0^3}{\epsilon^3} - \frac{7\beta_0\beta_1}{6\epsilon^2} + \frac{\beta_2}{3\epsilon}\right) a_s^3 \\ &+ \left(\frac{\beta_0^4}{\epsilon^4} - \frac{23\beta_1\beta_0^2}{12\epsilon^3} + \frac{5\beta_2\beta_0}{6\epsilon^2} + \frac{3\beta_1^2}{8\epsilon^2} - \frac{\beta_3}{4\epsilon}\right) a_s^4 + \mathcal{O}\left(a_s^5\right), \end{aligned} \tag{2.21}$$

where the coefficients $c_i^{[j]}$ are given explicitly up to order $i = 4$ in the expression, in terms of the β_i coefficients, which in turn are the expansion coefficients of the β function defined in Section 2.5. Note that the bare coupling is independent of the arbitrary scale μ, and thus a_s^R (hereafter simply referred to as a_s) must obey the differential equation for a_s as a function of the scale, which we will later call the renormalization group equation (RGE).

2.5 Renormalization Group

The renormalization group (RG) method has proven to be one of the most useful tools in QFT.

The renormalization group equation (RGE) is given by:

$$\frac{d}{d\ln\mu^2}\left(\frac{\alpha_s(\mu^2)}{4\pi}\right) = \beta(\mu) = -\sum_{i\geq 0} \beta_i \left(\frac{\alpha_s(\mu^2)}{4\pi}\right)^{i+2} \tag{2.22}$$

it shows that the dependence of the renormalization scale μ on the renormalized coupling is governed by the β function. The first two coefficients, β_0 [23, 24] and β_1 [28–31], are

[1] Dimensional regularization is well-known for preserving both gauge invariance and Lorentz invariance, which is why most modern perturbative QFT calculations employ it.

independent of the renormalization scheme and can be written as:

$$\beta_0 = \frac{11}{3}C_A - \frac{4}{3}T_F N_f, \tag{2.23}$$

$$\beta_1 = \frac{34}{3}C_A^2 - \frac{20}{3}C_A T_F N_f - 4C_F T_F N_f. \tag{2.24}$$

There are various arbitrary renormalization schemes. In the $\overline{\rm MS}$ scheme, the subsequent coefficients of the β function[2] [37–39] are:

$$\begin{aligned}\beta_2 =& \frac{2857}{54}C_A^3 - \frac{1415}{27}C_A^2 T_F N_f - \frac{205}{9}C_F C_A T_F N_f + 2C_F^2 T_F N_f \\ &+ \frac{44}{9}C_F T_F^2 N_f^2 + \frac{158}{27}C_A T_F^2 N_f^2\end{aligned} \tag{2.25}$$

$$\begin{aligned}\beta_3 =& C_A^4\left(\frac{150653}{486} - \frac{44}{9}\zeta_3\right) + \frac{d_A^{abcd}d_A^{abcd}}{N_A}\left(-\frac{80}{9} + \frac{704}{3}\zeta_3\right) \\ &+ C_A^3 T_F N_f\left(-\frac{39143}{81} + \frac{136}{3}\zeta_3\right) + C_A^2 C_F T_F N_f\left(\frac{7073}{243} - \frac{656}{9}\zeta_3\right) \\ &+ C_A C_F^2 T_F N_f\left(-\frac{4204}{27} + \frac{352}{9}\zeta_3\right) + \frac{d_F^{abcd}d_A^{abcd}}{N_A}N_f\left(\frac{512}{9} - \frac{1664}{3}\zeta_3\right) \\ &+ 46C_F^3 T_F N_f + C_A^2 T_F^2 N_f^2\left(\frac{7930}{81} + \frac{224}{9}\zeta_3\right) + C_F^2 T_F^2 N_f^2\left(\frac{1352}{27} - \frac{704}{9}\zeta_3\right) \\ &+ C_A C_F T_F^2 N_f^2\left(\frac{17152}{243} + \frac{448}{9}\zeta_3\right) + \frac{d_F^{abcd}d_F^{abcd}}{N_A}N_f^2\left(-\frac{704}{9} + \frac{512}{3}\zeta_3\right) \\ &+ \frac{424}{243}C_A T_F^3 N_f^3 + \frac{1232}{243}C_F T_F^3 N_f^3,\end{aligned} \tag{2.26}$$

[2]The coefficients of the β function in the momentum-subtraction (MOM) scheme [32–34] and in Landau gauge are presented in [35, 36]

$$
\begin{aligned}
\beta_4 = {} & C_A^5\left(\frac{8296235}{3888} - \frac{1630}{81}\zeta_3 + \frac{121}{6}\zeta_4 - \frac{1045}{9}\zeta_5\right) \\
& + \frac{d_A^{abcd}d_A^{abcd}}{N_A}C_A\left(-\frac{514}{3} + \frac{18716}{3}\zeta_3 - 968\zeta_4 - \frac{15400}{3}\zeta_5\right) \\
& + C_A^4 T_F N_f\left(-\frac{5048959}{972} + \frac{10505}{81}\zeta_3 - \frac{583}{3}\zeta_4 + 1230\zeta_5\right) \\
& + C_A^3 C_F T_F N_f\left(\frac{8141995}{1944} + 146\zeta_3 + \frac{902}{3}\zeta_4 - \frac{8720}{3}\zeta_5\right) \\
& + C_A^2 C_F^2 T_F N_f\left(-\frac{548732}{81} - \frac{50581}{27}\zeta_3 - \frac{484}{3}\zeta_4 + \frac{12820}{3}\zeta_5\right) \\
& + C_A C_F^3 T_F N_f\left(3717 + \frac{5696}{3}\zeta_3 - \frac{7480}{3}\zeta_5\right) - C_F^4 T_F N_f\left(\frac{4157}{6} + 128\zeta_3\right) \\
& + \frac{d_A^{abcd}d_A^{abcd}}{N_A}T_F N_f\left(\frac{904}{9} - \frac{20752}{9}\zeta_3 + 352\zeta_4 + \frac{4000}{9}\zeta_5\right) \\
& + \frac{d_F^{abcd}d_A^{abcd}}{N_A}C_A N_f\left(\frac{11312}{9} - \frac{127736}{9}\zeta_3 + 2288\zeta_4 + \frac{67520}{9}\zeta_5\right) \\
& + \frac{d_F^{abcd}d_A^{abcd}}{N_A}C_F N_f\left(-320 + \frac{1280}{3}\zeta_3 + \frac{6400}{3}\zeta_5\right) \\
& + C_A^3 T_F^2 N_f^2\left(\frac{843067}{486} + \frac{18446}{27}\zeta_3 - \frac{104}{3}\zeta_4 - \frac{2200}{3}\zeta_5\right) \\
& + C_A^2 C_F T_F^2 N_f^2\left(\frac{5701}{162} + \frac{26452}{27}\zeta_3 - \frac{944}{3}\zeta_4 + \frac{1600}{3}\zeta_5\right) \\
& + C_F^2 C_A T_F^2 N_f^2\left(\frac{31583}{18} - \frac{28628}{27}\zeta_3 + \frac{1144}{3}\zeta_4 - \frac{4400}{3}\zeta_5\right) \\
& + C_F^3 T_F^2 N_f^2\left(-\frac{5018}{9} - \frac{2144}{3}\zeta_3 + \frac{4640}{3}\zeta_5\right) \\
& + \frac{d_F^{abcd}d_A^{abcd}}{N_A}T_F N_f^2\left(-\frac{3680}{9} + \frac{40160}{9}\zeta_3 - 832\zeta_4 - \frac{1280}{9}\zeta_5\right) \\
& + \frac{d_F^{abcd}d_F^{abcd}}{N_A}C_A N_f^2\left(-\frac{7184}{3} + \frac{40336}{9}\zeta_3 - 704\zeta_4 + \frac{2240}{9}\zeta_5\right) \\
& + \frac{d_F^{abcd}d_F^{abcd}}{N_A}C_F N_f^2\left(\frac{4160}{3} + \frac{5120}{3}\zeta_3 - \frac{12800}{3}\zeta_5\right) \\
& + C_A^2 T_F^3 N_f^3\left(-\frac{2077}{27} - \frac{9736}{81}\zeta_3 + \frac{112}{3}\zeta_4 + \frac{320}{9}\zeta_5\right) \\
& + C_A C_F T_F^3 N_f^3\left(-\frac{736}{81} - \frac{5680}{27}\zeta_3 + \frac{224}{3}\zeta_4\right) \\
& + C_F^2 T_F^3 N_f^3\left(-\frac{9922}{81} + \frac{7616}{27}\zeta_3 - \frac{352}{3}\zeta_4\right) \\
& + \frac{d_F^{abcd}d_F^{abcd}}{N_A}T_F N_f^3\left(\frac{3520}{9} - \frac{2624}{3}\zeta_3 + 256\zeta_4 + \frac{1280}{3}\zeta_5\right) \\
& + C_A T_F^4 N_f^4\left(\frac{916}{243} - \frac{640}{81}\zeta_3\right) - C_F T_F^4 N_f^4\left(\frac{856}{243} + \frac{128}{27}\zeta_3\right).
\end{aligned}
\tag{2.27}
$$

where ζ_i denotes the Riemann zeta function, and C_F and C_A are the quadratic Casimir operators for the fundamental and adjoint representations of the color Lie algebra, respectively. The symbol $d^{abc} = \mathrm{Tr}\big(\{\frac{\lambda^a}{2}, \frac{\lambda^b}{2}\}\frac{\lambda^c}{2}\big)$, and T_F is the trace normalization for the fundamental representation. The exact definitions of the color structures $d_F^{abcd}d_A^{abcd}$ and $d_F^{abcd}d_F^{abcd}$ appearing below can be found in [40].

For fermions transforming under the fundamental representation and the standard normalization of the $SU(N)$ generators, these **color factors** take the values

$$\begin{aligned} T_F =& \frac{1}{2}, \quad C_A = N, \quad C_F = \frac{N_A}{2N} = \frac{N^2-1}{2N}, \quad \frac{d_A^{abcd}d_A^{abcd}}{N_A} = \frac{N^2\left(N^2+36\right)}{24}, \\ & \frac{d_F^{abcd}d_A^{abcd}}{N_A} = \frac{N\left(N^2+6\right)}{48}, \quad \frac{d_F^{abcd}d_F^{abcd}}{N_A} = \frac{N^4-6N^2+18}{96N^2}. \end{aligned} \tag{2.28}$$

For QCD, which is an $SU(3)_C$ color gauge theory, the relevant color factors and terms are:

$$\begin{aligned} T_F = \frac{1}{2}, \quad C_A = 3, \quad C_F = \frac{4}{3}, \\ \frac{d_A^{abcd}d_A^{abcd}}{N_A} = 45, \quad \frac{d_F^{abcd}d_A^{abcd}}{N_A} = \frac{15}{4}, \quad \frac{d_F^{abcd}d_F^{abcd}}{N_A} = \frac{5}{24}. \end{aligned} \tag{2.29}$$

In the massless limit ($m_q = 0$), the theory's dynamics is governed by two physical parameters: the number of flavors N_f and the number of colors N_c. The exact analytic solution to Eq. (2.22) is given by:

$$\int_{\alpha_s(\mu_0)}^{\alpha_s(\mu)} \frac{1}{\beta\left(a_s\right)} d\left(\frac{\alpha_s}{4\pi}\right) = -\int_{\mu_0^2}^{\mu^2} \frac{dQ^2}{Q^2}, \tag{2.30}$$

By truncating the β function at the first order in perturbation theory and integrating Eq. 2.30, one obtains the 1-loop coupling solution:

$$a_s\left(\mu\right) = \frac{a_s\left(\mu_\lambda\right)}{1 + a_s\left(\mu_\lambda\right)\beta_0 \ln\left(\mu^2/\mu_\lambda^2\right)} \tag{2.31}$$

where, for notational simplicity, we define $a_s = \alpha_s/(4\pi)$. This expression allows a known (experimentally measured) strong coupling at a specific scale μ to be connected to an unknown value $\alpha_s\big(\mu_\lambda\big)$ at another scale. In more practical terms, the solution can be recast by introducing the QCD scale parameter, Λ. At first order in β_0, we have

$$\Lambda^2 \equiv \mu^2 e^{-\frac{4\pi}{\beta_0 \alpha_x(\mu^2)}} \tag{2.32}$$

which leads to the well-known one-loop solution:

$$a_s\left(\mu\right) = \frac{1}{\beta_0 \ln(\mu^2/\Lambda^2)} \tag{2.33}$$

Using the coupling displacement relation, in an arbitrary λ-renormalization scheme, two different scales can be connected to each other via the displacement

$$a_s(\mu) = a_s\left(\mu_\lambda\right) + \sum_{n\geq 1} \frac{1}{n!} \frac{d^n a_s(\mu)}{\left(d\ln\mu^2\right)^n}\bigg|_{\mu=\mu_\lambda} (-\lambda)^n, \tag{2.34}$$

where $-\lambda = \ln\left(\mu^2/\mu_\lambda^2\right)$.

By generalizing this displacement relation and introducing a k-th power in the running coupling, we obtain the following **Generalized Displacement Relation**:

$$
\begin{aligned}
a(\mu_0)^k = {} & a(\mu_\lambda)^k + \beta_0 k\lambda a(\mu_\lambda)^{k+1} + a(\mu_\lambda)^{k+2}\left[\frac{k}{2!}(k+1)\lambda^2\beta_0^2 + k\lambda\beta_1\right] \\
& + a(\mu_\lambda)^{k+3}\left[\frac{k}{3!}(k+1)(k+2)\lambda^3\beta_0^3 + \frac{k}{2!}(2k+3)\lambda^2\beta_1\beta_0 + k\lambda\beta_2\right] \\
& + a(\mu_\lambda)^{k+4}\left[\frac{k}{4!}(k+1)(k+2)(k+3)\lambda^4\beta_0^4 + \frac{k}{3!}\Big(11+3k(k+4)\Big)\lambda^3\beta_0^2\beta_1\right. \\
& \left. + \frac{k(k+2)}{2!}\lambda^2(\beta_1^2+2\beta_0\beta_2) + k\lambda\beta_3\right] + a(\mu_\lambda)^{k+5}\left[\frac{k}{5!}(k+1)(k+2)(k+3)(k+4)\lambda^5\beta_0^5\right. \\
& + \frac{2k}{4!}(2k+5)\Big(k(k+5)+5\Big)\lambda^4\beta_0^3\beta_1 + \frac{\beta_0\lambda^3 k}{3!}\Big(\beta_1^2\left[3k(k+5)+17\right] \\
& \left. + 3\beta_0\beta_2(k+2)(k+3)\Big) + \frac{k(2k+5)\lambda^2}{2!}\left(\beta_1\beta_2+\beta_0\beta_3\right) + k\lambda\beta_4\right] \\
& + a(\mu_\lambda)^{k+6}\left[\frac{\lambda^6}{6!}\beta_0^6 k(k+1)(k+2)(k+3)(k+4)(k+5)\right. \\
& + \frac{\lambda^5}{5!}\beta_0^4\beta_1 k\Big(5k(k+6)\left[k(k+6)+15\right]+274\Big) + \frac{\beta_0^2 k(k+3)\lambda^4}{4!}\Big(\beta_1^2\left[6k(k+6)+43\right] \\
& + 4\beta_0\beta_2(k+2)(k+4)\Big) + \frac{k\lambda^3}{3!}\Big(\beta_1^3(k+2)(k+4) + 2\beta_0\beta_2\beta_1\left[3k(k+6)+25\right] \\
& \left. + 3\beta_0^2\beta_3(k+3)^2\Big) + \frac{k(k+3)\lambda^2}{2!}\left(\beta_2^2+2\beta_1\beta_3+2\beta_0\beta_4\right) + k\lambda\beta_5\right] + \mathcal{O}\left(a^{k+7}\right).
\end{aligned}
\tag{2.35}
$$

Chapter 3

Renormalization Scale Setting

The choice of renormalization scale and scheme in perturbative QCD calculations introduces ambiguities that can affect the precision of theoretical predictions. Although renormalization group (RG) invariance ensures that physical quantities are independent of both the scheme and the scale, in fixed-order truncated calculations these dependencies persist and can lead to systematic uncertainties. To address this issue, several scale-setting methods have been developed to minimize such ambiguities and improve the convergence of perturbative series.

Among the most common approaches are the Fastest Apparent Convergence (FAC) method [41–43], the Principle of Minimum Sensitivity (PMS) [44–47], and the Brodsky–Lepage–Mackenzie (BLM) method [48]. Each of these approaches addresses the problem from a different perspective. FAC selects the renormalization scale such that higher-order corrections vanish, thus optimizing the convergence of the series. PMS, on the other hand, seeks to minimize the dependence on unphysical parameters, such as the renormalization scale and scheme, through a direct optimization over these variables. Finally, the BLM method sets an effective renormalization scale such that the scheme-dependent terms are absorbed into the effective coupling constant, thereby improving convergence and eliminating scheme ambiguities. The main focus of this work is centered on the BLM method.

3.1 Brodsky–Lepage–Mackenzie Method (BLM)

The **Brodsky–Lepage–Mackenzie** (BLM) method, proposed in 1983 [48], provides a solution to the ambiguities associated with the choice of renormalization scale and scheme in perturbative Quantum Chromodynamics (pQCD). This approach is inspired by the Gell-Mann–Low scheme used in Quantum Electrodynamics (QED), where the renormalization scale is naturally fixed by associating it with the virtual photon exchange. A classic example in QED is electron–muon scattering, where the renormalization scale is chosen as $\mu = t$, effectively eliminating all the β-function coefficients in the perturbative QED calculations.

In the context of QCD, the BLM method provides an automatic procedure to set the appropriate renormalization scale, optimizing the convergence of perturbative expansions in pQCD. This method identifies and absorbs the terms proportional to the β_0 coefficient of the β-function (referred to as non-conformal terms), allowing the perturbative series to be reorganized such that the non-conformal contributions vanish at the adjusted renormalization scale. This leads to improved precision in theoretical predictions.

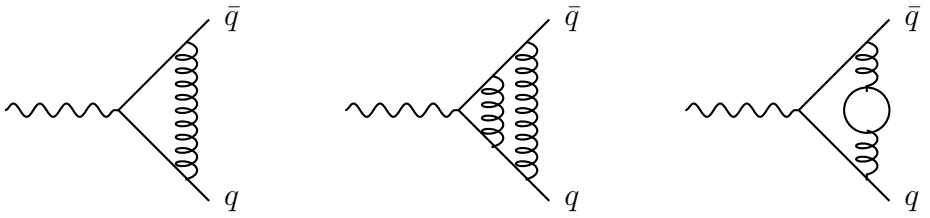

Figure 3.1: Ejemplos de diagramas de Feynman para correnciones de un vertice a 1- y 2-loop.

A general expression for an observable in pQCD in any renormalization scheme is:

$$\mathscr{P}_\ell\left(\mu_r\right) = c_{0,0} + \sum_{i\geq 1}\sum_{j=0}^{i-1} c_{i,j}\left[N_f\right]^j a_s\left(\mu_r\right)^{\ell+i-1} \tag{3.1}$$

where i denotes the perturbative order, $c_{i,j}$ are the perturbative coefficients, ℓ is the power of a_s at the Born level, and N_f represents the number of active quark flavors. In this expression, the coefficients $c_{i,j}$ (with $j \neq 0$) contain contributions associated with internal fermion loops (indexed by j).

The BLM method absorbs the β_0-dependent contributions contained in the perturbative coefficients of a physical quantity into the effective renormalization scale (at first order in perturbation theory), a procedure known as the *absorption of non-conformal terms*. To illustrate this, consider the physical quantity from Eq. (3.1) for $i = 2$, which can be written as:

$$\mathscr{P}_\ell\left(\mu_r\right) = c_{0,0} + c_{1,0}a_s(\mu_r)^\ell + \left(c_{2,0} + c_{2,1}N_f\right)a_s(\mu_r)^{\ell+1}, \tag{3.2}$$

where the non-conformal dependence arises from the $\mathcal{O}\left(a_s^{\ell+1}\right)$ order. As an illustrative example, Figure 3.1 shows the QCD-type corrections to a vertex (with $\ell = 1$). At one-loop level, the correction is proportional to $g_s^2 \sim a_s$ due to the coupling of a gluon with a quark and anti-quark, corresponding to the coefficient $c_{1,2}$. At two-loop level, we have the correction from the exchange of two gluons associated with $c_{2,0}$ and the quark bubble correction associated with $c_{2,1}$, both of which contribute terms proportional to a_s^2. Thus, the BLM method eliminates the non-conformal contributions from the $c_{2,1}$ term, which is related to β_0 from Eq. (2.23), by absorbing these contributions into the effective coupling using the one-loop displacement relation in Eq. (2.35). Therefore, the observable under this prescription is expressed as

$$\mathscr{P}_\ell|_{\text{BLM}} = t_{0,0} + t_{1,0}a_s\left(Q_1\right) + t_{2,0}a_s\left(Q_1\right)^2, \tag{3.3}$$

where $t_{n,0}$ with $n = 0, 1, 2$ are the *conformal coefficients*, and Q_1 is the BLM scale. Note that the observable in Eq. (3.3) is scheme-independent, *i.e.*, it does not depend on N_f. Therefore, the perturbative expansion remains unchanged across quark thresholds, since all vacuum polarization effects due to the production of new quarks can be absorbed into the effective coupling. Consequently, the BLM procedure can always be applied to various processes, such as effective cross sections or decay rates.

The non-conformal term can be absorbed into the running coupling if and only if the following scale setting condition is satisfied:

$$Q_1 = \mu_0 e^{-\frac{t_{2,1}}{2\ell t_{1,0}}}, \tag{3.4}$$

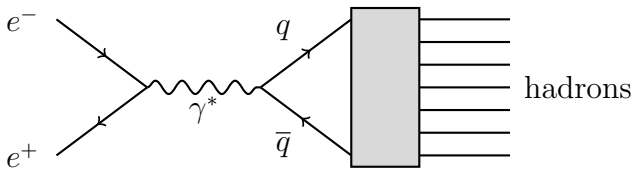

Figure 3.2: Annihilation process $e^+e^- \to$ hadrons with an intermediate photon.

the coefficient $t_{2,1}$ corresponds to terms that accompany β_0 and originate from its dependence on N_f; in this work, we will refer to them as *non-conformal coefficients*.

The BLM method preserves all renormalization group (RG) properties of existence and uniqueness, reflexivity, symmetry, and transitivity[1]. The RG invariance of BLM maintains the scheme-independent transformations that relate different couplings in various renormalization schemes [50–53]. These are known as commensurate scale relations (CSRs), and it has been shown that although the expansion coefficients under different renormalization schemes may differ, after a proper scale setting, one can determine a relation between the effective couplings that leads to an invariant result for the computed observable. Using this approach, it is also possible to extend conformal properties to renormalizable gauge theories, such as the generalized Crewther relation [54].

In the Abelian limit $N_c \to 0$, the BLM method reduces to the Gell-Mann–Low scheme in QED, and the results match perfectly.

The simplest observables in perturbative QCD are those that do not involve hadrons in the initial state and are fully inclusive with respect to the details of the final state. A typical example is the total cross section for electron–positron annihilation into hadrons at a center-of-mass energy Q, as shown in Figure 3.2, for which one can write:

$$R_{e^+e^-}(Q) \equiv \frac{\sigma_{tot}\left(e^+e^- \to \gamma^* \to \text{ hadrons }\right)}{\sigma\left(e^+e^- \to \gamma^* \to \mu^+\mu^-\right)}. \tag{3.5}$$

In the parton model, where quarks are treated as free particles, the cross section for producing a quark–antiquark pair of a specific flavor is exactly the same as that for producing a $\mu^+\mu^-$ pair, except for a factor of the quark's electric charge squared, Q_f^2, and a factor of N_C arising from the color charge, since each quark flavor comes in three colors. It is assumed that the quarks will subsequently "fragment" into hadrons. The theoretical expectation at the Born level, neglecting quark masses, is

$$R_{e^+e^-}|_{\text{Born}} \equiv R_0 = N_c \sum_{f=1}^{N_f} Q_f^2, \tag{3.6}$$

where N_f is the number of active quark flavors with masses below the square root of the process energy. The expression for R_0 is purely an electroweak prediction for the ratio.

Quarks, however, are not free; they can radiate gluons and exchange virtual gluons, giving rise to QCD corrections. Figure 3.3 provides a pictorial illustration of such processes.

The QCD corrections to the process presented in Eq. (3.5) at leading order, where the ratio is defined as $\mathcal{R}_{e^+e^-} = R_{e^+e^-}/R_0$, can be expressed as:

$$\mathcal{R}_{e^+e^-}(\mu) = c_0 + c_1 a_s(\mu) + c_2 a_s(\mu)^2 + \mathcal{O}\left(a_s^3\right) \tag{3.7}$$

[1]For further details on the RG properties, see [49]

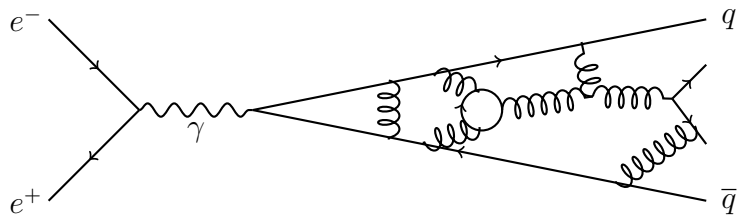

Figure 3.3: Pictorial illustration of the QCD corrections to the electron–positron annihilation into hadrons.

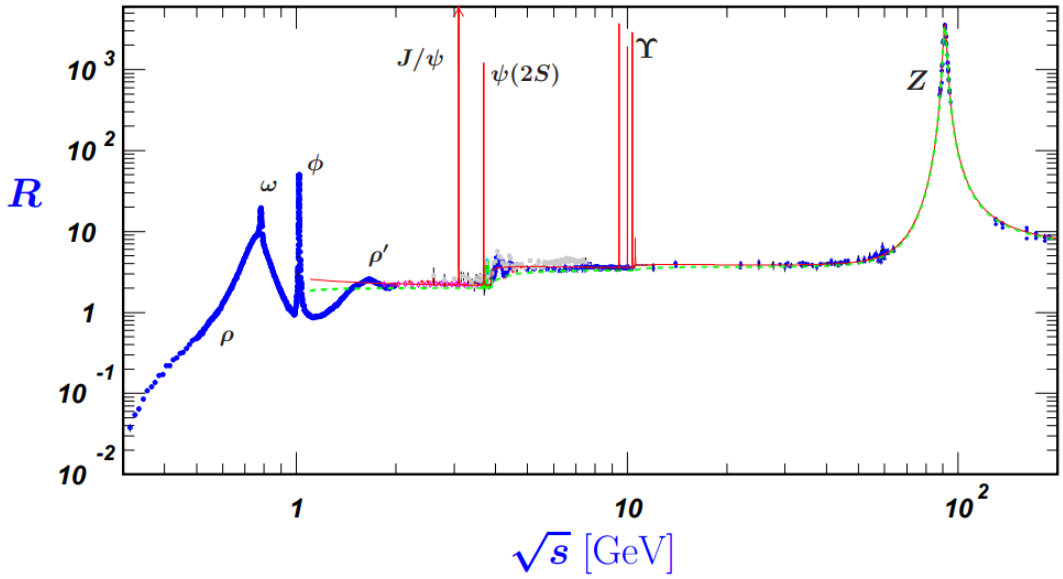

Figure 3.4: Datos sobre $R_{e^+e^-}$, comparados con la predicción del modelo de quarks (línea verde discontinua) y el resultado perturbativo QCD (línea roja sólida). Los errores de los datos por encima de 2 GeV son sólo estadísticos. Figura tomada de PDG-2022 [1].

where the NLO coefficients were computed in the $\overline{\text{MS}}$ scheme by [14, 15, 55, 56]:

$$\begin{aligned} c_0 &= 1, \\ c_1 &= 4, \\ c_2 &= \left(\frac{41}{8} - \frac{11}{3}\zeta_3\right) C_A - \frac{1}{8} C_F + \left(\frac{2}{3}\zeta_3 - \frac{11}{12}\right) N_f. \end{aligned} \tag{3.8}$$

For the corresponding expressions including Z-boson exchange and finite quark mass effects, see Refs. [57–59]. Figure 3.4 shows the available experimental measurements of the total hadronic production cross section, including the contribution from Z-boson exchange, normalized to the electromagnetic muon production cross section $\sigma(e^+e^- \to \mu^+\mu^-) = 4\pi\alpha(s)^2/3s$. Reference [60] demonstrates that the integral over the $R_{e^+e^-}$ series is related to the hadronic decay of the τ lepton across a range of invariant masses.

Characteristically, we observe that the coefficients of the series corresponding to pQCD observables, such as in Eq. (3.7), increase order by order, resulting in a slow convergence. This situation becomes significantly worse near thresholds or in the presence of tight kinematic cuts. Strictly speaking, the poor convergence is due to the fact that the series expansion for

an observable is not merely an expansion in α_s, but rather in $\left(\ln \frac{\mu^2}{Q^2}\ \alpha_s(\mu)\right)$.

The scale dependence for electron–positron annihilation can be expressed explicitly as

$$\mathcal{R}_{e^+e^-}(Q) = \hat{c}_0(\mu_r/Q) + \hat{c}_1(\mu_r/Q)\, a_s(\mu_r) + \hat{c}_2(\mu_r/Q)\, a_s(\mu_r)^2 + \mathcal{O}\left(a_s^3\right) \tag{3.9}$$

where

$$\begin{aligned} \hat{c}_0(\mu_r/Q) =& c_0, \\ \hat{c}_1(\mu_r/Q) =& c_1, \\ \hat{c}_2(\mu_r/Q) =& c_2 + \pi\beta_0 c_1 \ln\left(\frac{\mu_r^2}{Q^2}\right). \end{aligned} \tag{3.10}$$

Note that at higher orders, the coefficients $\hat{c}_k(\mu_r/Q)$ generate a long logarithmic dependence of the form $\ln^{k-1}(\mu_r^2/Q^2)$. If the full series were summed, the μ_r dependence of the coefficients would cancel out, and the final result would be independent of the choice of the scale μ_r, as physical observables should not depend on unphysical scales. However, truncating the series at a fixed order N introduces a residual μ_r dependence at order $\mathcal{O}(a_s^{N+1})$, which implies an uncertainty in the prediction of $R_{e^+e^-}$ due to the arbitrariness in the choice of scale (in other words, a scale-setting ambiguity is introduced).

In the **Conventional Scale Setting** (CSS) approach, the initial scale is fixed directly to the typical momentum transfer of the process, Q, with the aim of eliminating the large logarithms that emerge at higher orders. Uncertainties related to the scale choice are usually estimated by varying Q within the range $[Q/2, 2Q]$. Although this is not a rigorous prescription for determining the uncertainty, it is motivated by the requirement that no large logarithms should be introduced in the calculation due to large scale hierarchies. It is commonly assumed that increasing the perturbative order reduces the ambiguities associated with scale and scheme choices, under the notion that incorporating more loop corrections yields more accurate theoretical predictions in comparison with experimental results. However, this does not guarantee the level of precision obtained through conventional scale setting. Rather, it represents only a preliminary approach to addressing the divergent nature of perturbative series, which also include renormalon divergences that grow factorially as $n!\,(\beta_0\alpha_s)^n$, along with other asymptotic perturbative divergences that can spoil theoretical predictions.

Numerically, the electron–positron annihilation into hadrons in the conventional (Conv.) case, for $N_f = 5$, with $\alpha_s(M_Z) = 0.1180 \pm 0.0009$,

$$\mathcal{R}^{\rm NLO}_{e^+e^-}\left(\sqrt{s} = 31.6\ {\rm GeV}\right)\big|_{\rm Conv.} = 1.047^{+0.007}_{-0.005}. \tag{3.11}$$

Figure 3.5 shows the result for $\mathcal{R}_{e^+e^-}$ under conventional scale setting. In panel (a), the results are shown above the expected level, and the convergence achieved by the truncated expansion up to NLO is evident; however, a strong dependence on the renormalization scale value remains. In panel (b), the shaded region represents the uncertainty in the estimate obtained by varying the scale within the previously mentioned range (*i.e.*, $\mu_r \sim [Q/2, 2Q]$). Note that different choices of the renormalization scale can lead to significantly different results when higher-order corrections are included. This highlights the need for a more principled argument for choosing the proper renormalization scale in fixed-order predictions, which can be guided by comparing theoretical results with experimental data.

The main issues with CSS stem from the lack of a well-defined prescription for determining the appropriate renormalization scale or the correct range for its variation. Suppression of

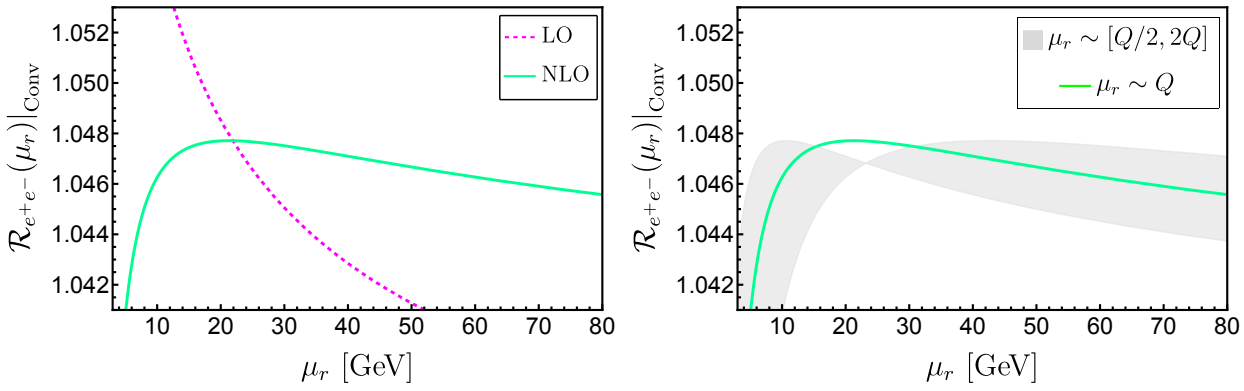

Figure 3.5: Renormalization scale dependence of the total cross-section ratio for electron–positron annihilation into hadrons under conventional scale setting. (a) One-loop (dashed line) and two-loop (solid line) QCD corrections. (b) The uncertainty associated with conventional scale setting, obtained by varying the scale in the range $[Q/2, 2Q]$. Results are shown for $N_f = 5$, with an initial renormalization scale $\mu_r^{\rm init} = 31.6$ GeV.

scale dependence is only possible by increasing the perturbative order in α_s, but this does not guarantee that choosing $\mu_r = Q$ will yield a reliable theoretical prediction across different physical processes. This limitation restricts both the predictive power and the systematization of scale-setting procedures. For instance, in some cases the scale is chosen as the center-of-mass energy, while in others it is taken as the mass of the heavy quarks—without a strong underlying criterion. In terms of predictive uncertainties, CSS incorporates the errors from uncalculated higher-order terms that are missing in the truncated series.

The large amount of high-precision experimental data expected in the near future—particularly due to the high collision energy and luminosity of the Large Hadron Collider (LHC)—will demand increasingly accurate and refined theoretical predictions. CSS appears to be, at best, a **fortunate guess**; its results suffer from large uncertainties, and the perturbative series converges poorly, regardless of whether large logarithms or renormalon contributions are resummed. Furthermore, in this context, it becomes nearly impossible to distinguish between Standard Model (SM) and Beyond the Standard Model (BSM) signals. In many cases, improved higher-order calculations are not expected to be available in the short term.

On the other hand, as noted at the beginning of this section, the BLM method provides an excellent optimization strategy to address the ambiguities introduced by conventional scale setting. Applying the BLM method at NLO to electron–positron annihilation into hadrons, we obtain

$$\mathcal{R}_{e^+e^-}|_{\rm BLM} = 1 + a_s\left(Q_1\right) + 1.332 a_s\left(Q_1\right)^2 \tag{3.12}$$

where the BLM scale is $Q_1 = 0.708\ Q$, and the coefficients are independent of the renormalization scheme.

Figure 3.6 shows the result for $\mathcal{R}_{e^+e^-}$ using the BLM method at leading order (dotted line) and next-to-leading order (solid line), as well as CSS at leading order (dashed line) and next-to-leading order (dash-dotted line). Note that the results obtained with BLM exhibit greater stability with respect to the renormalization scale μ_r already at leading order, in contrast to the CSS approach, where stability is only achieved by incorporating higher-order corrections in the perturbative expansion.

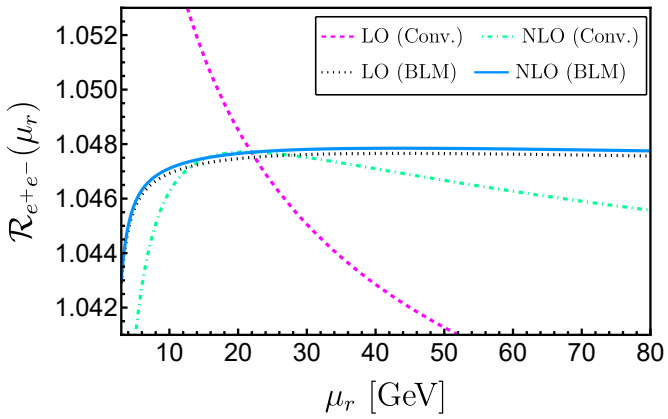

Figure 3.6: Total electron–positron annihilation ratio into hadrons with QCD corrections up to NLO versus the renormalization scale μ_r, using conventional scale setting (Conv.) and the BLM method.

Chapter 4

The Principle of Maximum Conformality

This section introduces the **Principle of Maximum Conformality** (PMC) [61–65], which extends the BLM method [48] to higher orders in perturbation theory. PMC systematically resolves the ambiguities associated with the choice of renormalization scale and scheme by providing a method to set one or more optimal scales at each perturbative order, such that all non-conformal terms are absorbed into the running coupling in the perturbative QCD expansion. This results in a *maximally conformal* series consistent with the principles of the renormalization group.

We refer to PMC-I (Principle of Maximum Conformality, Type I) as the first approach, in which different renormalization scales are assigned at each perturbative order and the non-conformal terms are absorbed iteratively, order by order. This strategy enables a hierarchical resummation of the non-conformal terms into the running behavior of the coupling. A second approach, PMC-II (Principle of Maximum Conformality, Type II), absorbs all non-conformal terms simultaneously at all orders of perturbation theory by defining either several or a single effective scale. It is worth noting that PMC is not the only way to extend the BLM method to higher orders; alternative approaches such as sequential BLM (seBLM) have been proposed in Refs. [66–68].

Throughout this discussion, we will demonstrate how the PMC method provides a solution to the scale- and scheme-setting ambiguities, yielding accurate perturbative predictions free of renormalon terms, which typically cause divergence at high orders.

4.1 PMC Type I

The **PMC-I** (Principle of Maximum Conformality, Type I) approach [61] constitutes a systematic extension of the BLM method. In this framework, a different *effective renormalization scale* is assigned to each order in the perturbative series, with the non-conformal terms—i.e., the terms dependent on the β_i coefficients—being absorbed iteratively. In this way, each effective scale Q_i is determined such that the associated β_i terms vanish at that specific order, yielding a *conformal* perturbative series free from renormalon contributions and with suppressed dependence on the arbitrary initial renormalization scale. This procedure improves the convergence of the series and yields physical predictions that are independent of the renormalization scheme and scale. In the following, we detail the mathematical steps

required to implement PMC-I and derive the explicit expressions for scale setting at LO, NLO, and NNLO.

For the purposes of this procedure, we rewrite the observable from Eq. (3.1) in the following form:

$$\begin{aligned}\frac{\mathscr{P}_\ell - c_{0,0}}{c_{1,0}} \equiv \mathscr{D}_\ell &= a_s\left(\mu_r\right)^\ell + \sum_{i=1}^{2} d_{2,i} N_f^{i-1} a_s^{\ell+1}\left(\mu_r\right) + \sum_{i=1}^{3} d_{3,i} N_f^{i-1} a_s\left(\mu_r\right)^{\ell+2} \\ &\quad + \sum_{i=1}^{4} d_{4,i} N_f^{i-1} a_s\left(\mu_r\right)^{\ell+3} + \mathcal{O}\left(a_s^{\ell+4}\right) \\ &= a_s\left(\mu_r\right)^\ell + \left(d_{2,0} + d_{2,1} N_f\right) a_s\left(\mu_r\right)^{\ell+1} + \left(d_{3,0} + d_{3,1} N_f + d_{3,2} N_f^2\right) a_s\left(\mu_r\right)^{\ell+2} \\ &\quad + \left(d_{4,0} + d_{4,1} N_f + d_{4,2} N_f^2 + d_{4,3} N_f^3\right) a_s\left(\mu_r\right)^{\ell+3} + \mathcal{O}\left(a_s^{\ell+4}\right)\end{aligned} \tag{4.1}$$

where the coefficients $c_{0,0}$ and $c_{1,0}$ are independent of the initial renormalization scale.

For $\mathscr{D}_\ell$ at N^{3}LO, the primary goal is to absorb all N_f-dependent terms into the coupling a_s order by order, through iterative PMC scale settings. This procedure ensures that the non-conformal terms associated with the β_i coefficients are systematically eliminated at each step. The process is outlined as follows. The first step is to absorb the higher-order N_f terms at each perturbative order, i.e., the terms $d_{2,1}N_f$, $d_{3,2}N_f^2$, and $d_{4,3}N_f^3$ must be eliminated by fixing a specific PMC scale Q_1, via the scale shift $\mu_r \to Q_1$. In this way, we obtain:

$$\begin{aligned}\mathscr{D}'_\ell &= a_s\left(Q_1\right)^\ell + d'_{2,0} a_s\left(Q_1\right)^{\ell+1} + \left(d'_{3,0} + d'_{2,1} N_f\right) a_s\left(Q_1\right)^{\ell+2} \\ &\quad + \left(d'_{4,0} + d'_{4,1} N_f + d'_{4,2} N_f^2\right) a_s\left(Q_1\right)^{\ell+3}.\end{aligned} \tag{4.2}$$

The second PMC scale setting, Q_2, at NLO absorbs the terms $d'_{3,1}N_f$ and $d'_{4,2}N_f^2$ into $a_s^{\ell+2}$, yielding:

$$\mathscr{D}''_\ell = a_s(Q_1)^\ell + d'_{2,0} a_s(Q_2)^{\ell+1} + d''_{3,0} a_s(Q_2)^{\ell+2} + (d''_{4,0} + d''_{4,1} N_f) a_s(Q_2)^{\ell+3} \tag{4.3}$$

Finally, the third PMC scale setting, Q_3, at NNLO absorbs the term $d''_{4,1}N_f$ into $a_s^{\ell+3}$, and is expressed as:

$$\mathscr{D}'''_\ell \equiv \mathscr{D}_\ell|_{\text{PMC}} = a_s\left(Q_1\right)^\ell + d'_{2,0} a_s\left(Q_2\right)^{\ell+1} + d''_{3,0} a_s\left(Q_3\right)^{\ell+2} + d'''_{4,0} a_s\left(Q_3\right)^{\ell+3} \tag{4.4}$$

where $d'_{2,0}$, $d''_{3,0}$, and $d'''_{4,0}$ are the conformal coefficients, i.e., they are independent of the initial scale and the renormalization scheme. The elimination of the N_f-dependent terms associated with the β_i coefficients is achieved via the sequential scale shifts $\mu_r \to Q_1$, $Q_1 \to Q_2$, and $Q_2 \to Q_3$. At the $a_s^{\ell+3}$ order, the scale from the previous order is repeated. This is due to the lack of information required to determine a new scale Q_4; therefore, the PMC scale at this order is set equal to Q_3. The determination of the coefficients is carried out step by step through the sequential adjustments $\mathscr{D}_\ell = \mathscr{D}'_\ell$, $\mathscr{D}'_\ell = \mathscr{D}''_\ell$, and $\mathscr{D}''_\ell = \mathscr{D}'''_\ell$, while simultaneously transforming the coefficients into their conformal counterparts. The relation between the initial coefficients of $\mathscr{D}_\ell$ and those appearing at each step of the scale-setting procedure is provided in Appendix B.

On the other hand, the effective PMC scales responsible for absorbing the renormalization scheme dependence are given by a perturbative series expansion in powers of a_s. The

PMC scales Q_i are determined order by order up to NNLO using the following formula:

$$\ln\frac{Q_1^2}{\mu_r^2}=\ln\frac{Q_{10}^2}{\mu_r^2}+\frac{x\beta_0}{4}\ln\frac{Q_{10}^2}{\mu_r^2}a_s\left(\mu_r\right)+\frac{y}{16}\left(\beta_0^2\ln^2\frac{Q_{10}^2}{\mu_r^2}-\beta_1\ln\frac{Q_{10}^2}{\mu_r^2}\right)a_s^2\left(\mu_r\right)+\mathcal{O}\left(a_s^3\right), \quad (4.5)$$

$$\ln\frac{Q_2^2}{Q_1^2}=\ln\frac{Q_{20}^2}{Q_1^2}+\frac{z\beta_0}{4}\ln\frac{Q_{20}^2}{Q_1^2}a_s\left(Q_1\right)+\mathcal{O}\left(a_s^2\right), \quad (4.6)$$

$$\ln\frac{Q_3^2}{Q_2^2}=\ln\frac{Q_{30}^2}{Q_2^2}+\mathcal{O}\left(a_s\right), \quad (4.7)$$

where Q_{i0} $(i=1,2,3)$ are fully determined from the elimination of the terms $d_{2,1}N_f$, $d'_{3,1}N_f$, and $d'_{4,1}N_f$, respectively, and the effective parameters x, y, and z are defined as follows:

$$x = \frac{3(\ell+1)d_{2,1}^2-6\ell d_{3,2}}{\ell d_{2,1}}, \quad (4.8)$$

$$y = \frac{(\ell+1)(2\ell+1)d_{2,1}^3-6\ell(\ell+1)d_{2,1}d_{3,2}+6\ell^2 d_{4,3}}{\ell d_{2,1}^2}, \quad (4.9)$$

$$z = \frac{3(\ell+2)d_{3,1}'^2-6(\ell+1)d'_{2,0}d'_{4,2}}{(\ell+1)d'_{2,0}d'_{3,1}}. \quad (4.10)$$

which are used to eliminate the terms $d_{3,2}N_f^2$, $d'_{4,2}N_f^2$, and $d_{4,3}N_f^3$.

From the analysis, we find that

$$\ln\frac{Q_{10}^2}{\mu_r^2} = \frac{6d_{2,1}}{\ell}, \quad (4.11)$$

$$\ln\frac{Q_{20}^2}{Q_1^2} = \frac{6d'_{3,1}}{(\ell+1)d'_{2,0}}, \quad (4.12)$$

$$\ln\frac{Q_{30}^2}{Q_2^2} = \frac{6d''_{4,1}}{(\ell+2)d''_{3,0}}. \quad (4.13)$$

This method provides a fundamental tool for ensuring scheme independence in physical QCD predictions. The coefficients $d_{j,i}$ (with $j>i$) are scheme-dependent. This implies that different renormalization schemes, such as the $\overline{\text{MS}}$ scheme or the Gell-Mann–Low (GM-L) scheme, will lead to different values of the PMC scales; however, the final result for a physical observable must remain invariant under such choices. This invariance is achieved by iteratively adjusting the renormalization scales to absorb the non-conformal terms into the effective coupling and by establishing commensurate scale relations between observables in different schemes [53]. For instance, starting from the observable $R_{e^+e^-}(Q)$, one can define an effective coupling constant $\alpha_s^R(Q)$ that encapsulates all radiative corrections and allows predictions to be related under different renormalization conventions. A notable example is the scale displacement $e^{-5/3}$ that connects $\alpha_s^{\overline{\text{MS}}}$ and $\alpha_s^{\text{GM-L}}$, ensuring consistency between both schemes. These relations highlight the capability of the PMC method to interpret any scheme as a special case of a universal coupling function, thereby preserving the theoretical consistency of physical predictions.

N_f	c_0	c_1	$c'_{2,0}$	$c''_{3,0}$	$c'''_{4,0}$
3	1	4	1.3584	−1486.52	21101.2
4	1	4	1.3584	−1497.11	$21101.2 - 34.1333\kappa$
5	1	4	1.3584	−1488.93	$21101.2 - 7.75758\kappa$

Table 4.1: Coefficients for the perturbative expansion of $\mathcal{R}_{e^+e^-}$ under PMC-I scale setting.

4.1.1 Electron–Positron Annihilation in PMC-I

Electron–positron annihilation into hadrons, through the measurement of its total cross sections, constitutes one of the most precise methods for determining the value of α_s. The annihilation process up to order α_s^4 can be expressed as follows:

$$\mathcal{R}_{e^+e^-}(\mu) = c_0 + c_1 a_s(\mu) + c_2 a_s(\mu)^2 + c_3 a_s(\mu)^3 + c_4 a_s(\mu)^4, \tag{4.14}$$

where the first three coefficients are presented in Eq. (3.8). The coefficients c_3 and c_4 [69] are given by:

$$c_3 = -424.764 - 76.8083 N_f - 0.33152 N_f^2 - 79.36 \frac{\left(\sum_f Q_f\right)^2}{\sum_f Q_f^2}, \tag{4.15}$$

$$c_4 = -40092.2 + 4805.12 N_f - 204.134 N_f^2 + 5.504 N_f^3 + 256\kappa \frac{\left(\sum_f Q_f\right)^2}{\sum_f Q_f^2}. \tag{4.16}$$

and κ is a very small, poorly defined quantity. An estimate for κ can be obtained indirectly from PDG data [1] by comparing the coefficients[1],

$$\kappa \approx -17.828 + 0.575 N_f. \tag{4.17}$$

Applying the PMC Type I method, the following series is obtained:

$$\mathcal{R}_{e^+e^-}|_{\text{PMC-I}} = c_0 + c_1 a_s(Q_1) + c'_{2,0} a_s(Q_2)^2 + c''_{3,0} a_s(Q_3)^3 + c'''_{4,0} a_s(Q_3)^4 \tag{4.18}$$

where the coefficients are presented in Table 4.1. The perturbative scales are determined as follows:

4.2 PMC Type II

The main idea of the PMC Type II method (or PMC-II) is the introduction of the $\mathcal{R}$-renormalization scheme [70, 71], which generalizes the conventional scheme used in dimensional regularization (DR) [26, 27]. In this scheme, a constant $-\delta$ is subtracted in addition to the standard $\ln 4\pi - \gamma_E$ subtraction of the $\overline{\text{MS}}$ scheme:

$$\mu^2 = \mu_\delta^2 \exp\left(\ln(4\pi) - \gamma_E - \delta\right). \tag{4.19}$$

The subtraction δ defines an infinite set of renormalization schemes, where physical results remain independent of δ, i.e., independent of the scheme. Since PMC predictions do not depend on the choice of renormalization scheme, PMC scale setting satisfies the principles of renormalization group (RG) invariance [72].

[1] This value does not correspond to a rigorous estimate.

4.2.1 Generalization of an Observable

An observable in pQCD under an arbitrary renormalization scheme $\mathcal{R}$ can be written as the following expansion:

$$\mathscr{P}_\ell(Q) = t_0 + \sum_{n\geq 0} t_{n+1}\left(Q,\mu_0\right) a_s\left(\mu_0\right)^{\ell+n} \tag{4.20}$$

where μ_0 is the initial renormalization scale and Q is the kinematic scale of the process. In the ideal case, the observable is independent of the renormalization scale, which is achieved by summing the entire perturbative series. However, in practice, this is not feasible due to the mathematical complexity of higher-order terms. Once the series is truncated, it becomes sensitive to the renormalization scale and to a specific scheme, introducing an ambiguity conditioned by theoretical conventions. Using the coupling displacement relation, in any scheme $\mathcal{R}$,

The observable in Eq. (4.20) can be written as

$$\begin{aligned}
\mathscr{P}_\ell(Q) = {} & t_0 + t_1 a_s(\mu)^\ell + a_s(\mu)^{\ell+1}\left[\beta_0\lambda\ell t_1 + t_2\right] + a_s(\mu)^{\ell+2}\Bigg[\frac{\beta_0^2\lambda^2\ell(\ell+1)t_1}{2!} + \beta_0\lambda(\ell+1)t_2 \\
& + \beta_1\lambda\ell t_1 + t_3\Bigg] + a_s(\mu)^{\ell+3}\Bigg[\frac{\beta_0^3\lambda^3\ell(\ell+1)(\ell+2)t_1}{3!} + \frac{\beta_0^2\lambda^2(\ell+1)(\ell+2)t_2}{2!} \\
& + \frac{\beta_1\beta_0\lambda^2\ell(2\ell+3)t_1}{2!} + \beta_0\lambda(\ell+2)t_3 + \beta_1\lambda(\ell+1)t_2 + \beta_2\lambda\ell t_1 + t_4\Bigg] + a_s\left(\mu\right)^{\ell+4} \\
& \times\Bigg[\frac{\beta_0^2\lambda^2(\ell+2)(\ell+3)t_3}{2!} + \lambda(\ell+1)t_2\left(\beta_2 + \frac{\beta_0^3\lambda^2(\ell+2)(\ell+3)}{3!} + \frac{\beta_1\beta_0\lambda(2\ell+5)}{2!}\right) \\
& + \lambda\ell t_1\Bigg(\beta_3 + \frac{\beta_0^4\lambda^3(\ell+1)(\ell+2)(\ell+3)}{4!} + \frac{\beta_1\beta_0^2\lambda^2(3\ell(\ell+4)+11)}{3!} \\
& + \frac{\left(\beta_1^2+2\beta_0\beta_2\right)\lambda(\ell+2)}{2!}\Bigg) + \beta_0\lambda(\ell+3)t_4 + \beta_1\lambda(\ell+2)t_3 + t_5\Bigg] + a_s\left(\mu\right)^{\ell+5} \\
& \times\Bigg[\frac{\beta_0^2\lambda^2(\ell+3)(\ell+4)t_4}{2!} + \lambda(\ell+2)t_3\left(\beta_2 + \frac{\beta_0^3\lambda^2(\ell+3)(\ell+4)}{3!} + \frac{\beta_1\beta_0\lambda(2\ell+7)}{2!}\right) \\
& + \lambda(\ell+1)t_2\Bigg(\beta_3 + \frac{\beta_0^4\lambda^3(\ell+2)(\ell+3)(\ell+4)}{4!} + \frac{\beta_1\beta_0^2\lambda^2(3(\ell+1)(\ell+5)+11)}{3!} \\
& + \frac{\left(\beta_1^2+2\beta_0\beta_2\right)\lambda(\ell+3)}{2!}\Bigg) + \lambda\ell t_1\Bigg(\beta_4 + \frac{\beta_0^5\lambda^4(\ell+1)(\ell+2)(\ell+3)(\ell+4)}{5!} \\
& + \frac{2\beta_1\beta_0^3\lambda^3(2\ell+5)(\ell(\ell+5)+5)}{4!} + \frac{\beta_0\lambda^2\left(\beta_1^2(3\ell(\ell+5)+17)+3\beta_0\beta_2(\ell+2)(\ell+3)\right)}{2!} \\
& + \frac{\left(\beta_1\beta_2+\beta_0\beta_3\right)\lambda(2\ell+5)}{2!}\Bigg) + \beta_0\lambda(\ell+4)t_5 + \beta_1\lambda(\ell+3)t_4 + t_6\Bigg] + \mathcal{O}\left(a_s^{\ell+6}\right),
\end{aligned} \tag{4.21}$$

where $\lambda = \ln\left(\mu_\lambda^2/\mu_0^2\right)$. The above expression explicitly shows the scheme dependence. The choice of the initial scale is arbitrary and is not the final argument of the running coupling; the final scales will be independent of the initial renormalization scale.

In a conformal (or scale-invariant) theory, where $\beta_i = 0$, the λ dependence disappears from the observable's expression. Therefore, by absorbing all β_i-dependent terms into the

effective coupling at each order, we obtain a final result that is independent of the initial choice of scale and scheme. Although the method is not exact, it leads to a strong suppression of the initial scale dependence. Moreover, in the final result, the coefficients should be completely conformal. The use of the $\mathcal{R}$-scheme allows us to rigorously justify this. From the explicit form of Eq. (4.21), it is easy to confirm that

$$\frac{\partial \mathscr{P}_\ell}{\partial \lambda} = -\beta(a_s)\frac{\partial \mathscr{P}_\ell}{\partial a_s}. \tag{4.22}$$

where the scheme invariance of the physical prediction requires that $\partial \mathscr{P}_\ell/\partial\lambda = 0$.

The idea is that the scales in the coupling constant should be set in such a way that the non-conformal terms associated with the coefficients of the β-function are eliminated, leaving only scheme-independent (conformal) terms. In this way, the finite-order theoretical prediction becomes scheme-independent, thus satisfying the requirements of the renormalization group. The criterion of scheme invariance is a fundamental theoretical principle of RG and must hold regardless of the truncation order of the series. This differs from the general principle that ensures the all-orders expression for a physical observable is invariant under changes in the renormalization scale and scheme, i.e., $d\mathscr{P}/d\mu_0 = 0$. The final series obtained corresponds to the theory where $\beta(a) = 0$, known as the conformal series. This result shows that, at any order, PMC dictates that all non-conformal terms in the perturbative series must be resummed into the running coupling.

Eq. (4.21) clearly exposes the pattern of β_i terms that appear in the coefficients at each order of the perturbative expansion. The $\mathcal{R}$-scheme provides a unified framework for describing predictions in pQCD. Additional conclusions can also be drawn: since no specific value of δ is privileged, it can be observed that certain coefficients associated with the β_i terms exhibit degeneracy. For instance, the terms $\beta_0 a_s^2$ and $\beta_1 a_s^3$ share coefficients that can be equated.

In this way, for example, if we define

$$\begin{aligned}
&t_{1,0} \equiv t_1, \qquad && t_{2,1} \equiv t_1\lambda_1 = t_1 \ln\left(\mu^2/\mu_0^2\right), \\
&t_{2,0} \equiv t_2, \qquad && t_{3,1} \equiv t_2\lambda_2 = t_2 \ln\left(\mu^2/\mu_0^2\right), \\
&t_{3,0} \equiv t_3, \qquad && t_{3,2} \equiv t_1 \ln^2\left(\mu^2/\mu_0^2\right), \\
&\quad\vdots
\end{aligned} \tag{4.23}$$

the general expression in Eq. (4.21) can be rewritten as:

$$\begin{aligned}\mathscr{P}_\ell = & t_0 + t_{1,0}a_s^\ell(Q) + \left[t_{2,0} + \ell\beta_0 t_{2,1}\right] a_s^{\ell+1}(Q) + \Bigg[t_{3,0} + \ell\beta_1 t_{2,1} + (\ell+1)\beta_0 t_{3,1} \\ & + \frac{\ell(\ell+1)}{2}\beta_0^2 t_{3,2}\Bigg] a_s^{\ell+2}(Q) + \Bigg[t_{4,0} + \ell\beta_2 t_{2,1} + (\ell+1)\beta_1 t_{3,1} + (\ell+2)\beta_0 t_{4,1} \\ & + \frac{\ell(3+2\ell)}{2}\beta_0\beta_1 t_{3,2} + \frac{(\ell+1)(\ell+2)}{2}\beta_0^2 t_{2,1} + \frac{\ell(\ell+1)(\ell+2)}{3!}\beta_0^3 t_{4,3}\Bigg] a_s^{\ell+3}(Q) \\ & + \Bigg[t_{5,0} + \beta_1(\ell+2)t_{4,1} + \beta_2(\ell+1)t_{3,1} + \beta_3\ell t_{2,1} + \beta_0(\ell+3)t_{5,1} \\ & + \frac{\left(\beta_1^2 + 2\beta_0\beta_2\right)\ell(\ell+2)t_{3,2}}{2!} + \frac{\beta_1\beta_0(\ell+1)(2\ell+5)t_{4,2}}{2!} + \frac{\beta_0^2(\ell+2)(\ell+3)t_{5,2}}{2!} \\ & + \frac{\beta_1\beta_0^2\ell(3\ell(\ell+4)+11)t_{4,3}}{3!} + \frac{\beta_0^3(\ell+1)(\ell+2)(\ell+3)t_{5,3}}{3!} \\ & + \frac{\beta_0^4\ell(\ell+1)(\ell+2)(\ell+3)t_{5,4}}{4!}\Bigg] a_s^{\ell+4}(Q) + \mathcal{O}\left(a_s^{\ell+5}\right).\end{aligned} \tag{4.24}$$

In this notation, the conformal and non-conformal parts of the perturbative coefficients are denoted by $t_{i,0}$ and $t_{i,j}$, respectively.

4.2.2 Multi-Scale Renormalization Setting in PMC-II

Rewriting the series from Eq. (4.24) into a skeleton-type expansion:

$$\begin{aligned}\mathscr{P}_\ell\left(Q^2\right) = & a(Q)^\ell\Bigg[t_{1,0} + \ell\left(\beta_0 a(Q) + \beta_1 a(Q)^2 + \beta_2 a(Q)^3\right) t_{2,1} + \frac{\ell}{2}\Big((\ell+1)\beta_0^2 a(Q)^2 \\ & + (3+2\ell)\beta_0\beta_1 a(Q)^3\Big) t_{3,2} + \frac{\ell(\ell+1)(\ell+2)}{3!}\beta_0^3 t_{4,3} a(Q)^3\Bigg] \\ & + a(Q)^{\ell+1}\left[t_{2,0} + (\ell+1)\left(\beta_0 a(Q) + \beta_1 a(Q)^2\right) t_{3,1} + \frac{(\ell+1)(\ell+2)}{2}\beta_0^2 t_{4,2} a(Q)^2\right] \\ & + a(Q)^{\ell+2}\left[t_{3,0} + (\ell+2)\beta_0 t_{4,1} a(Q)\right] \\ & + a(Q)^{\ell+3}\left[t_{4,0}\right] + \mathcal{O}\left(a^{\ell+4}\right).\end{aligned} \tag{4.25}$$

At this point, we can define new effective scales Q_i. All terms linear in β can then be resummed through the following definition:

$$\begin{aligned} t_{1,0}a_s\left(Q_1\right)^\ell = & t_{1,0}a_s\left(Q\right)^\ell - \ell\, a_s\left(Q\right)^{\ell-1}\beta\left(a_s\right)t_{2,1}, \\ t_{2,0}a_s\left(Q_2\right)^{\ell+1} = & t_{2,0}a_s\left(Q\right)^{\ell+1} - (\ell+1)\, a_s\left(Q\right)^{\ell}\beta\left(a_s\right)t_{3,1}, \\ t_{3,0}a_s\left(Q_3\right)^{\ell+2} = & t_{3,0}a_s\left(Q\right)^{\ell+2} - (\ell+2)\, a_s\left(Q\right)^{\ell+1}\beta\left(a_s\right)t_{4,1}, \\ & \vdots, \\ t_{k,0}a_s\left(Q_k\right)^{k} = & t_{k,0}a_s\left(Q\right)^{k} - k a\left(Q\right)^{k-1}\beta\left(a_s\right)t_{k+1,1}. \end{aligned} \tag{4.26}$$

At the same time, from the displacement relation given in Eq. (2.35), the running coupling can be expressed in terms of $a_s\left(Q_k\right)^k$:

$$\begin{aligned} a_s\left(Q_k\right)^k = & a_s\left(Q\right)^k + k\ a_s\left(Q\right)^{k-1}\beta\left(a_s\right)\ln\frac{Q_k^2}{Q^2} \\ & + \frac{k}{2}a_s\left(Q\right)^{k-2}\left[\beta\frac{d\beta}{da_s}a_s\left(Q\right) + (k-1)\,\beta\left(a_s\right)^2\right]\ln^2\frac{Q_k^2}{Q^2} + \cdots \end{aligned} \tag{4.27}$$

Considering the k-th power of the running coupling from Eqs. (4.26) and (4.27), one finds that the new renormalization scale satisfies:

$$-\frac{t_{k+1,1}}{t_{k,0}} = \ln\frac{Q_k^2}{Q^2} + \frac{1}{2}\left[\frac{\partial\beta}{\partial a_s} + (k-1)\frac{\beta}{a_s}\right]\ln^2\frac{Q_k^2}{Q^2} + \cdots \tag{4.28}$$

Therefore, the PMC procedure simultaneously determines the scale at each order. The PMC scales Q_k are determined up to N^{3}LO using the following formula:

$$\ln\left(\frac{Q_k}{Q}\right)^2 = \frac{\tau_{k,1} + \Delta_k^{(1)}\left(a_s\right)\tau_{k,2} + \Delta_k^{(2)}\left(a_s\right)\tau_{k,3}}{1 + \Delta_k^{(1)}\left(a_s\right)\tau_{k,1} + \left(\Delta_k^{(1)}\left(a_s\right)\right)^2\left(\tau_{k,2} - \tau_{k,1}\right) + \Delta_k^{(2)}\left(a_s\right)\tau_{k,1}^2}, \tag{4.29}$$

where

$$\tau_{k,j} = (-1)^j\,\frac{t_{k+j,j}}{t_{k,0}}, \tag{4.30}$$

$$\Delta_k^{(1)}\left(a_s\right) = \frac{1}{2!}\left[\frac{\partial\beta}{\partial a_s} + (k+\ell-2)\,\frac{\beta}{a_s}\right]. \tag{4.31}$$

$$\begin{aligned} \Delta_k^{(2)}\left(a_s\right) = & \frac{1}{3!}\left[\beta\frac{\partial^2\beta}{\partial a_s^2} + \left(\frac{\partial\beta}{\partial a_s}\right)^2 + 3\,(k+\ell-2)\,\frac{\beta}{a_s}\frac{\partial\beta}{\partial a_s}\right. \\ & \left. + (k+\ell-2)\,(k+\ell-3)\,\frac{\beta^2}{a_s^2}\right], \end{aligned} \tag{4.32}$$

Finally, the pQCD prediction for $\mathscr{P}_\ell$ after setting the PMC scales Q_k is expressed as:

$$\begin{aligned} \mathscr{P}_\ell|_{\rm PMC} = & \ t_{0,0} + t_{1,0}a_s(Q_1)^\ell + t_{2,0}a_s(Q_2)^{\ell+1} + t_{3,0}a_s(Q_3)^{\ell+2} \\ & + t_{4,0}a_s(Q_4)^{\ell+3} + \mathcal{O}(a_s^{\ell+4}). \end{aligned} \tag{4.33}$$

The PMC scales are perturbative in nature, meaning that more loop terms are required to achieve higher-precision predictions. For instance, Q_4 remains unknown because the $\{\beta_i\}$ terms at order a_s^{p+4} are needed. Nevertheless, Q_4 can be set equal to the last determined scale, Q_3, which ensures the scheme independence of our prediction, as discussed in Ref. [73].

4.2.3 Single-Scale Setting (PMCs)

In the previous subsection, we presented the multi-scale PMC method, which involves considerable theoretical analysis. We now introduce an alternative all-orders single-scale

approach, known as PMCs (single-scale PMC), which simplifies the implementation and automation of PMC scale setting. In essence, the PMCs provides an average value for the multiple PMC scales while retaining the central predictions of the full PMC framework. It has also been observed that the single PMCs scale exhibits both stability and improved convergence as the perturbative order increases.

Let us begin by rewriting Eq. (4.24) in a more compact form as follows:

$$\mathscr{P}_\ell\,(Q) = \sum_{n=1}^{\infty}\sum_{m=0}^{n-1}\left(r_{n,0} + (n+\ell-1)(-1)^m\; r_{n+m,m}(Q/\mu)\;\beta(a_s)\;\Delta_n^{(m-1)}\,a_s^{-1}(\mu)\right)a_s^{n+\ell+1}(\mu), \tag{4.34}$$

where the $\Delta_n(a_s)$ factors are defined in Eq. (4.30).

Here, as before, $r_{n,0}$ are the dimensionless conformal coefficients, and

$$r_{n+m,m}(Q/\mu) = \sum_{k=0}^{m} C_k^m\;\hat{r}_{n+m-k,m-k}\;\ln^k\left(\frac{\mu^2}{Q^2}\right), \tag{4.35}$$

with $C_k^m = m!/\left[k!(m-k)!\right]$. The numerical coefficients $\hat{r}_{n+m-k,\,m-k}$ are provided in Appendix **??**. Note, in particular, that $r_{n,0} = \hat{r}_{n,0}$ is purely numerical and independent of Q/μ.

We can now introduce a single effective scale Q_s, determined by requiring that all non-conformal terms vanish simultaneously, that is:

$$\sum_{n\geq 1, m\geq 1, 0\leq k\leq m}(-1)^j \ln^k\frac{Q_m^2}{Q^2}\left[n\beta\left(a_{Q_\star}\right)a_{Q_\star}^{n-1}\right]C_m^k\Delta_n^{(m-1)}\left(a_{Q_s}\right)\hat{r}_{n+m-k,m-k} = 0, \tag{4.36}$$

which leads to:

$$\ln\frac{Q_s^2}{Q^2} = T_0 + T_1 a_s(Q) + T_2 a_s^2(Q) + \mathcal{O}\left(a_s^3\right), \tag{4.37}$$

where the T_i are process-dependent coefficients. The single effective scale Q_s can be determined at NNLL order, with the first three coefficients given by:

$$\begin{aligned} T_0 &= -\frac{\hat{r}_{2,1}}{\hat{r}_{1,0}}, \\ T_1 &= \frac{(\ell+1)\left(\hat{r}_{2,0}\hat{r}_{2,1} - \hat{r}_{1,0}\hat{r}_{3,1}\right)}{\ell\;\hat{r}_{1,0}^2} + \frac{(\ell+1)\left(\hat{r}_{2,1}^2 - \hat{r}_{1,0}\hat{r}_{3,2}\right)}{2\hat{r}_{1,0}^2}\beta_0, \end{aligned} \tag{4.38}$$

$$\begin{aligned} T_2 = {}& \frac{(\ell+1)^2\left(\hat{r}_{1,0}\hat{r}_{2,0}\hat{r}_{3,1} - \hat{r}_{2,0}^2\hat{r}_{2,1}\right) + \ell(\ell+2)\left(\hat{r}_{1,0}\hat{r}_{2,1}\hat{r}_{3,0} - \hat{r}_{1,0}^2\hat{r}_{4,1}\right)}{\ell^2\hat{r}_{1,0}^3} \\ &+ \frac{(\ell+2)\left(\hat{r}_{2,1}^2 - \hat{r}_{1,0}\hat{r}_{3,2}\right)}{2\hat{r}_{1,0}^2}\beta_1 - \frac{1}{2\ell\;\hat{r}_{1,0}^3}\Big[\ell(\ell+1)\hat{r}_{2,0}\hat{r}_{2,1}^2 + (\ell+1)(\ell+2)\hat{r}_{1,0}^2\hat{r}_{4,2} \\ &+ (\ell+1)^2\left(\hat{r}_{2,0}\hat{r}_{2,1}^2 - 2\hat{r}_{1,0}\hat{r}_{2,1}\hat{r}_{3,1} - \hat{r}_{1,0}\hat{r}_{2,0}\hat{r}_{3,2}\right)\Big]\beta_0 + \frac{1}{6\hat{r}_{1,0}^3}\Big[(\ell+1)(\ell+2) \\ &\times\left(\hat{r}_{1,0}\hat{r}_{2,1}\hat{r}_{3,2} - \hat{r}_{1,0}^2\hat{r}_{4,3}\right) + (\ell+1)(1+2\ell)\left(\hat{r}_{1,0}\hat{r}_{2,1}\hat{r}_{3,2} - \hat{r}_{2,1}^3\right)\Big]\beta_0^2. \end{aligned} \tag{4.39}$$

4.3 Aniquilación electrón-positrón a hadrones en PMC-II

Chapter 5

Relation Between Pole and Running Masses of Heavy Quarks

The mass of quarks plays an important role in the phenomenology of high-energy physics. For example, the b-quark mass is essential for determining B-meson decays and is the dominant decay channel of the Higgs boson into a quark pair, while the top-quark mass is used indirectly to determine the Higgs boson mass.

At lowest order in perturbation theory, it is not necessary to choose a renormalization scheme when considering quantum corrections to quark masses, which are defined differently depending on the renormalization scheme. One of the most widely used renormalization schemes is the modified minimal subtraction scheme, $\overline{\rm MS}$, which corresponds to a specific choice of the finite parts of the counterterms. In this case, the renormalized mass and coupling constant explicitly depend on the renormalization scale through the renormalization group equations (RGE), i.e., the scale of the physical process. Another commonly used renormalization scheme is the on-shell subtraction scheme, in which the renormalized mass is defined at all orders as the pole position of the particle propagator.

High-order QCD corrections to the quark mass ratio have been calculated up to $\mathcal{O}(\alpha_s^3)$ [74, 75] and $\mathcal{O}(\alpha_s^4)$ [76–78], where it is argued that the renormalization scale should be set to the typical momentum of the process in order to eliminate large logarithms. This estimated scale is then varied over an arbitrary range to assess its uncertainty. However, this conventional procedure leads to scheme-dependent predictions and thus violates the fundamental principle of renormalization group invariance.

The pQCD series for the relation between the pole mass and the mass in other schemes exhibits a convergence problem, since the higher-order contributions grow factorially as $n!\,(\beta_0\alpha_s)^n$. This issue is not always resolved within the conventional renormalization procedure, where the choice of subtraction scheme and renormalization scale is not free from ambiguities.

5.1 Quark Mass Relations in Perturbative QCD

In this section, we present the relation between the pole mass and the running mass for heavy quarks using the PMC method. Following this section, we will demonstrate that the mass obtained under the PMC approach is independent of the initial choice of subtraction scheme used in the calculations, up to the order of the expansion.

The primary relation between the pole mass and the running mass [77–81] arises from the renormalization of the bare mass m_0, which is given by

$$m_0 = Z^{\rm OS}\, M, \quad \text{and} \quad m_0 = Z^{\overline{\rm MS}}\, \overline{m}, \tag{5.1}$$

where M and $\overline{m}$ are the pole and $\overline{\rm MS}$ running quark masses, respectively, and $Z^{\rm OS}$ and $Z^{\overline{\rm MS}}$ are the corresponding renormalization constants. We thus consider the relation between the pole and running masses for heavy quarks, namely:

$$H_q\left(\mu\right) = \frac{M}{\overline{m}\left(\mu\right)} = \frac{Z^{\overline{\rm MS}}}{Z^{\rm OS}}. \tag{5.2}$$

The renormalized expression in Eq. (5.2) can be written as a standard QCD perturbative series:

$$H_q\left(\mu\right) = \frac{M}{\overline{m}\left(\mu\right)} = 1 + \sum_{n\geq 1} h_n \left[a_s(\mu)\right]^n, \tag{5.3}$$

where n denotes the perturbative order, α_s is the strong coupling constant, and the h_n coefficients are given by

$$h_n = h_{n,0} + h_{n,1} N_f + h_{n,2} N_f^2 + \cdots + h_{n,n-1} N_f^{n-1}. \tag{5.4}$$

Here, N_f is the number of active quark flavors. The N_f-dependent terms arise from UV-divergent diagrams of the process, which dynamically depend on the virtuality of the underlying quark and gluon subprocesses. We will show an optimal way to set the scales at each perturbative order using the PMC method, in contrast to the conventional approach, thereby yielding a relation that converges to the final value.

Similarly, the inverse relation [77–81] is given by

$$\overline{H}_q\left(\mu\right) = \frac{\overline{m}(\mu)}{M} = 1 + \sum_{n\geq 1} \overline{h}_n \left[a_s(\mu)\right]^n, \tag{5.5}$$

where the $\overline{h}_n$ are perturbative coefficients, which—similarly to Eq. (5.4)—will be useful for determining the mass in the modified minimal subtraction scheme.

5.2 Determination of the Pole Mass and the $\overline{\rm MS}$ Mass for Heavy Quarks within the PMC Framework

In this section, we present an improved analysis of the relation between the pole mass and the $\overline{\rm MS}$ mass for heavy quarks using the PMC method. Before applying the PMC formalism, it is necessary to obtain the scale dependence of the mass ratio from the previous N_f-dependent mass relation at a fixed scale. This can be achieved using the scale evolution of the strong coupling constant up to four-loop level, as given by Eq. (2.35), namely:

$$\begin{aligned} a_s(Q^*) = a_s(Q) - \beta_0 \ln\left(\frac{Q^{*2}}{Q^2}\right) a_s^2(Q) + \left[\beta_0^2 \ln^2\left(\frac{Q^{*2}}{Q^2}\right) - \beta_1 \ln\left(\frac{Q^{*2}}{Q^2}\right)\right] a_s^3(Q) \\ + \left[-\beta_0^3 \ln^3\left(\frac{Q^{*2}}{Q^2}\right) + \frac{5}{2}\beta_0\beta_1 \ln^2\left(\frac{Q^{*2}}{Q^2}\right) - \beta_2 \ln\left(\frac{Q^{*2}}{Q^2}\right)\right] a_s^4(Q) + \mathcal{O}\left(a_s^5\right), \end{aligned} \tag{5.6}$$

where Q^* and Q are two arbitrary renormalization scales.

Choosing the heavy quark pole mass as the initial renormalization scale, the expression for the pole mass from Eq. (5.3), dependent on the number of active quark flavors N_f, can be written as

$$\begin{aligned} H_q = 1 + h_{1,0} a_s(\mu_r^{\rm init}) + (h_{2,0} + h_{2,1} N_f)\, a_s^2(\mu_r^{\rm init}) + \left(h_{3,0} + h_{3,1} N_f + h_{3,2} N_f^2\right) a_s^3(\mu_r^{\rm init}) \\ + \left(h_{4,0} + h_{4,1} N_f + h_{4,2} N_f^2 + h_{4,3} N_f^3\right) a_s^4(\mu_r^{\rm init}) + \mathcal{O}(a_s^5). \end{aligned} \tag{5.7}$$

The coefficients $h_{i,j}$ up to four-loop level are provided in Ref. [77]:

$$\begin{aligned} &h_{1,0} = 1.333, && h_{2,0} = 14.485, \\ &h_{2,1} = -1.041, && h_{3,0} = 217.903, \\ &h_{3,1} = -27.961, && h_{3,2} = 0.653, \\ &h_{4,0} = 4357.4 \pm 1.64, && h_{4,1} = -(834.548 \pm 0.04), \\ &h_{4,2} = -45.431, && h_{4,3} = -0.678. \end{aligned} \tag{5.8}$$

The $\mathcal{R}_\delta$-scheme [70, 71] reveals a specific degeneracy of the coefficients across different perturbative orders in the series, ensuring a one-to-one correspondence between the N_f terms and the $\{\beta_i\}$ terms through Eq. (5.6), order by order in the expansion. Based on this, Eq. (5.7) can be rewritten in terms of the $\{\beta_i\}$ structure of Eq. (4.24), up to order a_s^4:

$$\begin{aligned} H_q = 1 + r_{1,0} a_s(\mu_r^{\rm init}) + (r_{2,0} + \beta_0 r_{2,1})\, a_s^2(\mu_r^{\rm init}) + \left(r_{3,0} + \beta_1 r_{2,1} + 2\beta_0 r_{3,1} + \beta_0^2 r_{3,2}\right) a_s^3(\mu_r^{\rm init}) \\ + \left(r_{4,0} + \beta_2 r_{2,1} + 2\beta_1 r_{3,1} + \frac{5}{2}\beta_0\beta_1 r_{3,2} + 3\beta_0 r_{4,1} + 3\beta_0^2 r_{4,2} + \beta_0^3 r_{4,3}\right) a_s^4(\mu_r^{\rm init}). \end{aligned} \tag{5.9}$$

Here, for future convenience, we have transformed the N_f-series into the required $\{\beta_i\}$-series. The coefficients β_0, β_1, and β_2 are given in Eqs. (2.23) and (2.25). The $r_{i,0}$ with $i = 1, \ldots, 4$ are scale-invariant conformal coefficients, while the $r_{i,j}$ with $1 \le j < i \le 4$ are non-conformal coefficients that must be absorbed into the coupling.

Applying the PMC method, we absorb all non-conformal coefficients that govern the running behavior of the coupling into the strong coupling itself. The non-conformal terms are eliminated, and the resulting pQCD series becomes a conformal mass ratio:

$$\begin{aligned} H_q^{\rm PMC} &= 1 + r_{1,0} a_s(Q_1) + r_{2,0} a_s^2(Q_2) + r_{3,0} a_s^3(Q_3) + r_{4,0} a_s^4(Q_4) \\ &= 1 + 0.424307 \alpha_s(Q_1) - 0.272706 \alpha_s^2(Q_2) + 3.27051 \alpha_s^3(Q_3) + 1.84591 \alpha_s^4(Q_4), \end{aligned} \tag{5.10}$$

where the conformal coefficients are independent of the renormalization scale μ_r. The final series becomes scheme-independent up to the given order, eliminating the ambiguity of the conventional renormalization scheme. Here, Q_k ($k = 1, \ldots, 4$) are the PMC scales for the mass relation between the pole and running masses, determined by Eq. (4.29).

The inverse relation, comparing the running mass to the pole mass, $\overline{H}_q$, is conventionally determined at $\mathcal{O}(a_s^4)$ for a renormalization scale $\mu_r^{\rm init} = M$ as:

$$\begin{aligned} \overline{H}_q = 1 + \bar{h}_{1,0} a_s(\mu_r^{\rm init}) + \left(\bar{h}_{2,0} + \bar{h}_{2,1} N_f\right) a_s^2(\mu_r^{\rm init}) + \left(\bar{h}_{3,0} + \bar{h}_{3,1} N_f + \bar{h}_{3,2} N_f^2\right) a_s^3(\mu_r^{\rm init}) \\ + \left(\bar{h}_{4,0} + \bar{h}_{4,1} N_f + \bar{h}_{4,2} N_f^2 + \bar{h}_{4,3} N_f^3\right) a_s^4(\mu_r^{\rm init}), \end{aligned} \tag{5.11}$$

where the coefficients are given in [77]:

$$\begin{aligned}
&\bar{h}_{1,0} = -1.333, && \bar{h}_{2,0} = -15.374,\\
&\bar{h}_{2,1} = 1.041, && \bar{h}_{3,0} = -226.283,\\
&\bar{h}_{3,1} = 28.229, && \bar{h}_{3,2} = -0.653,\\
&\bar{h}_{4,0} = -4455.25 \pm 1.64, && \bar{h}_{4,1} = 845.941 \pm 0.04,\\
&\bar{h}_{4,2} = -45.517, && \bar{h}_{4,3} = 0.678.
\end{aligned} \tag{5.12}$$

Applying PMC scale setting yields the following conformal series:

$$\begin{aligned}
\overline{H}_q^{\rm PMC} &= 1 + \overline{r}_{1,0} a_s(\overline{Q}_1) + \overline{r}_{2,0} a_s^2(\overline{Q}_2) + \overline{r}_{3,0} a_s^3(\overline{Q}_3) + \overline{r}_{4,0} a_s^4(\overline{Q}_4) \\
&= 1 - 0.424307\alpha_s(\overline{Q}_1) + 0.182631\alpha_s^2(\overline{Q}_2) - 3.39816\alpha_s^3(\overline{Q}_3) - 1.60253\alpha_s^4(\overline{Q}_4),
\end{aligned} \tag{5.13}$$

where $\overline{Q}_k$ $(k = 1, \ldots, 4)$ are the PMC scales at each perturbative order, determined via Eqs. (4.29), (4.30), (4.31), and (4.32), using the conformal coefficients $\overline{r}_{i,0}$ and the non-conformal coefficients $\overline{r}_{i,j}$ of the inverse relation.

The results presented in this section, $H_q^{\rm PMC}$ and $\overline{H}_q^{\rm PMC}$, originate from series initially computed in the On-shell and $\overline{\rm MS}$ schemes, respectively. After applying the PMC formalism, they become scheme-independent. The initial schemes serve only as a starting point for deriving the generalized mass relations, from which one can determine the heavy quark masses $M_q^{\rm PMC}$ and their corresponding mass differences $\Delta M_q^{\rm PMC}$ within the PMC framework.

5.3 Numerical Results and Discussion

For the numerical calculations, we use the current central values for the charm, bottom, and top quark masses as reported in PDG-2022 [1], namely:

$$\begin{aligned}
&\overline{m}_c(\overline{m}_c^2) = 1.27 \pm 0.02 \text{ GeV}, \quad \alpha_s(\overline{m}_c) = 0.38 \pm 0.03,\\
&\overline{m}_b(\overline{m}_b^2) = 4.18^{+0.04}_{-0.03} \text{ GeV}, \quad \alpha_s(\overline{m}_b) = 0.233 \pm 0.008,
\end{aligned} \tag{5.14}$$

and for the top quark, based on cross-section measurements,

$$\overline{m}_t(\overline{m}_t^2) = 162.5^{+2.1}_{-1.5} \text{ GeV}, \quad \alpha_s(\overline{m}_t) = 0.1083, \tag{5.15}$$

as well as the pole masses of the quarks [1] for determining the $\overline{\rm MS}$ masses:

$$\begin{aligned}
&M_c = 1.67 \pm 0.07 \text{ GeV}, \quad M_b = 4.78 \pm 0.06 \text{ GeV},\\
&M_t = 172.5 \pm 0.7 \text{ GeV}, \quad \alpha_s(M_Z) = 0.1181.
\end{aligned} \tag{5.16}$$

5.3.1 Charm Quark Mass Relations

The determination of the charm quark mass plays a crucial role in the estimation of the Cabibbo-Kobayashi-Maskawa (CKM) matrix parameters. The relation between its pole and running masses, including QCD corrections $\mathcal{O}(\alpha_s)$, has been computed up to three loops [82] and four loops [78]. The results for H_c are presented in Table 5.1, where $H_c^{(i)}$ denotes the approximate mass ratio at each perturbative order with $i =$ LO, NLO, etc. We

fix $\mu_r = \mu^{\rm init} = 2$ GeV for the conventional scale setting, and for the PMC approach we also take $\mu^{\rm init} = 2$ GeV as the initial scale.

For H_c, we introduce four PMC scales. As stated in Section 4.2, Eq. (4.29), and due to the lack of a_s^5 information, the optimal scale at $\mathcal{O}(a_s^4)$ cannot be fixed, so we set $Q_4^{(c)}$ equal to the last determined PMC scale of the process.

The PMC multi-scales are:

$$Q_1^{(c)} = 1.136 \text{ GeV}, \quad Q_2^{(c)} = 0.950 \text{ GeV}, \quad Q_3^{(c)} = 1.006 \text{ GeV}, \tag{5.17}$$

which are all smaller than $\mu^{\rm init}$, showing that different $\{\beta_i\}$ structures govern the dynamics at each perturbative order.

The perturbative QCD corrections to the charm mass ratio yield:

$$H_c^{\rm PMC} = 1 + 0.2408 - 0.1165 + 0.7962 + 0.2806. \tag{5.18}$$

	$H_c^{(1)}$	$H_c^{(2)}$	$H_c^{(3)}$	$H_c^{(4)}$	$\overline{H}_c^{(1)}$	$\overline{H}_c^{(2)}$	$\overline{H}_c^{(3)}$	$\overline{H}_c^{(4)}$
Conv.	1.16124	1.31224	1.51842	1.88291	0.949974	0.934186	0.927642	0.924158
PMCs	1.10309	1.08699	1.13389	1.14032	0.947721	0.950494	0.944138	0.943769
PMC	1.24077	1.12431	1.92046	2.20104	0.944683	0.949485	0.941559	0.941064

Table 5.1: Numerical results for the charm quark mass ratio H_c and its inverse $\overline{H}_c$ using conventional scale setting (Conv.), PMCs, and PMC, corrected up to four-loop level. The initial scale is $\mu_r^{\rm init} = 2$ GeV (and $\mu_r^{\rm init} = M_Z$ [1]).

An alternative approach is the single-scale PMC (PMCs), which helps to suppress residual scale dependence when it becomes significant. The idea is to set an effective single scale. The details of the procedure are described in Subsection 4.2.3. In our case, the single scale is determined from the following perturbative relation, fixed up to the next-to-next-to-leading-log ($\rm N^2LL$) level:

$$\ln\left(\frac{Q_s^{(c)}}{Q}\right)^2 = -1.171 + 12.56\, a_s(Q) + 104.8\, a_s^2(Q), \tag{5.19}$$

where $Q = \mu_r^{\rm init}$, and the coefficients are determined using Eq. (4.38).

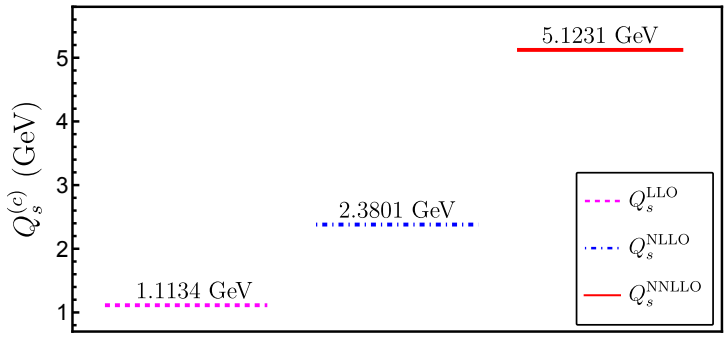

Figure 5.1: PMC single-scale values for H_c, determined up to NNLL. $\mu_r^{\rm init} = 2$ GeV.

The PMCs single-scale values are shown in Fig. 5.1, up to N^{2}LL order: $Q_s^{(c)} = 1.1134$ GeV. The scales satisfy $Q_s^{(c),\mathrm{LL}} < Q_s^{(c),\mathrm{NLL}} < Q_s^{(c),\mathrm{N^2LL}}$.

The best result for the PMC pole mass of the charm quark is obtained via the PMCs scale setting, which improves the convergence of the observables. The pole masses for each approximation are:

$$\begin{aligned} M_c^{\mathrm{PMC}}|_{\mathrm{NLO}} &= 1.40^{+0.05}_{-0.02}\ \mathrm{GeV}, \\ M_c^{\mathrm{PMC}}|_{\mathrm{N^2LO}} &= 1.38^{+0.03}_{-0.02}\ \mathrm{GeV}, \\ M_c^{\mathrm{PMC}}|_{\mathrm{N^3LO}} &= 1.44^{+0.14}_{-0.05}\ \mathrm{GeV}, \\ M_c^{\mathrm{PMC}}|_{\mathrm{N^4LO}} &= 1.45^{+0.17}_{-0.05}\ \mathrm{GeV}. \end{aligned} \tag{5.20}$$

The perturbative PMC pole mass M_c^{PMC} contributes to the central value reported in [1] and is consistent with the results in [78, 79].

The uncertainties in Eq. (5.20) are estimated by varying the PMCs single scale between N^{2}LL and NLL levels, i.e., $Q_s^{(c),\mathrm{N^2LL}} \pm |Q_s^{(c),\mathrm{N^2LL}} - Q_s^{(c),\mathrm{NLL}}|$.

To quantify the theoretical prediction, we define the error as:

$$E(M_q) = \frac{\left|M_q^{\mathrm{data}} - M_q\right|}{1\ \mathrm{GeV}}, \tag{5.21}$$

which compares the numerical result with experimental or phenomenological data. For the charm quark, the conventional setting yields $E(M_q^{\mathrm{Conv.}}) \simeq 0.7$, while our result gives $E(M_q^{\mathrm{PMCs}}) \simeq 0.2$.

The inverse ratio values $\overline{H}_c$ from Eq. (5.5) for the charm quark are listed in Table 5.1 for PMC and PMCs, compared with the conventional setting. The resulting pole and running masses from the PMC approach are shown in Table 5.2. Finally, the PMC pole–running mass difference for the charm quark, $\Delta M_c = M_c - \overline{m}_c$, yields an improved estimate: $\Delta M_c^{\mathrm{PMC}} \sim 100$ MeV.

	M_c (GeV)	$\overline{m}_c$ (GeV)	$\lvert\Delta M_c\rvert$ (GeV)
Conv.	2.39 ± 0.04	$1.54^{+0.02}_{-0.03}$	0.847947
PMCs	$1.45^{+0.17}_{-0.05}$	$1.576^{+0.0012}_{-0.0013}$	0.108979
PMC	2.79 ± 0.04	1.57 ± 0.07	0.939072

Table 5.2: Pole mass values using the input from Eq. (5.14), running mass values using Eq. (5.16), and their difference for the charm quark using conventional (Conv.), PMCs, and PMC scale settings.

5.3.2 Bottom Quark Mass Relations

The bottom quark plays an important role in modern particle physics, and a precise knowledge of its mass parameter is necessary for accurate theoretical predictions. For instance, an accurate bottom quark mass is required for calculations involving b meson decays, which are often proportional to the fifth power of the quark mass [76].

	$H_b^{(1)}$	$H_b^{(2)}$	$H_b^{(3)}$	$H_b^{(4)}$	$\overline{H}_b^{(1)}$	$\overline{H}_b^{(2)}$	$\overline{H}_b^{(3)}$	$\overline{H}_b^{(4)}$
Conv.	1.09462	1.14138	1.17515	1.20652	0.949889	0.935519	0.930128	0.927575
PMCs	1.09197	1.07916	1.11247	1.11654	0.947965	0.950712	0.944444	0.944082
PMC	1.11393	1.08096	1.15252	1.16382	0.94520	0.949855	0.942191	0.941717

Table 5.3: Numerical results for the mass ratio H_b of the bottom quark and its inverse $\overline{H}_b$, using conventional scale setting (Conv.), PMCs and PMC, up to four-loop corrections. $\mu_r^{init} = 2$ GeV (and $\mu_r^{init} = M_Z$).

The perturbative mass relations for the bottom quark, including QCD corrections, have been computed up to three loops in Ref. [83] and up to four loops in Refs. [75, 77, 78]. Using the PMC formalism for the b quark, we obtain the following numerical series:

$$H_b^{\rm PMC} = 1 + 0.1140 - 0.03297 + 0.07156 + 0.01129, \tag{5.22}$$

in contrast to values quoted for $\mathcal{O}(\alpha_s^3)$ in [84] and $\mathcal{O}(\alpha_s^4)$ in [76, 78]. The PMC multi-scale setting yields the following effective scales:

$$Q_1^{(b)} = 1.129 \text{ GeV}, \quad Q_2^{(b)} = 0.5682 \text{ GeV}, \quad Q_3^{(b)} = 1.006 \text{ GeV}, \tag{5.23}$$

and $Q_4^{(b)}$ is fixed equal to the last known scale. Optionally, using the single-scale PMC (PMCs) at N^{2}LL, the mass ratio H_b is shown in Table 5.3. The initial renormalization scale is taken as 2 GeV for the conventional setting, and the PMCs scale is determined from Fig. 5.2 by:

$$\ln\left(\frac{Q_s^{(b)}}{Q}\right)^2 = -1.1714 + 12.38\, a_s(Q) + 96.38\, a_s^2(Q). \tag{5.24}$$

The resulting PMC pole masses for the bottom quark are:

$$\begin{aligned} M_b^{\rm PMC}|_{\rm NLO} &= 4.66^{+0.03}_{-0.02} \text{ GeV}, \\ M_b^{\rm PMC}|_{\rm N^2LO} &= 4.52^{+0.03}_{-0.02} \text{ GeV}, \\ M_b^{\rm PMC}|_{\rm N^3LO} &= 4.82^{+0.04}_{-0.02} \text{ GeV}, \\ M_b^{\rm PMC}|_{\rm N^4LO} &= 4.86^{+0.03}_{-0.02} \text{ GeV}, \end{aligned} \tag{5.25}$$

Uncertainties are estimated by varying the multi-scales $Q_k^{(b)}$ $(k = 1, 2, 3)$ within the conventional range. Note that the bottom quark mass is not a physical observable, and therefore carries an inherent $\Lambda_{\rm QCD}$ uncertainty of order 0.3 GeV. This cannot be removed via the OPE, and dominates over PMC-induced uncertainty. Thus, central values from PMC should be understood within this limitation.

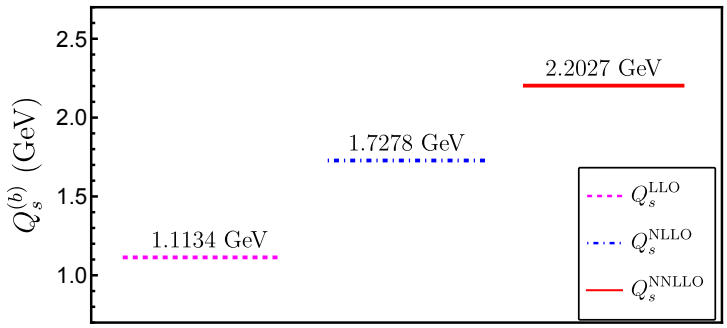

Figure 5.2: Single PMC scale Q_s for H_b determined up to NNLL. $\mu_r^{init} = 2$ GeV.

Our PMC prediction, $M_b^{\rm PMC} = 4.84$ GeV, is much closer to the PDG(2022) value $M_b = 4.78 \pm 0.06$ GeV [1], with an error measure $E(M_b^{\rm PMC}) \simeq 0.08$, as compared to $E(M_b^{\rm Conv.}) \simeq 0.26$ from the conventional scale setting. Additionally, the second PMC approach is also consistent with the PDG central value. The inverse ratio $\overline{H}_b^{\rm PMC}$ at $\mathcal{O}(\alpha_s^4)$ is shown in Table 5.3.

In the conventional setting, M_b shows strong scale dependence, as depicted in Fig. 5.3. This sensitivity results from the arbitrary scale choice and poor convergence. In contrast, Fig. 5.4(a) and (b) show improved stability and convergence using PMC and PMCs, respectively.

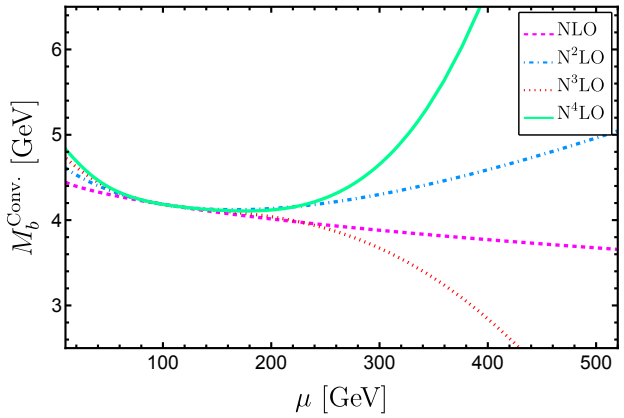

Figure 5.3: QCD corrections to M_b at one (dashed), two (dash-dotted), three (dotted), and four-loop (solid) orders using conventional scale setting. $N_f = 5$, $\mu_r^{init} = 2$ GeV.

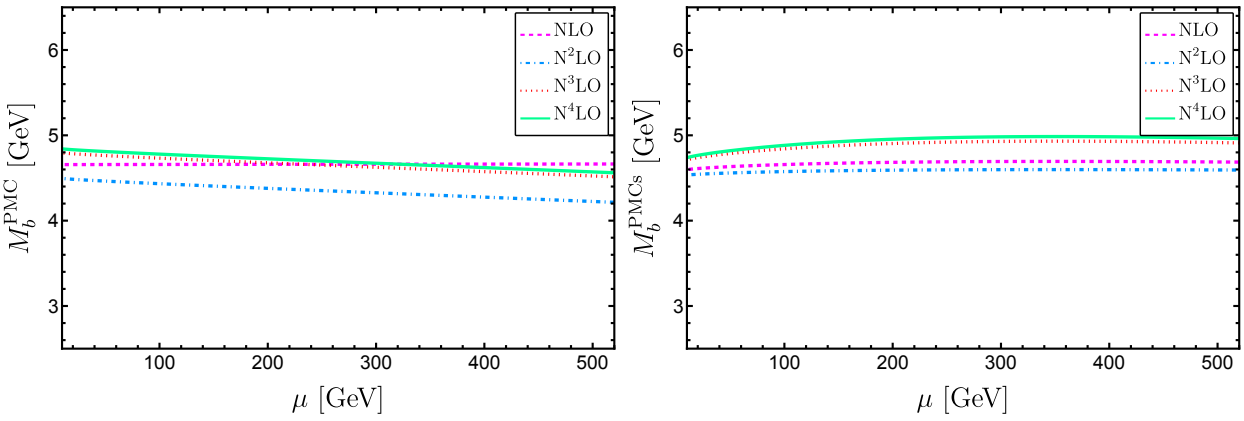

Figure 5.4: QCD corrections to M_b using (a) multi-scale PMC and (b) single-scale PMCs at one (dashed), two (dash-dotted), three (dotted), and four-loop (solid) levels. $\mu_r^{init} = 2$ GeV.

	M_b (GeV)	$\overline{m}_b$ (GeV)	$\lvert\Delta M_b\rvert$ (GeV)
Conv.	$5.04^{+0.86}_{-0.51}$	$4.43^{+0.05}_{-0.06}$	0.609
PMCs	$4.67^{+0.06}_{-0.04}$	$4.512^{+0.003}_{-0.006}$	0.155
PMC	$4.86^{+0.03}_{-0.02}$	4.50 ± 0.06	0.363

Table 5.4: Pole mass values using input from Eq. (5.14), running masses from Eq. (5.16), and their difference for the bottom quark, using conventional scale setting (Conv.), PMCs, and PMC.

5.3.3 Top Quark Mass Relations

The top quark mass is a fundamental theoretical parameter extracted from experimental data at the Tevatron and the LHC [1, 85]. The renormalized top quark mass, expressed in terms of the pole-to-running mass relation with QCD corrections up to $\mathcal{O}(\alpha_s^3)$ and $\mathcal{O}(\alpha_s^4)$, has been determined in [76–79, 83], and including mixed QCD-EW corrections $(\alpha\alpha_s)$ in [86, 87]. The pole mass is sensitive to low-momentum contributions, which leads to significant perturbative corrections. Thus, truncating the series at a fixed order inevitably introduces scale and scheme dependence. The Principle of Maximum Conformality (PMC) significantly improves the mass ratio predictions for the top quark, yielding results that are independent of the renormalization scheme. The PMC mass ratio (and its inverse) at various perturbative orders is presented in Table 5.5, using conventional, PMC, and PMCs scale settings, with an initial scale $\mu_r^{\rm init} = 80$ GeV. The PMC ratio up to $\mathcal{O}(\alpha_s^4)$ reads:

$$H_t^{\rm PMC} = 1 + (49.5 - 5.00 + 5.43 + 0.363) \times 10^{-3}, \tag{5.26}$$

This result exhibits better convergence compared to the conventional result in Eq. (5.9). The effective PMC scales determined are:

$$Q_1^{(t)} = 44.86 \text{ GeV}, \quad Q_2^{(t)} = 16.24 \text{ GeV}, \quad Q_3^{(t)} = 40.25 \text{ GeV}. \tag{5.27}$$

These values are independent of the initial renormalization scale, except for a residual dependence from the truncated β-function, which is below the quoted precision. Table 5.5

shows the corresponding PMCs results, where the single effective scale is displayed in Fig. 5.5, evaluated up to NNLL order. The PMC pole mass predictions for the top quark at different perturbative orders are:

$$\begin{aligned} M_t^{\rm PMC}|_{\rm NLO} &= 172.1 \pm 0.6 \text{ GeV}, \\ M_t^{\rm PMC}|_{\rm N^2LO} &= 171.3 \pm 0.6 \text{ GeV}, \\ M_t^{\rm PMC}|_{\rm N^3LO} &= 172.2 \pm 0.6 \text{ GeV}, \\ M_t^{\rm PMC}|_{\rm N^4LO} &= 172.3 \pm 0.6 \text{ GeV}. \end{aligned} \tag{5.28}$$

The PMC pole mass prediction for the top quark represents a significant improvement over the conventional determination. The current central value is 172.5 GeV [1], which contributes to the value determined from top-quark pair production at hadron colliders [88].

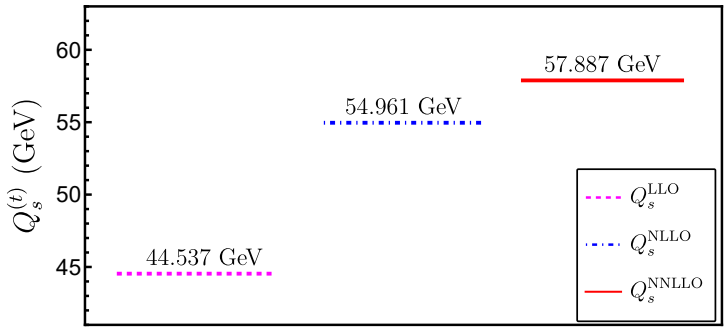

Figure 5.5: Single-scale PMC value for H_t, determined up to NNLL. $\mu_r^{\rm init} = 80$ GeV.

Figure 5.6 shows the renormalization scale dependence of the top-quark pole mass M_t under the conventional approach, up to four loops, using Eq. (5.9) and an initial scale $\mu_r^{\rm init} = 80$ GeV. The numerical results for M_t after applying PMC multi-scale and PMCs single-scale optimization are displayed in Fig. 5.7, where the scale dependence is effectively suppressed. This is attributed to the systematic determination of PMC effective scales, which improves theoretical precision over the conventional approach. Figure 5.7(a) corresponds to the multi-scale case, and Fig. 5.7(b) corresponds to the single-scale scenario.

The final PMC results for the top quark pole and running masses are listed in Table 5.6, showing notable improvement. The PMC correction to the top quark mass serves as a reliable input in electroweak precision tests such as the $\Delta\rho$ parameter [89], and has been studied in the PMC framework in [90]. Moreover, the mass difference between the PMC pole and running top quark masses from both initial schemes is found to be $\Delta M_t^{\rm PMC} = 9.7$ GeV.

	$H_t^{(1)}$	$H_t^{(2)}$	$H_t^{(3)}$	$H_t^{(4)}$	$\overline{H}_t^{(1)}$	$\overline{H}_t^{(2)}$	$\overline{H}_t^{(3)}$	$\overline{H}_t^{(4)}$
Conv.	1.04595	1.05574	1.05876	1.05995	0.949889	0.93699	0.932718	0.930977
PMCs	1.04788	1.04441	1.04911	1.04941	0.948011	0.950753	0.944502	0.944141
PMC	1.04952	1.04456	1.04999	1.05035	0.94571	0.950193	0.94278	0.942327

Table 5.5: Numerical results for the mass ratio H_t of the top quark and its inverse $\overline{H}_t$ under conventional scale setting (Conv.), PMCs and PMC, respectively, corrected up to four-loop level. $\mu_r^{\rm init} = 80$ GeV (and $\mu_r^{\rm init} = M_Z$).

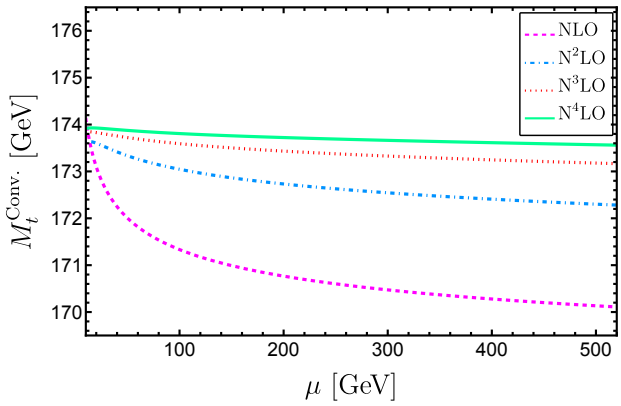

Figure 5.6: QCD correction to M_t at one (dotted), two (dot-dashed), three (dashed), and four-loop (solid) levels under conventional scale setting. For $N_f = 6$ and $\mu_r^{\rm init} = 80$ GeV.

	M_t (GeV)	$\overline{m}_t$ (GeV)	$\lvert\Delta M_t\rvert$ (GeV)
Conv.	$173.8^{+1.3}_{-1.0}$	$160.6^{+1.8}_{-1.4}$	13.2097
PMCs	172.10 ± 0.06	$162.86^{+0.08}_{-0.09}$	9.23861
PMC	172.3 ± 0.6	162.6 ± 0.7	9.70624

Table 5.6: Values obtained for the pole mass using the input from Eq. (5.15), the running mass from Eq. (5.16), and their difference for the top quark using conventional (Conv.), PMCs, and PMC scale settings.

5.4 Final Discussion

The conventional determination of the heavy-quark mass ratios assigns an arbitrary range and systematic error to fixed-order pQCD corrections, thereby violating the fundamental principle of renormalization group invariance. The Principle of Maximum Conformality (PMC) formalism provides a solution to this issue by systematically setting the renormalization scale of the process, leading to a consistent connection between the pole and running masses. The results obtained using the PMC are independent of the initial choice of the renormalization scale. The PMC scale is determined through the absorption of non-conformal terms into the running coupling, which represents a significant theoretical advantage, as these scales are derived rather than arbitrarily chosen.

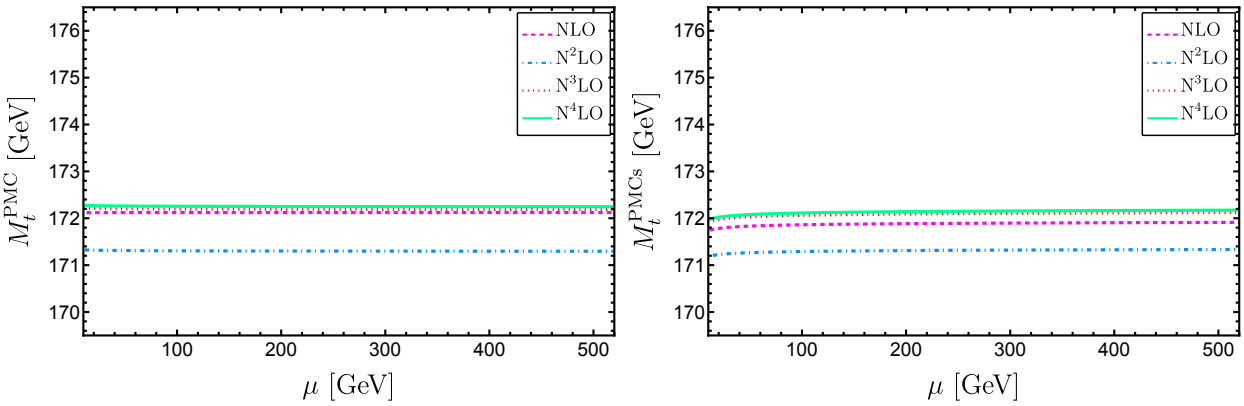

Figure 5.7: QCD correction to the top quark pole mass M_t under (a) PMC multi-scale and (b) PMCs single-scale optimization, at one (dotted), two (dot-dashed), three (dashed), and four-loop (solid) levels. For $\mu_r^{\rm init} = 80$ GeV.

A second improvement of the PMC formalism is that a different effective scale is set at each perturbative order, which enhances the convergence of the perturbative series. In scenarios where the series convergence is slow, it is advantageous to adopt a universal single PMC scale, which further stabilizes the prediction of the observable. In this work, this situation occurs in the determination of the mass ratio for the charm quark, where the single-scale PMC prediction outperforms the multi-scale version in terms of stability and convergence.

The results obtained in this study are: $M_b^{\rm PMC} = 4.86^{+0.03}_{-0.02}$ GeV, $M_t^{\rm PMC} = 172.3 \pm 0.6$ GeV, and $\overline{m}_t^{\rm PMC} = 162.6 \pm 0.7$ GeV. These results improve the achievable precision in various Standard Model tests and enhance sensitivity to possible new physics signals, as the PMC formalism eliminates the ambiguities associated with the renormalization scheme and scale. The PMC pole masses can be reliably used in threshold phenomena [91, 92], where more accurate mass corrections can significantly impact predictions for heavy-quark production cross sections.

Chapter 6

The PMC Approach to the Electroweak Parameter ρ

The parameter ρ is used to describe the ratio between charged and neutral currents in the weak interaction [93]. In particular, ρ is related to the ratio between the W and Z boson masses and is used to predict shifts in the W boson mass and the effective leptonic weak mixing angle due to loop corrections. It can be expressed as

$$\rho = 1 + \delta\rho, \tag{6.1}$$

with

$$\delta\rho = \frac{\Pi_{ZZ}(0)}{M_Z^2} - \frac{\Pi_{WW}(0)}{M_W^2}, \tag{6.2}$$

where $\Pi_{ZZ}(0)$ and $\Pi_{WW}(0)$ are the transverse parts of the Z and W boson self-energies evaluated at zero external momentum.

The precision determination of ρ is crucial for testing the internal consistency of the Standard Model (SM) and for probing new physics beyond it. The parameter $\delta\rho$ in the on-shell (OS) top-quark mass definition can be written as

$$\delta\rho_{\rm OS} = \rho_0\, \delta P(\mu), \tag{6.3}$$

with the prefactor ρ_0 defined as

$$\rho_0 = \frac{N_C G_F}{8\sqrt{2}\pi^2} M_t^2. \tag{6.4}$$

Here, the Fermi constant is given by $G_F = 1.16638 \times 10^{-5}$ GeV^{-2} [1], and N_C is the color factor, with $N_C = 3$ for quarks and $N_C = 1$ for leptons. Meanwhile, QCD corrections up to the four-loop level are included in δP [94–99]:

$$\delta P(\mu) = 1 + d_1 a_s(\mu) + d_2 a_s^2(\mu) + d_3 a_s^3(\mu), \tag{6.5}$$

where the coefficients d_i are listed in Appendix C.

The goal of this section is to apply the PMC scale-setting procedure to refine the values of ρ_0 and δP[1]. The determination of the top-quark mass is generally crucial for computing

[1] A PMC study of the δP factor using a single-scale approach was conducted in Ref. [90]. In this work, we extend the PMC method to adjust both ρ_0 and δP using both multi-scale and single-scale settings.

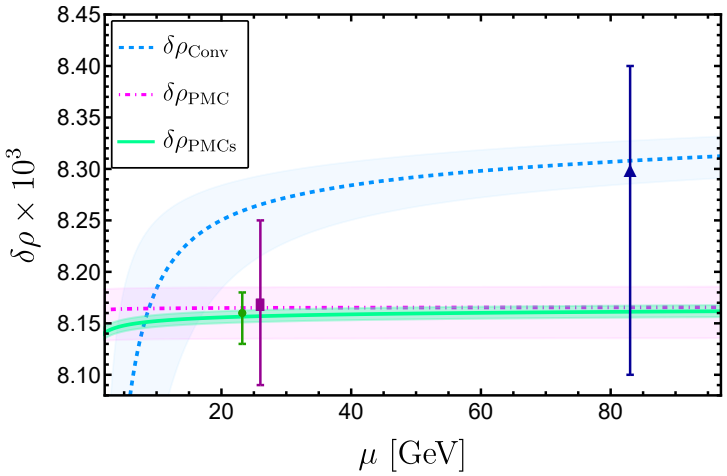

Figure 6.1: Renormalization scale dependence of $\delta\rho$. Dashed line: conventional scale setting; dotted line: PMC multi-scale setting; solid line: PMCs single-scale setting.

$\delta\rho$. In our study, $M_t(\mu)$ is obtained by optimizing the scale setting of the observable H_q in Eq. (5.7), where the PMC prescription yields M_t. Using the calculations presented in Subsection 5.3.3, Eq. (6.4) gives

$$\begin{aligned}
\rho_0 &= 9.282 \pm 0.009 \times 10^{-3}, \quad \text{(PMCs)} \\
\rho_0 &= 9.30 \pm 0.09 \times 10^{-3}, \quad \text{(PMC)} \\
\rho_0 &= 9.47^{+0.11}_{-0.14} \times 10^{-3}, \quad \text{(Conventional)}
\end{aligned} \tag{6.6}$$

On the other hand, the PMC approach for δP is expressed as

$$\delta P^{\rm PMC} = 1 + r_1^{\rm conf}\alpha_s(Q_1) + r_2^{\rm conf}\alpha_s^2(Q_2) + r_3^{\rm conf}\alpha_s^3(Q_3), \tag{6.7}$$

where $r_i^{\rm conf}$ are the conformal coefficients listed in Appendix C. These coefficients are independent of the initial renormalization scale choice. Using Eqs. (4.29)–(4.32), in the multi-scale PMC setting we find

$$Q_1 = 26.11 \text{ GeV}, \quad Q_2 = 84.08 \text{ GeV}, \tag{6.8}$$

and Q_3 is set equal to the last determined scale.

For the single-scale PMCs setting, we have

$$\delta P^{\rm PMCs} = 1 + r_1^{\rm conf}\alpha_s(Q_s^{\rm NLL}) + r_2^{\rm conf}\alpha_s^2(Q_s^{\rm NLL}) + r_3^{\rm conf}\alpha_s^3(Q_s^{\rm NLL}), \tag{6.9}$$

where $Q_s^{\rm LL} = 26.43$ GeV and $Q_s^{\rm NLL} = 23.96$ GeV (see Appendix **??**).

Numerically, the renormalization scale dependence of the four-loop QCD correction to the electroweak parameter $\delta\rho$ is shown in Fig. 6.1. The dashed line indicates a stronger dependence associated with the conventional method. The dotted and solid lines represent the PMC multi-scale and single-scale settings, respectively. In all cases, the shaded bands reflect the associated uncertainties.

Due to the perturbative nature of the single-scale approach, we observe that the minimal residual dependence stabilizes at higher energies compared to the multi-scale result.

The significant stability of $\delta\rho$ achieved using PMC is attributed to the elimination of the renormalization scale ambiguity and the systematic absorption of non-conformal terms into the running coupling.

The triangular, square, and circular markers on the plot correspond to the central values of $\delta\rho$ obtained using the conventional, PMC multi-scale, and PMCs single-scale settings, respectively. The same input parameters used in this section and in Section 5.3 yield the following results:

$$\begin{aligned} \delta\rho &= 8.16^{+0.02}_{-0.03} \times 10^{-3}, && \text{(PMCs)} \\ \delta\rho &= 8.17 \pm 0.08 \times 10^{-3}, && \text{(PMC)} \\ \delta\rho &= 8.3^{+0.1}_{-0.2} \times 10^{-3}. && \text{(Conventional)} \end{aligned} \tag{6.10}$$

The uncertainty in the conventional case is estimated by varying μ in the range $[M_t/2, 2M_t]$, whereas in the PMC case it is obtained by considering the difference between NLL and LL scale determinations, along with other propagated errors.

6.1 Final Discussion

As an application, this work focuses on the relevance of the electroweak parameter ρ in describing weak interactions and its connection to the W and Z boson masses. The precision of ρ is essential for testing the internal consistency of the Standard Model and for probing new physics. To achieve this, we use the PMC scale-setting procedure applied to the top-quark mass (see Section 5.3) to refine the values of ρ_0 and δP.

In particular, the determination of $\delta\rho$ is found to lie within the range $8.16^{+0.02}_{-0.03} \times 10^{-3}$ to $8.3^{+0.1}_{-0.2} \times 10^{-3}$ in the PMC approach, compared to $8.3^{+0.1}_{-0.2} \times 10^{-3}$ using the conventional method. These results highlight the enhanced stability and precision achieved using PMC, as seen in Fig. 6.1. Overall, this section emphasizes the value of the PMC scale-setting framework in determining key Standard Model parameters and its capability to remove renormalization scale ambiguities, thereby improving the accuracy of theoretical predictions. The results obtained have important implications for Standard Model tests and the search for new physics in future experiments.

Chapter 7

Hadronic Decay of the W Boson

The study of the hadronic decay width of the W boson plays an important role within the Standard Model and has been measured by several collaborations, such as D0 [100], ATLAS [101], LHCb [102], and CMS [103], where the average leptonic decay branching fraction per flavor is estimated to be $(10.89 \pm 0.08)\%$, and the inclusive hadronic decay branching fraction is $(67.32 \pm 0.23)\%$.

Improving the predictions of the hadronic decay of the W boson directly impacts our knowledge of the fundamental free parameters of the theory. This decay can be used as an excellent estimator of the strong coupling constant, $\alpha_s(Q)$, which determines the scale of strong interactions described theoretically by QCD; this estimation has implications for reducing theoretical uncertainties in all high-precision perturbative QCD (pQCD) calculations. Furthermore, it can be used indirectly to determine the sum of the first two rows of the CKM matrix, thereby helping to test the unitarity of this matrix for all quarks lighter than the top quark. Theoretical predictions of the hadronic decay width of the W boson have improved in recent decades due to the inclusion of electroweak (EW) and mixed (EW-QCD) corrections, although QCD-type corrections still introduce uncertainties under the premise of renormalization group invariance [104].

The aim is to improve the prediction of the hadronic decay width of the W boson through an optimal treatment of perturbative QCD corrections. Conventionally, the renormalization scale of the process, μ_r, is chosen to be equal to the mass of the W boson, M_W; in principle, the decay result should be independent of M_W, but due to the truncation of the perturbative series, M_W appears in the calculated expressions. This choice of $\mu_r = M_W$ therefore raises an issue of ambiguity in the choice of the renormalization scale and scheme. By applying the Principle of Maximum Conformality (PMC), we suppress this ambiguity and improve the theoretical estimates of the W boson hadronic decay.

7.1 Hadronic Decay Width of the W Boson

The hadronic decay width of the W boson can be expressed as [103]:

$$\Gamma_W^{(\mathrm{had})} = \Gamma_0 + \Gamma_{\mathrm{QCD}} + \Gamma_{\mathrm{EW}} + \Gamma_{\mathrm{mix}}, \tag{7.1}$$

where Γ_0 denotes the tree-level contribution. In the massless quark limit, this contribution reads:

$$\Gamma_0 = \frac{\sqrt{2} G_F N_c}{12\pi} M_W^3 \sum_{i=u,c} \sum_{j=d,s,b} |V_{ij}|^2 , \tag{7.2}$$

which depends on the number of colors N_c (= 3 for quarks), the Fermi constant G_F, the W boson mass M_W, and the sum of the squared CKM matrix elements V_{ij}, excluding kinematically forbidden channels (i.e., those involving the top quark).

The term $\Gamma_{\rm QCD}$ includes the pure QCD corrections, which will be the main focus of this section. On the other hand, $\Gamma_{\rm EW}$ represents the electroweak corrections, as found in [105–108], and $\Gamma_{\rm mix}$ accounts for the mixed EW-QCD corrections [109–111], i.e., corrections proportional to the squared ratio of quark-to-boson masses, which are strongly suppressed compared to the other corrections.

The QCD corrections to the decay of the W boson into hadrons can be expressed as:

$$\Gamma_{\rm QCD} = \Gamma_0 \sum_{n=1}^{\infty} \sum_{m=0}^{n-1} c_{n,m} \, {N_f}^m \, a_s^n, \tag{7.3}$$

where the coefficients $c_{n,m}$ arise from loop corrections and are known up to the fourth order in a_s [60]. The subscript n indicates the perturbative order (power of a_s), m is the number of internal fermion loops, and N_f is the number of active quark flavors (quarks lighter than the energy scale of the process).

As shown in a previous work [112], by using the scale displacement relation, the QCD correction $\Gamma_{\rm QCD}$ in Eq. (7.3) can be expressed as:

$$\Gamma_{\rm QCD}(Q) = \Gamma_0 \sum_{n=1}^{\infty} \sum_{m=0}^{n-1} \left(r_{n,0} + n(-1)^m \, r_{n+m,m}(Q/\mu) \, \beta(a_s) \, B_n^{(m-1)} \, a_s^{-1}(\mu) \right) a_s^n(\mu), \tag{7.4}$$

where the first three $B_n(a_s)$ factors are:

$$\begin{aligned} B_n^{(0)} &= 1, \quad B_n^{(1)} = \frac{1}{2}\left[\frac{\partial \beta}{\partial a_s} + (n-1)\frac{\beta}{a_s}\right], \\ B_n^{(2)} &= \frac{1}{3!}\left[\beta \frac{\partial^2 \beta}{(\partial a_s)^2} + \left(\frac{\partial \beta}{\partial a_s}\right)^2 + 3(n-1)\frac{\beta}{a_s}\frac{\partial \beta}{\partial a_s} + (n-1)(n-2)\frac{\beta^2}{a_s^2}\right]. \end{aligned} \tag{7.5}$$

Using the PMC method in the single-scale approach (PMCs), we obtain a maximally conformal expression for the pQCD series of $\Gamma_{\rm QCD}$:

$$\begin{aligned} \Gamma_{\rm QCD}|_{\rm PMCs} \;=\; \Gamma_0 \Big(& \hat{r}_{1,0} \, a_s(Q_s) + \hat{r}_{2,0} \, a_s^2(Q_s) + \hat{r}_{3,0} \, a_s^3(Q_s) \\ & + \hat{r}_{4,0} \, a_s^4(Q_s) + \mathcal{O}\left(a_s^5\right) \Big). \end{aligned} \tag{7.6}$$

This expression is said to have *maximum conformality* in the sense that it depends solely on the $\hat{r}_{n,0}$ coefficients and not on the $r_{n+m,m}(Q/\mu)$ ones, provided the correct value of Q_s is

used. The PMCs scale Q_s is determined by the following perturbative series:

$$\ln \frac{Q_s^2}{M_W^2} = T_0 + T_1 a_s\left(M_W\right) + T_2 a_s^2\left(M_W\right) + \mathcal{O}\left(a_s^3\right), \tag{7.7}$$

with coefficients:

$$T_0 = \frac{\hat{r}_{2,1}}{\hat{r}_{1,0}}, \tag{7.8}$$

$$T_1 = \frac{\left(\hat{r}_{2,1}^2 - \hat{r}_{1,0}\hat{r}_{3,2}\right)\beta_0}{\hat{r}_{1,0}^2} + \frac{2\left(\hat{r}_{2,0}\hat{r}_{2,1} - \hat{r}_{1,0}\hat{r}_{3,1}\right)}{\hat{r}_{1,0}^2}, \tag{7.9}$$

$$\begin{aligned} T_2 = {} & \frac{3\left(\hat{r}_{2,1}^2 - \hat{r}_{1,0}\hat{r}_{3,2}\right)\beta_1}{2\hat{r}_{1,0}^2} + \frac{\left(2\hat{r}_{1,0}\hat{r}_{3,2}\hat{r}_{2,1} - \hat{r}_{2,1}^3 - \hat{r}_{4,3}\hat{r}_{1,0}\right)\beta_0^2}{\hat{r}_{1,0}^3} \\ & + \frac{3\left(\hat{r}_{1,0}\hat{r}_{2,1}\hat{r}_{3,0} - \hat{r}_{1,0}^2\hat{r}_{4,1}\right) + 4\left(\hat{r}_{1,0}\hat{r}_{3,1}\hat{r}_{2,0} - \hat{r}_{2,1}\hat{r}_{2,0}\right)}{\hat{r}_{1,0}^3} \\ & + \frac{\left(4\hat{r}_{1,0}\hat{r}_{2,1}\hat{r}_{3,1} - 3\hat{r}_{1,0}^2\hat{r}_{4,2} + 2\hat{r}_{1,0}\hat{r}_{3,2}\hat{r}_{2,0} - 3\hat{r}_{2,1}^2\hat{r}_{2,0}\right)\beta_0}{\hat{r}_{1,0}^3}. \end{aligned} \tag{7.10}$$

The PMC single scale Q_s is nearly independent of the initial choice of renormalization scale μ_r, which is a key advantage of this method. As a result, the QCD correction to the W boson decay using the PMCs method, as given in Eq. (7.6), is similar to the expansion in Eq. (7.4), but it contains only conformal terms (i.e., $\beta = 0$), making it less sensitive to the initial renormalization scale and thus reducing the ambiguity associated with scheme and scale choices. The predictions obtained will be studied numerically in the following section.

7.2 Numerical Results

For our numerical analysis, we use the following input parameters: the mass of the W boson, $M_W = 80.377 \pm 0.012$ GeV, the strong coupling constant $\alpha_s(M_Z) = 0.1179 \pm 0.0009$, and the mass of the Z boson, $M_Z = 91.1876 \pm 0.0021$ GeV [1].

In the conventional renormalization scale-setting approach, the convergence of the perturbative series for $\Gamma_{\rm QCD}$ improves if we choose the kinematic scale equal to the renormalization scale, i.e., $\mu_r^{\rm init} = \mu_r$, typically taken as M_W in our case, in order to avoid large logarithmic corrections from scale ratios. Although this choice suppresses large logarithms, it introduces scale dependence, which generally leads to an ambiguity.

Figure 7.1(a) shows the renormalization scale dependence of $\Gamma_{\rm QCD}$ in the conventional scale setting, with $N_f = 5$, at various loop orders. At leading order (LO), a strong scale dependence is observed (dashed curve), which only diminishes when higher-loop corrections are included. In this figure, LO in QCD is shown as the magenta dashed line, next-to-leading order (NLO) as the red dash-dotted line, next-to-next-to-leading order ($\rm N^2LO$) as the thick blue dotted line, and next-to-next-to-next-to-leading order ($\rm N^3LO$) as the solid green line.

On the other hand, the PMC method provides a systematic way to suppress the ambiguity in the choice of μ_r by optimally determining the effective scale Q_s that absorbs the non-conformal terms in $\Gamma_{\rm QCD}$ at each order in perturbation theory. The application of the PMC method to $\Gamma_{\rm QCD}$ is shown in Fig. 7.1(b), where it is evident that already at LO (magenta dashed curve), there is little scale dependence in the region $\mu_r > 10$ GeV. The stability

of the higher orders NLO (dash-dotted curve), N^{2}LO (dotted curve), and N^{3}LO (solid curve) is due to the inclusion of the $r_{4,j}$ coefficients in the determination of the PMC single scale.

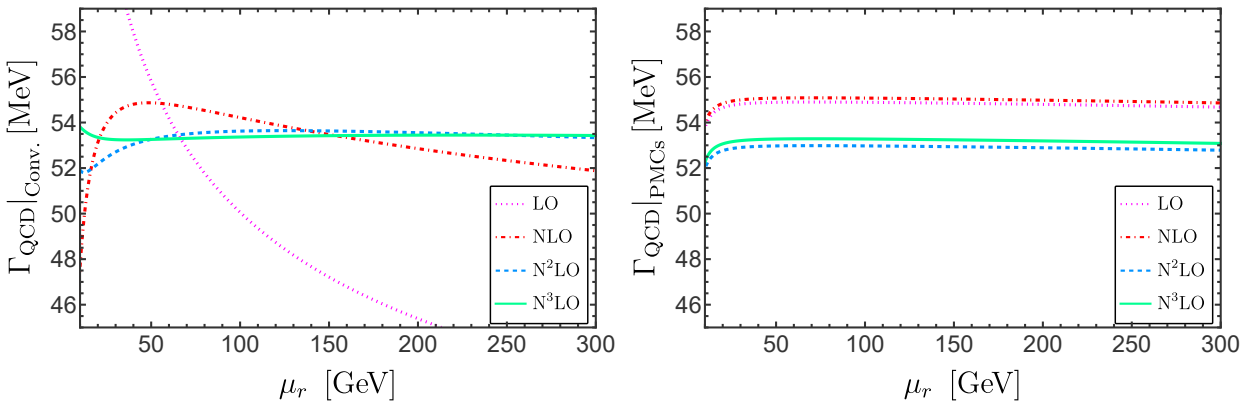

Figure 7.1: (a) QCD corrections up to four loops for $\Gamma_{\rm QCD}$ under conventional scale setting, and (b) using the PMC single-scale approach. We choose the number of active flavors as $N_f = 5$. Input parameters can be found in Section 7.2.

Considering only tree-level and QCD corrections to $\Gamma_W^{(\rm had)}$—i.e., neglecting $\Gamma_{\rm EW}$ and $\Gamma_{\rm mix}$ [see Eq. (7.1)]—and using $G_F = 1.166 \times 10^{-5}$ GeV^{-2} [1] and $\sum_{i,j} |V_{ij}|^2 = 1.984 \pm 0.021$ [103], we obtain:

$$\Gamma_W^{(\rm had)}\Big|_{\rm PMC}^{\mathcal{O}(\alpha_s^4)} = 1405.61 \pm 0.21 \text{ MeV}. \tag{7.11}$$

To obtain this result, the PMC single scale up to next-to-next-to-leading logarithmic order (N^{2}LL) was found to be $Q_s \sim 0.688 M_W$, which is lower than the typical conventional scale choice $\mu_r \sim M_W$, assumed to suppress large logarithms.

The relative sizes of the LO, NLO, N^{2}LO, and N^{3}LO contributions to $\Gamma_W^{(\rm had)}$ using the PMC method are:

$$\frac{\Gamma_{\rm QCD}^{(\rm LO)}}{\Gamma_W^{(\rm had)}} \simeq 0.039, \quad \frac{\Gamma_{\rm QCD}^{(\rm NLO)}}{\Gamma_W^{(\rm had)}} \simeq 10^{-4}, \quad \frac{\Gamma_{\rm QCD}^{(\rm N^2LO)}}{\Gamma_W^{(\rm had)}} \simeq -1.5 \times 10^{-3}, \quad \frac{\Gamma_{\rm QCD}^{(\rm N^3LO)}}{\Gamma_W^{(\rm had)}} \simeq 2.2 \times 10^{-5}.$$

The uncertainty in Eq. (7.11) is estimated by considering the PMC scale determination at NLL and N^{2}LL orders. Table 7.1 summarizes the corrections at each order and the total width obtained using PMCs, conventional scale setting, and results from Refs. [109, 111].

	Γ_0	$\Gamma^{(1)}_{\rm QCD}$	$\Gamma^{(2)}_{\rm QCD}$	$\Gamma^{(3)}_{\rm QCD}$	$\Gamma^{(4)}_{\rm QCD}$	$\Gamma^{(\rm had)}_W$
PMCs	1352.33	54.898	0.185737	−2.10097	0.302928	1405.61 ± 0.21
Conv.	1352.33	51.737	2.78935	−0.966785	−0.231709	$1405.66^{+6.36}_{-5.16}$
[109]	1408.98	54.087	2.727	−1.018	−0.245	1464.73
[111]	1392.17	52.345	2.773	−0.925	−0.221	1446.15

Table 7.1: Numerical results for QCD corrections to the hadronic decay of the W boson. Γ_0 denotes the tree-level contribution, $\Gamma^{(i)}_{\rm QCD}$ represents the correction at order i, and $\Gamma^{(\rm had)}_W$ is the total hadronic decay width including QCD corrections. Results are presented for the PMC single-scale setting, conventional scale setting, and previous literature. All values are in MeV. Input parameters are detailed in Section 7.2.

Figure **??** compares the W boson hadronic decay width, $\Gamma^{(\rm had)}_W$, as a function of the renormalization scale μ_r, using both the conventional scale setting and the PMC method. The black dashed curve represents the conventional method, showing moderate scale dependence within the shaded region ($\mu_r \in [M_W/2, 2M_W]$). This variation illustrates the inherent sensitivity of the conventional approach to the choice of μ_r, which can introduce theoretical uncertainties. In contrast, the solid magenta curve corresponds to the PMC single-scale setting, displaying reduced scale dependence, particularly outside the region where the scale ambiguity is most pronounced. The vertical line indicates the PMC-determined scale Q_s, which provides an optimal balance for improving perturbative series stability. While the conventional method yields reasonable predictions, PMC demonstrates a clear advantage in reducing theoretical uncertainty in $\Gamma^{(\rm had)}_W$.

To further quantify the scale dependence of the W boson hadronic decay width, we define the relative variation $\Delta\Gamma_W$ as:

$$\Delta\Gamma_W = \left(\frac{\Gamma_W(\mu_r) - \Gamma_W(M_W)}{\Gamma_W(M_W)}\right) \times 100, \tag{7.12}$$

which represents the relative deviation of $\Gamma_W(\mu_r)$, calculated at an arbitrary scale μ_r, from the reference value at $\mu_r = M_W$. This expression quantifies how the renormalization scale affects theoretical predictions, providing insight into the sensitivity of perturbative QCD calculations to the choice of scale.

Figure 7.2 displays the percentage variation $\Delta\Gamma_W$ as a function of the renormalization scale μ_r. Two curves are shown for comparison: the blue dotted curve ($\Delta\Gamma^{\rm Conv}_W$) represents the conventional method, showing larger oscillations, especially at low μ_r, indicating greater scale sensitivity. The solid green curve ($\Delta\Gamma^{\rm PMCs}_W$) represents the PMC method, exhibiting significantly reduced variation and a much flatter behavior across the entire scale range. The shaded bands around each curve denote theoretical uncertainties, with the PMC method also yielding smaller uncertainties compared to the conventional approach. This highlights the superior reliability of the PMC method in reducing theoretical uncertainties associated with arbitrary scale choices.

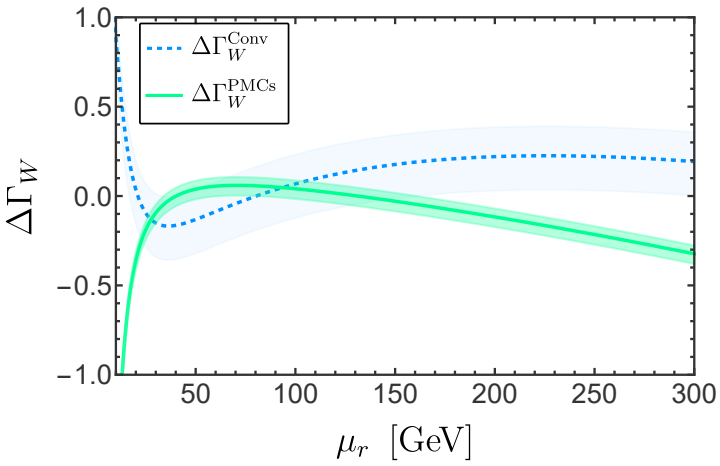

Figure 7.2: Comparison of the percentage relative variation of the W boson hadronic decay width, $\Delta\Gamma_W(\%)$, as a function of the renormalization scale μ_r. The blue dotted curve corresponds to the conventional scale-setting method, while the solid green curve represents the PMC method. Shaded regions indicate the associated theoretical uncertainties for each method.

7.3 Other Optimizations of the Renormalization Scale for W Boson Decay

In this section, we discuss the numerical results obtained using the PMC method and compare them with other scale-setting optimization strategies.

Applying the BLM method to the QCD corrections of the W boson decay width, $\Gamma_{\rm QCD}$, as given in Eq. (7.3), up to order $n = 2$, the resulting renormalization scale is $Q_{\rm BLM} = 0.708 M_W$.

For NNLO and higher orders, i.e., $n \geq 3$ in Eq. (7.3), the relationship between β_0 and N_f is no longer unique. Therefore, it is necessary to extend the BLM method to relate the coefficients that contain powers of N_f to those associated with the β-function coefficients β_0, β_1, and β_2.

One such extension is the BLM/PMC method [61, 63], which assigns a distinct renormalization scale at each order in the perturbative QCD series. All non-conformal terms in the perturbative series are absorbed into the running coupling, such that the remaining series mimics that of a conformal theory—i.e., with $\beta_i = 0$ for all i. Consequently, predictions obtained using the BLM/PMC method are scheme-independent. The procedure involves replacing the renormalization scale μ with appropriate effective scales until all higher-order N_f-dependent terms are fully absorbed into the running coupling, thereby eliminating the terms associated with the β-function coefficients β_i. Simultaneously, the perturbative coefficients are modified. In our case, applying the BLM/PMC method to the perturbative QCD corrections of the hadronic W boson decay in Eq. (7.3), we fix the effective scales order by order. It is worth noting that the fifth-order ($n = 5$) perturbative coefficients are not available, so the fourth renormalization scale is set equal to the last calculated one. Thus, we obtain $Q^*_{\rm BLM/PMC} = 0.740 M_W$.

Finally, Figure 7.3 shows the estimation of the hadronic decay width of the W boson up to the four-loop level as a function of the renormalization scale μ_r, comparing different scale-setting methods. The dot-dashed curve corresponds to the BLM method, which predicts a larger decay width; the dotted curve represents the BLM/PMC method, which yields a slightly smaller decay width but with reduced scale dependence. The dashed curve corresponds to the conventional scale-setting, which stabilizes only at higher orders. The solid

curve represents the PMC method, showing the least variation and providing a stable and nearly constant prediction over the entire μ_r range. From this comparison, it is evident that BLM-based methods exhibit reduced dependence on the renormalization scale, making them a robust option for precise predictions in QCD.

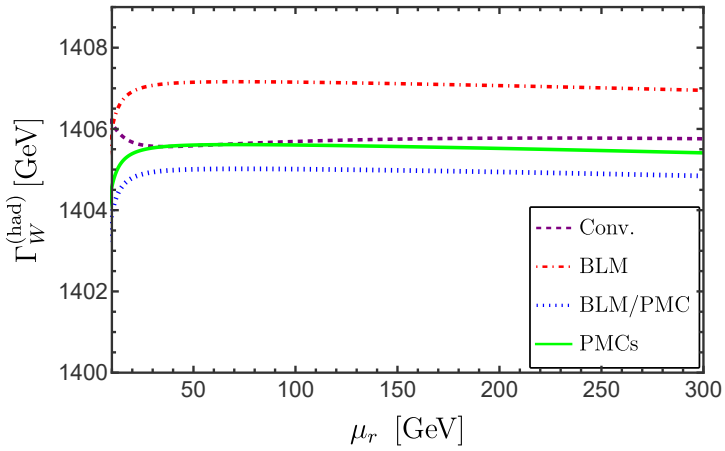

Figure 7.3: Inclusive hadronic decay width of the W boson, Γ^W_{had}, up to four-loop level under different scale-setting methods: conventional (dashed curve), BLM (dot-dashed curve), BLM/PMC (dotted curve), and PMC (solid curve). Input parameters are given in Section 7.2.

7.4 Indirect Extraction of $|V_{cs}|$

The hadronic decay width of the W boson, described in Eq. (7.1), involves contributions from the elements of the first two rows of the CKM matrix, corresponding to quarks lighter than the mass of the W boson. The current experimental values of the CKM matrix elements are given by [1]:

$$\begin{aligned} &|V_{ud}| = 0.97367 \pm 0.00032, && |V_{us}| = 0.22431 \pm 0.00085, \\ &|V_{ub}| = (3.82 \pm 0.20) \times 10^{-3}, && |V_{cd}| = 0.221 \pm 0.004, \\ &|V_{cs}| = 0.975 \pm 0.006, && |V_{cb}| = (41.1 \pm 1.2) \times 10^{-3}. \end{aligned} \tag{7.13}$$

Among these elements, the most relevant in the hadronic decays of the W boson are $|V_{ud}|$ and $|V_{cs}|$. However, the large uncertainty in the experimental value of $|V_{cs}|$ introduces a significant limitation to the precision of theoretical predictions for the hadronic decay width. This motivates an independent estimate of $|V_{cs}|$ based on theoretical methods.

Experimentally, the V_{cs} element of the CKM matrix is primarily determined through processes such as semileptonic decays of D mesons, where the decay width and form factors are combined to extract its value; leptonic decays of the D_s meson, which use the decay rate together with decay constants computed in lattice QCD; and decays of the W boson, such as $W \to c\bar{s}$, measured at colliders like LEP and the LHC [1]. These approaches yield values consistent with the unitary structure of the CKM matrix, although with significant uncertainties in the case of V_{cs}.

In this work, we apply the PMC method to improve the precision of the QCD corrections in the theoretical prediction of the hadronic decay width. Using the theoretical expression for the decay width along with the experimental values of all input parameters, we can indirectly

extract the charm-strange element of the CKM matrix, $|V_{cs}|$, obtaining:

$$|V_{cs}|_{\rm conv.} = 0.966^{+0.004}_{-0.005}, \quad (7.14)$$

$$|V_{cs}|_{\rm PMC} = 0.9667^{+0.0003}_{-0.0002}. \quad (7.15)$$

The quoted uncertainties were estimated by varying the renormalization scale μ_r within the range $\mu_r/2$ to $2\mu_r$ in the calculation up to N^{3}LO order.

These two estimates are consistent with each other and in good agreement with the average value reported by the PDG. The small difference observed highlights the utility of the PMC method in reducing the theoretical uncertainties associated with QCD corrections.

Chapter 8

Viability of PMC in Factorizable Hadronic Processes

Hadron colliders allow the exploration of physics at sub-nuclear scales, but theoretical predictions of their cross-sections require careful control of perturbative QCD approximations. A crucial ingredient is factorization in hard processes: according to the QCD factorization theorem, the hadronic cross-section can be separated into two components—a short-distance part, process-dependent and perturbatively calculable, and universal long-distance (non-perturbative) functions. This is schematically expressed as:

$$d\sigma_{AB\to X} = \sum_{a,b} \int dx_a dx_b \, f_{a/A}(x_a, \mu_F) f_{b/B}(x_b, \mu_F) \otimes \hat{\sigma}_{ab\to X}(x_a, x_b, Q; \mu_R, \mu_F) \, . \tag{8.1}$$

Here, $f_{a/A}(x, \mu_F)$ and $f_{b/B}(x, \mu_F)$ are the parton distribution functions (PDFs) describing the probability of finding partons a and b inside the initial hadrons A and B with momentum fraction x at the factorization scale μ_F. The factor $\hat{\sigma}_{ab\to X}$ is the short-distance partonic cross-section for producing the final state X from partons a and b, calculable as a perturbative series in the strong coupling constant $\alpha_s(\mu_R)$ evaluated at the renormalization scale μ_R. In some cases, particularly when X includes identified hadrons in the final state, the expression might additionally involve fragmentation functions (generically indicated by $\otimes F$) to describe the formation of final-state hadrons. The choice of scales μ_F and μ_R is, order by order, arbitrary and constitutes a significant source of theoretical uncertainty. This section explores the application of the Principle of Maximum Conformality (PMC) for optimally setting the renormalization scale μ_R in $\hat{\sigma}$, aiming to enhance the accuracy of predictions and eliminate scale-setting ambiguities.

8.1 Factorization Structure and Scale Setting in the Partonic Cross Section

In high-energy hadronic processes, factorization ensures that high-energy dynamics are encapsulated in $\hat{\sigma}_{ab}$, separated from the non-perturbative physics contained in PDFs. The partonic cross-section $\hat{\sigma}_{ab}$ is typically computed through a series expansion in powers of

$\alpha_s(\mu_R)$, for instance [63]:

$$\hat{\sigma}_{ab}\left(Q;\mu_R,\mu_F\right)=\hat{\sigma}_{ab}^{(0)}(Q)+\frac{\alpha_s\left(\mu_R\right)}{4\pi}\hat{\sigma}_{ab}^{(1)}\left(Q;\mu_R,\mu_F\right)+\left(\frac{\alpha_s\left(\mu_R\right)}{4\pi}\right)^2\hat{\sigma}_{ab}^{(2)}+\cdots, \tag{8.2}$$

where Q generically denotes the physical scale of the process (for example, the invariant mass of a lepton pair in Drell–Yan processes, the Higgs boson mass, etc.). At fixed order, the dependence on μ_R and μ_F appears such that the full physical cross-section $d\sigma_{AB\to X}$ would be invariant under scale changes if all orders were included. However, at truncated order, $d\sigma$ shows residual dependence on the unphysical scales μ_R and μ_F.

The proposal of PMC is to minimize this scale ambiguity. Practically, applying PMC to the partonic cross-section $\hat{\sigma}_{ab}$ involves identifying within perturbative calculations those contributions in higher-order coefficients stemming from the theory's evolution (terms involving β_0, β_1, etc., usually associated with the presence of N_f). Once isolated, these terms can be systematically handled using the PMC method.

8.2 Challenges and Benefits of Applying the PMC in Hadronic Processes

Applying the PMC to factorizable hadronic processes entails significant benefits but also presents practical challenges due to their greater complexity compared to simpler observables such as those from e^+e^- collisions We qualitatively discuss these aspects below

Elimination of scale ambiguity and improvement of precision The main benefit of the PMC is the elimination of the arbitrary dependence on μ_R By optimally setting the scale in $\hat{\sigma}_{ab}$ the associated theoretical uncertainty is drastically reduced For example in Higgs production in pp collisions it has been shown that applying the PMC suppresses the dependence of the prediction on variations in μ_R leaving only a mild residual higher-order dependence and the uncertainty from μ_F [113]

PMC predictions tend to converge more rapidly with the perturbative order by avoiding large renormalon contributions and show better agreement with existing experimental data than conventional fixed-scale estimates This was observed in the case of the Higgs cross section reported by ATLAS where the PMC prediction agreed within uncertainties with the measurement while the standard calculation with conventional scale setting showed larger deviations Likewise in $t\bar{t}$ pair production the NNLO prediction adjusted with PMC was consistent with data from Tevatron and LHC largely resolving previous discrepancies such as the difference in the top forward-backward asymmetry [63] In summary applying the PMC leads to more stable and precise predictions independent of arbitrary choices and thus more sensitive to the actual underlying physics

The presence of multiple scales and orders can be a challenge particularly in hadronic processes which often involve multiple characteristic scales For example in the production of heavy objects one may encounter the object mass M such as Higgs or top the center-of-mass energy $\sqrt{s}$ of the collider momentum transfer scales Q associated with differential observables like the p_T of a boson In addition strict application of the PMC generally introduces a different scale for each perturbative order multi-scale PMC In higher-order calculations NLO NNLO this implies that different terms in $\hat{\sigma}_{ab}$ are evaluated with α_s at different values of μ_R While this physically reflects the different typical virtualities at each order it complicates practical implementation since the total hadronic cross section is an integration convolution over a wide kinematic range A recent strategy to simplify this is the single-scale version of the PMC PMC-s which determines a single effective $\mu_R^{\rm PMC}$ that averages the effect of multiple scales order

by order This approximation captures the advantages of PMC with less algebraic complexity and comparative studies have shown that PMC-s essentially reproduces the same numerical results as multi-scale PMC in both integrated and differential observables Nevertheless there remains some ambiguity regarding how to choose the PMC scale at the highest computed order Recent investigations indicate that the definition of the scale at the highest order for which there is no next order to fully determine the β terms can introduce residual freedom Indeed it has been observed that different reasonable choices of that final scale can impact the result at a level comparable to the scale uncertainty in the conventional method This problem inherent to working at truncated order suggests that even with PMC it is prudent to assign an error associated with unknown higher-order terms However it is important to highlight that this ambiguity is of a different nature than that of conventional μ_R choice here it is limited only to the highest order and would disappear if an additional order were known whereas in the traditional approach the ambiguity persists at all orders

The convolution with PDFs and fragmentation functions unlike observables in e^+e^- where α_s appears isolated in hadronic processes the total cross section results from convoluting $\hat{\sigma}_{ab}$ with PDFs and possibly fragmentation functions This implies that the relevant effective scale may vary within the integration For example partonic contributions with very small $x_{a,b}$ correspond to subprocesses with lower invariant energy and could prefer a lower μ_R than those with large x values near the kinematic threshold In principle multi-scale PMC could accommodate this continuous variation assigning to each x region an appropriate scale through local β terms However in practical calculations it is common to apply the PMC at the level of integrated coefficients for example setting $\mu_R^{\rm PMC}$ after integrating over x The choice of μ_F adds another layer in general the PMC does not necessarily fix μ_F which is usually chosen to be of the order of Q to minimize large collinear logarithms in $\hat{\sigma}_{ab}$ The dependence on μ_F remains even after applying PMC since it is tied to the separation between perturbative and nonperturbative physics PDFs In realistic predictions sensitivity to μ_F is still evaluated separately to estimate the uncertainty associated with factorization It is worth noting that as the perturbative order increases the dependence on μ_F tends to decrease since the associated logarithmic terms are compensated by the DGLAP evolution of the PDFs In summary the presence of convolution integrals means that while the PMC eliminates the μ_R ambiguity in $\hat{\sigma}_{ab}$ the final prediction $d\sigma$ still carries uncertainty from PDFs both experimental from global fits and theoretical from the choice of μ_F Even so by eliminating renormalization uncertainty the PMC allows us to better isolate these other sources of error and thus focus on improving for instance the determination of PDFs with precise data

In summary the expected benefits of applying PMC in hadronic processes include i reduced theoretical uncertainty from renormalization scale which enhances the capacity of QCD tests to discriminate subtle effects or new physics ii more ordered and better converging perturbative series due to the absorption of β terms into the coupling iii invariance under the renormalization scheme and iv consistency with Abelian QED limits and other theoretical principles since the PMC reproduces in QCD the physically correct scale choice one would obtain in $\beta = 0$ theories or in the Abelian limit $N_C \to 0$

Among the challenges are the technical implementation of the PMC in complex high-order calculations where identifying β terms is not trivial the systematic handling of multiple scales without introducing new ambiguities and the coexistence with the factorization structure PDFs FFs ensuring that the optimal μ_R treatment in the short-distance part does not compromise the interpretation of the long-distance part fortunately the universality of PDFs guarantees that any improvement in the short-distance part translates directly into more reliable predictions without modifying the PDFs themselves So far existing studies indicate that the PMC is viable in a variety of processes and yields results compatible with data

supporting its use as a tool to improve the precision of perturbative QCD

8.3 Hadronic Processes as Candidates for the Application of the PMC

Not all hadronic processes present the same level of complexity when applying the Principle of Maximum Conformality (PMC). Some provide a more natural environment for its implementation. Below, we discuss several cases of interest.

In the context of lepton-hadron collisions, such as Deep Inelastic Scattering (DIS) $ep \to eX$, factorization also applies—a parton distribution function (PDF) in the proton and perturbatively calculable coefficient functions for observables such as structure functions F_2, etc. The situation is analogous to the Drell–Yan process in that there is typically a single hard scale, Q^2 (the momentum transferred by the lepton), which serves as the reference for both μ_R and μ_F. Implementing the PMC in DIS would mean setting the optimal renormalization scale in the Wilson coefficients of the structure functions. This could improve the extraction of PDFs from DIS data by reducing theoretical uncertainties. Similarly, in semi-inclusive processes such as hadron production in DIS (SIDIS) or polarized/transverse Drell–Yan processes, the elimination of scale ambiguities would help isolate genuine hadronic structure effects from perturbative uncertainties—for instance, transversity distribution functions, Sivers and Boer–Mulders effects.

In conclusion, the application of the PMC in hadronic processes involving perturbative factorization is both viable and promising. Processes such as Drell–Yan and heavy boson production provide clean scenarios for implementing conformal scale setting, while more complex cases (Higgs, top quark, semi-inclusive DIS) demonstrate the PMC's capacity to handle multiple scales and channels. Existing qualitative and quantitative studies suggest that the PMC can significantly improve the reliability of perturbative QCD predictions at hadron colliders [113]. Although technical challenges remain, particularly regarding scale setting at truncated orders and the treatment of μ_F, the PMC provides a theoretically solid framework to reduce longstanding systematic uncertainties in QCD, consistent with renormalization group (RG) invariance and conformality principles. When properly integrated into precision calculations, this approach will sharpen theory–experiment comparisons in particle physics, enhancing sensitivity to subtle effects and potentially paving the way for new discoveries with current and future collider data. Applications to Higgs and top-quark processes at the LHC have shown more stable predictions in closer agreement with experimental data. On the other hand, independent analyses emphasize the importance of carefully assigning PMC scales at finite orders to avoid introducing new uncertainties [114].

This chapter aims to provide guidance on the proposal of applying the PMC to factorized hadronic processes as a means to enhance the precision of perturbative QCD tests.

Chapter 9

Conclusions

This thesis addressed the fundamental problem of the ambiguity in the choice of the renormalization scale and renormalization scheme in perturbative QCD (pQCD). These ambiguities constitute a major source of theoretical uncertainty in high-energy process predictions. As a solution, the Principle of Maximum Conformality (PMC) was adopted and implemented. This method systematically absorbs the non-conformal terms into the strong coupling, thereby eliminating the artificial dependence on the renormalization scale in the perturbative series. In this way, the PMC ensures that the resulting predictions are renormalization group invariant and free from the arbitrary uncertainties associated with conventional scale setting.

Throughout this investigation, the PMC was successfully applied to several key contexts in particle physics: the relation between heavy quark masses in the pole (on-shell) and $\overline{\text{MS}}$ schemes, the electroweak parameter ρ of the Standard Model, and the hadronic decay width of the W boson. These case studies empirically demonstrated the advantages of the PMC over the conventional approach and highlighted its relevance in precision observables.

In the case of heavy quark masses, a consistent and high-precision connection between the pole mass and the $\overline{\text{MS}}$ mass was established for each quark, independently of the initial renormalization scale employed. Under the conventional approach, mass conversion required assigning an arbitrary scale range and assuming a systematic uncertainty; in contrast, the PMC removed this arbitrariness by determining an optimal scale order by order from first principles. In particular, it was shown that the multi-scale PMC assigns different effective scales at each perturbative order, significantly improving the convergence of the perturbative series. Furthermore, it was found that in scenarios with slowly converging series, such as for the charm quark, it is advantageous to employ a single-scale version of the PMC, which provides additional stability in the prediction.

Thanks to these optimizations, the resulting mass relations are more stable and precise than ever. For instance, the PMC-based calculation yielded a top quark pole mass of approximately 172.3 ± 0.6 GeV, with a corresponding $\overline{\text{MS}}$ mass of 162.6 ± 0.7 GeV. These values are consistent with experimental determinations but now obtained without scale ambiguity. Similarly, for the bottom quark, a pole mass of approximately 4.86 GeV was obtained, with a tiny theoretical uncertainty of about 0.02 GeV. These results represent a notable improvement in the achievable precision within the Standard Model: by eliminating scale dependence, the quark masses extracted using the PMC can be reliably used in threshold phenomena, such as heavy quark pair production near threshold, where more accurate mass values directly

impact the predicted cross sections.

This application of the PMC to heavy quark masses constitutes an original contribution of this thesis, providing a practical solution to the long-standing issue of mass definitions and their associated uncertainties in perturbative QCD.

Concerning the electroweak parameter ρ, which is related to the ratio of charged to neutral weak interactions (and sensitive to top quark loop corrections), it also benefited from the optimal scale setting provided by the PMC. Using the previously refined value of the top quark mass, the PMC was applied to fix the scale of the QCD corrections in the prediction of ρ. As a result, the theoretical uncertainty in the determination of $\delta\rho$ was reduced, and the dependence on the scale choice virtually disappeared. Numerically, the value obtained for $\delta\rho$ using the PMC was found to lie within the range $(8.2 \pm 0.1) \times 10^{-3}$, compared to $\sim 8.3 \times 10^{-3}$ from the conventional method with a larger uncertainty. That is, both approaches agree in the central value, but the PMC provides a more stable and precise estimate of this electroweak parameter.

This result reinforces the internal consistency of the Standard Model predictions: a more accurate determination of ρ improves precision tests, such as the prediction of the W boson mass or the effective weak mixing angle, and imposes tighter bounds on possible new physics effects that could manifest through subtle deviations in this parameter. The application of the PMC in the computation of ρ also represents a novel contribution of this thesis, demonstrating its usefulness beyond purely hadronic observables and extending it to high-impact electroweak quantities.

The hadronic decay width of the W boson constitutes another central contribution of this work. This observable, measured with increasing precision at collider experiments, is critical both for the determination of the strong coupling constant α_s from W decays and for tests of CKM matrix unitarity. In this thesis, the full computation of the hadronic width of the W boson up to order $\mathcal{O}(\alpha_s^4)$ ($\mathrm{N^3LO}$ in QCD) was carried out, implementing the PMC to set the optimal renormalization scale at each order. The most notable result is that the final prediction for the width exhibits no residual renormalization scale dependence within the truncated order, and an extremely reduced theoretical uncertainty.

Using the single-scale PMCs approach, an effective scale of approximately $0.69\, M_W$ was found, which yields a more balanced perturbative series with accelerated convergence. The obtained hadronic width is $\Gamma_W^{\mathrm{had}} \simeq 1405.6$ MeV (using current input parameters), with an estimated uncertainty of only ± 0.2 MeV. This level of precision contrasts sharply with the several MeV uncertainty affecting the conventional prediction under typical scale variation by a factor of 2. In other words, the PMC reduces the theoretical uncertainty by more than an order of magnitude for this observable, placing the prediction's precision at the level of current experimental uncertainties, or even below.

Thanks to this, it becomes possible to exploit the better-determined theoretical value to extract fundamental parameters. For instance, keeping the improved theoretical prediction of Γ_W^{had} fixed, an indirect extraction of the CKM matrix element $|V_{cs}|$ was performed. Using the most recent experimental data, the value of $|V_{cs}|$ obtained using the conventional method was approximately 0.966, while the PMC-based prediction yielded $|V_{cs}| \simeq 0.967$ with an uncertainty of just 0.03%. Both results are mutually consistent and in agreement with the PDG average, but the drastic reduction in uncertainty when using the PMC highlights the advantage of this approach: it allows for more stringent tests of CKM matrix unitarity and a more precise determination of α_s from W decays.

In summary, the theoretical improvement achieved in the hadronic W boson decay us-

ing the PMC represents an original and highly relevant contribution, as it directly impacts the interpretation of experimental results and the extraction of fundamental parameters in particle physics.

Finally, beyond the specific computations discussed, this thesis explored the feasibility of applying the PMC to more general factorizable hadronic processes, such as those relevant at hadron colliders. In a typical hadronic process (e.g., Drell–Yan production, heavy boson production, jets, Higgs production, etc.), the cross section is factorized into PDFs depending on a factorization scale μ_F and a perturbative partonic cross section that depends on the renormalization scale μ_R. The choice of both scales usually introduces significant uncertainty in the predictions.

Through a systematic discussion, it is argued that the PMC can be viably extended to optimally fix μ_R in the partonic sector even in the presence of factorization, thereby reducing the total theoretical ambiguity. The potential benefits of this application were highlighted: in relatively clean processes such as Drell–Yan or heavy boson production, the PMC would ensure that the perturbative calculation is conformal at each order, improving the stability of predictions under scale variation. In more complex cases with multiple intrinsic scales, such as Higgs or top production, or semi-inclusive DIS processes, the PMC has shown the capability to handle order-by-order dynamic scales and different production channels, albeit with additional technical challenges.

In particular, challenges were identified such as the treatment of the factorization scale (μ_F)—which remains fixed in this work—and the rigorous assignment of PMC scales to truncated orders without introducing new dependencies. Nonetheless, the evidence gathered (both from our analyses and from previous studies in the literature) suggests that the application of the PMC to collider processes is feasible and promising. In fact, recent studies indicate that applying the PMC leads to predictions for processes like Higgs or top production at the LHC that exhibit reduced dependence on renormalization parameters and improved agreement with experimental data, while also enhancing sensitivity to subtle effects.

In conclusion, this thesis not only presents concrete calculations where the PMC improves theoretical precision, but also provides guidelines and motivation for its broader adoption in hadronic phenomenology. Overall, the findings of this work underscore the relevance of the PMC as a solution to the scale-setting problem in perturbative QCD, consolidating its foundation in conformality principles and RG invariance. By suppressing unnecessary systematic uncertainties, the method strengthens the predictive power of the Standard Model, enabling more precise theory-experiment comparisons that help to better identify possible deviations attributable to new physics.

The results obtained—from heavy quark masses to W boson decays—constitute original contributions by the author to the field of high-energy particle physics, all aimed at improving the precision and reliability of theoretical predictions. These results have been documented in peer-reviewed publications and conference contributions, reflecting the contribution of this thesis to scientific knowledge.

9.1 Future Perspectives

This work opens several promising directions for future research. A natural first step is to apply the PMC formalism to an even broader range of hadronic processes at colliders, expanding upon those outlined in Chapter 8. For example, Drell–Yan lepton pair production, top quark pair production, heavy boson (W, Z) and Higgs production at the LHC, as well as

semi-inclusive DIS processes, are all prime candidates to benefit from conformal scale setting. Extending the use of the PMC to these processes would enable a generalized reduction of perturbative uncertainties in high-precision phenomenological analyses.

In parallel, it will be important to develop strategies to integrate the optimization of the factorization scale (μ_F) together with the renormalization scale, thereby addressing all sources of theoretical ambiguity in PDF-factorized calculations in a holistic manner. Another interesting direction is to investigate the behavior of the PMC when incorporating even higher perturbative orders or resummed series, examining how conformal stability evolves when approaching the complete theory limit.

From a phenomenological standpoint, integrating the PMC into global analysis tools in particle physics is a medium-term goal. This would involve implementing the PMC in observable calculation codes and global determinations of parameters such as α_s and PDFs. Such integration could significantly enhance the theoretical precision relied upon by experimental collaborations, maximizing discovery potential by reducing theoretical "noise."

Additionally, exploring the applicability of the PMC in theories beyond the Standard Model would be valuable for assessing whether the observed benefits persist in other frameworks. In short, the techniques and approaches developed in this thesis pave a promising path toward more reliable and accurate theoretical predictions in high-energy physics. The continuation and expansion of this research line will improve the interpretation of data from current and future experiments, enhancing sensitivity to potential new physics signals.

Thus, the legacy of this work lies not only in the specific results obtained, but also in having consolidated the PMC as a potential standard tool for the next generation of precision calculations in particle physics. This methodological progress will be essential to meet the challenges posed by the high-luminosity era and future high-energy collisions, ensuring that our theoretical predictions match the increasing experimental accuracy.

Appendix A

$SU(N)$ Group

As a gauge group, the unimodular unitary group $SU(N)$ is typically used. This group has dimension N^2-1 (the number of generators), and its fundamental representation acts on a complex space of dimension N. The group operators are unitary, satisfying $\omega^\dagger\omega = 1$, and unimodular, meaning that the determinant of the operator is equal to one. For infinitesimal transformations, one has:

$$1 = \det\omega = e^{\ln\det\omega} = e^{\mathrm{tr}\ln\omega} = e^{\mathrm{tr}\ln(1-i\Theta^a T_a)} = e^{-i\Theta^a \mathrm{tr} T_a}, \tag{A.1}$$

which implies $\mathrm{tr}(T_a) = 0$, i.e., the generators must be traceless matrices. In particular, there are $N-1$ diagonal traceless matrices.

In the case $N = 2$, i.e., for the group $SU(2)$, the generators are the Pauli matrices σ_i $(i = 1, 2, 3)$, whose standard representation is given by:

$$\sigma_1 = \begin{pmatrix} 0 & 1 \\ 1 & 0 \end{pmatrix}, \quad \sigma_2 = \begin{pmatrix} 0 & -i \\ i & 0 \end{pmatrix}, \quad \sigma_3 = \begin{pmatrix} 1 & 0 \\ 0 & -1 \end{pmatrix}. \tag{A.2}$$

The operators $T_a = \sigma_a/2$ satisfy the fundamental identity:

$$\sigma_a\sigma_b = i\epsilon_{abc}\sigma_c + \mathbb{I}_{2\times2}\delta_{ab}, \tag{A.3}$$

and thus form the Lie algebra of the group $SU(2)$:

$$[T_a, T_b] = i\epsilon_{abc}T_c. \tag{A.4}$$

The commutation relations for the generators of the $SU(2)$ group coincide with those of the generators of the $O(3)$ algebra. The group $SU(2)$ thus provides a double-valued representation of the three-dimensional rotation group.

In the case $N = 3$, we obtain the group $SU(3)$. Its generators $T_a = \lambda_a/2$ $(a = 1, \ldots, 8)$

are related to the Gell-Mann matrices, which are given by:

$$\lambda_1 = \begin{pmatrix} 0 & 1 & 0 \\ 1 & 0 & 0 \\ 0 & 0 & 0 \end{pmatrix}, \quad \lambda_2 = \begin{pmatrix} 0 & -i & 0 \\ i & 0 & 0 \\ 0 & 0 & 0 \end{pmatrix}, \quad \lambda_3 = \begin{pmatrix} 1 & 0 & 0 \\ 0 & -1 & 0 \\ 0 & 0 & 0 \end{pmatrix},$$
$$\lambda_4 = \begin{pmatrix} 0 & 0 & 1 \\ 0 & 0 & 0 \\ 1 & 0 & 0 \end{pmatrix}, \quad \lambda_5 = \begin{pmatrix} 0 & 0 & -i \\ 0 & 0 & 0 \\ i & 0 & 0 \end{pmatrix}, \quad \lambda_6 = \begin{pmatrix} 0 & 0 & 0 \\ 0 & 0 & 1 \\ 0 & 1 & 0 \end{pmatrix}, \tag{A.5}$$
$$\lambda_7 = \begin{pmatrix} 0 & 0 & 0 \\ 0 & 0 & -i \\ 0 & i & 0 \end{pmatrix}, \quad \lambda_8 = \frac{1}{\sqrt{3}} \begin{pmatrix} 1 & 0 & 0 \\ 0 & 1 & 0 \\ 0 & 0 & -2 \end{pmatrix}.$$

The group $SU(3)$ forms a Lie algebra with the following commutation relations:

$$[T_a, T_b] = i f_{abc} T_c, \tag{A.6}$$

where f_{abc} are the structure constants of the $SU(3)$ group.

Appendix B

PMC Coefficients Type I

Following a systematic step-by-step approach, we can determine the coefficients appearing in the PMC-I procedure. The conformal coefficients are given by:

$$d'_{2,0} = d_{2,0} + \frac{33}{2} d_{2,1}, \tag{B.1}$$

$$d''_{3,0} = d'_{3,0} + \frac{33}{2} d'_{3,1}, \tag{B.2}$$

$$d'''_{4,0} = d''_{4,0} + \frac{33}{2} d''_{4,1}. \tag{B.3}$$

On the other hand, the non-conformal coefficients are:

$$d'_{3,0} = \frac{1}{4\ell}\left[1089\,(\ell+1)\,d_{2,1}^2 + 153\ell d_{2,1} + 66\,(\ell+1)\,d_{2,0}d_{2,1} + (4d_{3,0} - 1089 d_{3,2})\,\ell\right] \tag{B.4}$$

$$d'_{3,1} = -\frac{1}{4\ell}\left[66(\ell+1)d_{2,1}^2 + 19\ell d_{2,1} + 4(\ell+1)d_{2,0}d_{2,1} - 4\ell\,(d_{3,1} + 33 d_{3,2})\right] \tag{B.5}$$

$$\begin{aligned} d'_{4,0} =& \frac{1}{64 d_{2,1}\ell^2}\Bigg[-40392 d_{4,3}\ell^3 + 143748 d_{2,1}^4\left(3 + 5\ell + 2\ell^2\right) \\ &+ 8 d_{2,1}\ell^2\,(8 d_{4,0} + 35937 d_{4,3} + 5049 d_{3,2}\ell) - 13464 d_{2,1}^3\ell\left(\ell^2 - 3\ell - 7\right) \\ &+ 72 d_{2,0}d_{2,1}(1+\ell)\left(34 d_{2,1}\ell - 242 d_{3,2}\ell + 121 d_{2,1}^2(3+2\ell)\right) \\ &+ 3 d_{2,1}^2\ell\left(2857\ell + 352 d_{3,0}(2+\ell) - 95832 d_{3,2}(3+2\ell)\right)\Bigg] \end{aligned} \tag{B.6}$$

$$
\begin{aligned}
d'_{4,1} =& \frac{1}{192 d_{2,1} \ell^2} \Bigg[22392 d_{4,3} \ell^3 - 52272 d_{2,1}^4 \left(3 + 5\ell + 2\ell^2\right) \\
& - 24 d_{2,1} \ell^2 \left(-8 d_{4,1} + 6534 d_{4,3} + 933 d_{3,2} \ell\right) \\
& - 48 d_{2,0} d_{2,1} (1 + \ell) \left(19 d_{2,1} \ell - 132 d_{3,2} \ell + 66 d_{2,1}^2 (3 + 2\ell) \right) \\
& + d_{2,1}^2 \ell \Big(- 5033 \ell - 192 d_{3,0} (2 + \ell) + 3168 d_{3,1} (2 + \ell) + 52272 d_{3,2} (8 + 5\ell) \Big) \\
& + 24 d_{2,1}^3 \ell \Big(- 1871 + \ell \left(-627 + 311 \ell\right) \Big) \Bigg]
\end{aligned}
\tag{B.7}
$$

Appendix C

Complete and PMC QCD correction coefficients at the four-loop level of the δP

Here, we first include the perturbative coefficients of the observable δP introduced in Sec. 6.

$$
\begin{aligned}
d_1 &= -2.14 C_F, && \text{(C.1)}\\
d_2 &= -4.42 C_F + 7.23 C_F^2 + C_A C_F \left(-6.29 - 31.5 \ln \frac{\mu^2}{M_t^2}\right) && \text{(C.2)}\\
&\quad + N_f C_F \left(21.4 + 0.36 \ln \frac{\mu^2}{M_t^2}\right),\\
d_3 &= -0.785 C_F^3 + C_F^2 T \left(8.30 + N_f \left(-8.74 - 1.62 \ln \frac{\mu^2}{M_t^2}\right)\right) && \text{(C.3)}\\
&\quad + C_A C_F^2 \left(17.2 + 5.92 \ln \frac{\mu^2}{M_t^2}\right) + C_A^2 C_F \left(-31.0 - \ln \frac{\mu^2}{M_t^2} - 1.80 \ln^2 \frac{\mu^2}{M_t^2}\right)\\
&\quad + C_F T^2 \left(-3.86 + N_f \left(7.61 - 1.69 \ln \frac{\mu^2}{M_t^2}\right)\right.\\
&\quad \left. - 6.4 \times 10^{-10} \ln \frac{\mu^2}{M_t^2} + 10^{-10} \ln^2 \frac{\mu^2}{M_t^2} + N_f^2 \left(-3.45 + 1.79 \ln \frac{\mu^2}{M_t^2} - 0.24 \ln^2 \frac{\mu^2}{M_t^2}\right)\right.\\
&\quad \left. + C_A C_F T \left(-25.4 - 4.64 \ln \frac{\mu^2}{M_t^2} + N_f \left(24.8 + \ln \frac{\mu^2}{M_t^2} + 1.31 \ln^2 \frac{\mu^2}{M_t^2}\right)\right)\right).
\end{aligned}
$$

The PMC conformal coefficients $r_i^{\rm conf}$ for the pertubative serie of δP up to four-loop level, is given by

$$r_1^{\rm conf} = -0.68 C_F, \tag{C.4}$$

$$r_2^{\rm conf} = -0.45 C_F + 0.73 C_F^2 - 0.64 C_A C_F + \frac{5.96 C_A C_F}{T}, \tag{C.5}$$

$$r_3^{\rm conf} = \frac{C_F}{T}\Bigg(C_A^2(-29.6T - 3.6) + C_A C_F(16.4T - 5.69) - 24.7 C_A T^2 + T\left(-0.78 C_F^2 + 8.30 C_F T - 3.86 T^2\right)\Bigg), \tag{C.6}$$

where $C_F = 4/3$, $C_A = 3$, and $T = 1/2$ are the known $SU(3)$ color factors.

Appendix D

Reduced Perturbative Coefficients for the Hadronic Decay of the W Boson

In this appendix, we present the reduced coefficients $\hat{r}_{i,j}$ for the perturbative series of the hadronic decay of the W boson, discussed in Chapter 7. These coefficients can be obtained from the two-point correlator related to the Adler function, as computed in [14, 55, 56, 59, 60, 115–117], and are expressed as:

$$\hat{r}_{1,0} = 3C_F, \tag{D.1}$$

$$\hat{r}_{2,0} = \frac{730}{3} - \frac{121C_A}{3T} - 176\zeta_3 + \frac{88C_A}{3T}\zeta_3, \tag{D.2}$$

$$\hat{r}_{2,1} = \frac{11}{T} - \frac{8}{T}\zeta_3, \tag{D.3}$$

$$\begin{aligned}\hat{r}_{3,0} = {} & \frac{174058}{9} - 17648\zeta_3 + \frac{8800}{3}\zeta_5 - \frac{1}{T}\left(\frac{172634C_A}{27} - 77C_A^2 - 121C_AC_F\right. \\ & \left. -\frac{46112C_A}{9}\zeta_3 + 56C_A^2\zeta_3 + 88C_AC_F\zeta_3 + 4400C_A\zeta_5\right) + \frac{1}{T^2}\left(\frac{36542C_A^2}{81}\right. \\ & \left. +\frac{9196C_A^2}{27}\zeta_3\right) - \pi^2\left(\frac{484}{3} - \frac{484C_A}{9T} + \frac{121C_A^2}{27T^2}\right),\end{aligned} \tag{D.4}$$

$$\hat{r}_{3,1} = \frac{1}{T}\left(\frac{7847}{9} - \frac{55C_A}{2} - \frac{33C_F}{2} - \frac{2096}{3}\zeta_3 + 20C_A\zeta_3 + 12C_F\zeta_3 + \frac{200}{3}\zeta_5\right), \tag{D.5}$$

$$\begin{aligned}\hat{r}_{3,2} = {} & \frac{302}{9T^2} - \frac{76}{3T^2}\zeta_3 - \pi^2\frac{1}{3T^2} - \frac{1}{T^2}\left(\frac{3322C_A}{27} - \frac{836C_A}{9}\zeta_3\right) \\ & -\pi^2\left(\frac{22}{3T} - \frac{11C_A}{9T^2}\right),\end{aligned} \tag{D.6}$$

$$\hat{r}_{4,0} = \frac{144939499}{81} - \frac{45547960}{27}\zeta_3 + 174240\zeta_3^2 + \frac{527560}{9}\zeta_5 - \frac{117040}{3}\zeta_7 \tag{D.7}$$
$$-\frac{1}{T}\left(\frac{143484077C_A}{162} - \frac{109858C_A^2}{9} - \frac{3157C_A^3}{24} - \frac{172634C_AC_F}{9} + \frac{1661C_A^2C_F}{3}\right.$$
$$+\frac{847C_AC_F^2}{2} + \frac{45547960}{27}\zeta_3 - \frac{2148080C_A}{3}\zeta_3 + \frac{29344C_A^2}{3}\zeta_3 + \frac{287C_A^3}{3}$$
$$+\frac{46112C_AC_F}{3}\zeta_3 - \frac{1208C_A^2C_F}{3}\zeta_3 - 308C_AC_F^2\zeta_3 + 38720C_A\zeta_3^2 - \frac{1305700C_A}{27}\zeta_5$$
$$\left.-\frac{2800C_A^2}{3}\zeta_5 - \frac{4400C_AC_F}{3}\zeta_5 - \frac{58520C_A}{9}\zeta_7\right) + \frac{1}{T^2}\left(\frac{126491101C_A^2}{772}\right.$$
$$-\frac{46508C_A^3}{27} - \frac{73084C_A^2C_F}{27} - \frac{4919255C_A^2}{54}\zeta_3 + \frac{11704C_A^3}{9}\zeta_3 + \frac{18392C_A^2C_F}{9}\zeta_3$$
$$\left.+\frac{4840C_A^2}{3}\zeta_3^2 - \frac{503360C_A^2}{27}\zeta_5\right) - \frac{1}{T^3}\left(\frac{8160361C_A^3}{1458} - \frac{270193C_A^3}{81}\zeta_3 - \frac{13310C_A^3}{9}\zeta_5\right)$$
$$+\pi^2\left(\frac{99550}{3} + \frac{49786C_A}{3T} - \frac{308C_A^2}{3T} - \frac{484C_AC_F}{3T} - \frac{71753C_A^2}{27T^2} + \frac{154C_A^3}{9T^2}\right.$$
$$\left.+\frac{242C_A^2C_F}{9T^2} + \frac{14641C_A^3}{108T^3} + 21296\zeta_3 - \frac{10648C_A}{T}\zeta_3 + \frac{5324C_A^2}{3T^2}\zeta_3 - \frac{2662C_A^3}{27T^3}\zeta_3\right),$$

$$\hat{r}_{4,1} = \frac{1}{T}\left(\frac{13044007}{162} - \frac{78470C_A}{27} + \frac{649C_A^2}{18} - \frac{15694C_F}{9} + \frac{77C_F^2}{2} + \frac{4367C_AC_F}{36}\right. \tag{D.8}$$
$$-\frac{195280\zeta_3}{3} + 3520\zeta_3^2 + \frac{20960C_A\zeta_3}{9} - \frac{236}{9}C_A^2\zeta_3 - 28C_F^2\zeta_3 + \frac{4192C_F\zeta_3}{3}$$
$$\left.-\frac{794}{9}C_AC_F\zeta_3 - \frac{118700\zeta_5}{27} - \frac{2000}{9}C_A\zeta_5 - \frac{400C_F\zeta_5}{3} - \frac{5320\zeta_7}{9}\right)$$
$$+\frac{1}{T^2}\left(-\frac{11499191C_A}{486} + \frac{49075C_A^2}{81} + \frac{1661C_AC_F}{3} + \frac{447205C_A\zeta_3}{27} - \frac{12350}{27}C_A^2\zeta_3\right.$$
$$\left.-418C_AC_F\zeta_3 - \frac{880}{3}C_A\zeta_3^2 + \frac{91520C_A\zeta_5}{27}\right) + \frac{1}{T^3}\left(\frac{741851C_A^2}{486} - \frac{24563C_A^2\zeta_3}{27}\right.$$
$$\left.-\frac{1210C_A^2\zeta_5}{3}\right) + \pi^2\left(-\frac{4526}{3T} + \frac{220C_A}{9T} + \frac{44C_F}{3T} + \frac{968\zeta_3}{T} + \frac{13046C_A}{27T^2}\right.$$
$$\left.-\frac{325C_A^2}{54T^2} - \frac{968C_A\zeta_3}{3T^2} - \frac{11C_AC_F}{2T^2} + \frac{242\zeta_3C_A^2}{9T^3} - \frac{1331C_A^2}{36T^3}\right),$$

$$\hat{r}_{4,2} = -\frac{1}{T}\left(\frac{869C_A}{72}\frac{121C_F}{12} - \frac{79C_A\zeta_3}{9} - \frac{22C_F\zeta_3}{3}\right) + \frac{1}{T^2}\left(+\frac{1045381}{324}\right. \tag{D.9}$$
$$-\frac{3775C_A}{27} - \frac{755C_F}{9} + 40\zeta_3^2 + \frac{950C_A\zeta_3}{9} + \frac{190C_F\zeta_3}{3} - \frac{40655\zeta_3}{18}$$
$$\left.-\frac{4160\zeta_5}{9}\right) + \frac{1}{T^3}\left(\frac{2233\zeta_3C_A}{9} + 110\zeta_5C_A - \frac{67441C_A}{162}\right) - \pi^2\left(\frac{593}{9T^2}\right.$$
$$\left.-\frac{25C_A}{18T^2} - \frac{5C_F}{6T^2} - \frac{44\zeta_3}{T^2} - \frac{121C_A}{12T^3} + \frac{22C_A\zeta_3}{3T^3}\right),$$
$$\hat{r}_{4,3} = \frac{1}{T^3}\left(\frac{6131}{54} - \frac{203\zeta_3}{3} - 30\zeta_5\right) - \pi^2\left(\frac{11}{4T^3} - \frac{2\zeta_3}{T^3}\right). \tag{D.10}$$

The factors proportional to π^2 originate from the analytic continuation in the Euclidean region, as noted in [118]. The factors T, C_A, and C_F correspond to the color factors of the $SU(3)_C$ gauge group. The symbols ζ_i denote the Riemann zeta function.

References

[1] **Particle Data Group** Collaboration, R. L. Workman *et al.*, "Review of Particle Physics," *PTEP* **2022** (2022) 083C01.

[2] T. Muta, *Foundations of Quantum Chromodynamics: An Introduction to Perturbative Methods in Gauge Theories, (3rd ed.)*, vol. 78 of *World scientific Lecture Notes in Physics*. World Scientific, Hackensack, N.J., 3rd ed., 2010.

[3] Y. V. Kovchegov and E. Levin, *Quantum chromodynamics at high energy*. Cambridge University Press, 2013.

[4] B. L. Ioffe, V. S. Fadin, and L. N. Lipatov, *Quantum chromodynamics: Perturbative and nonperturbative aspects*, vol. 30. Cambridge University Press, 2010.

[5] M. E. Peskin, *An introduction to quantum field theory*. CRC press, 2018.

[6] N. N. Bogoliubov, D. V. Shirkov, and E. M. Henley, "Introduction to the theory of quantized fields," *Physics Today* **13** no. 7, (1960) 40–42.

[7] L. D. Faddeev, *Gauge fields: an introduction to quantum theory*. CRC Press, 2018.

[8] J. D. Bjorken and S. D. Drell, "Relativistic quantum fields,".

[9] M. Gell-Mann, "A Schematic Model of Baryons and Mesons," *Phys. Lett.* **8** (1964) 214–215.

[10] G. Zweig, *An SU(3) model for strong interaction symmetry and its breaking. Version 2*, pp. 22–101. 2, 1964.

[11] M. Y. Han and Y. Nambu, "Three Triplet Model with Double SU(3) Symmetry," *Phys. Rev.* **139** (1965) B1006–B1010.

[12] Y. Nambu, "Systematics of hadrons in subnuclear physics," tech. rep., Univ. of Chicago, IL (United States), 1966.

[13] S. L. Adler and W. A. Bardeen, "Absence of higher order corrections in the anomalous axial vector divergence equation," *Phys. Rev.* **182** (1969) 1517–1536.

[14] T. Appelquist and H. Georgi, "e+ e- annihilation in gauge theories of strong interactions," *Phys. Rev. D* **8** (1973) 4000–4002.

[15] A. Zee, "Electron positron annihilation in stagnant field theories," *Phys. Rev. D* **8** (1973) 4038–4041.

[16] M. Gell-Mann, "Symmetries of baryons and mesons," *Phys. Rev.* **125** (1962) 1067–1084.

[17] Y. Ne'eman, "Derivation of strong interactions from a gauge invariance," *Nucl. Phys.* **26** (1961) 222–229.

[18] D. H. Coward *et al.*, "ELECTRON - PROTON ELASTIC SCATTERING AT HIGH MOMENTUM TRANSFERS," *Phys. Rev. Lett.* **20** (1968) 292–295.

[19] E. D. Bloom *et al.*, "High-Energy Inelastic e p Scattering at 6-Degrees and 10-Degrees," *Phys. Rev. Lett.* **23** (1969) 930–934.

[20] M. Breidenbach, J. I. Friedman, H. W. Kendall, E. D. Bloom, D. H. Coward, H. C. DeStaebler, J. Drees, L. W. Mo, and R. E. Taylor, "Observed behavior of highly inelastic electron-proton scattering," *Phys. Rev. Lett.* **23** (1969) 935–939.

[21] J. D. Bjorken, "Asymptotic Sum Rules at Infinite Momentum," *Phys. Rev.* **179** (1969) 1547–1553.

[22] *Proceedings, Colloquium on Renormalization of Yang-Mills Fields, Marseille, June 19-23, 1972*. 1972.

[23] D. J. Gross and F. Wilczek, "Ultraviolet Behavior of Nonabelian Gauge Theories," *Phys. Rev. Lett.* **30** (1973) 1343–1346.

[24] H. D. Politzer, "Reliable Perturbative Results for Strong Interactions?," *Phys. Rev. Lett.* **30** (1973) 1346–1349.

[25] S. R. Coleman and D. J. Gross, "Price of asymptotic freedom," *Phys. Rev. Lett.* **31** (1973) 851–854.

[26] C. G. Bollini and J. J. Giambiagi, "Dimensional renormalization: The number of dimensions as a regularizing parameter," *Nuovo Cim. B* **12** (1972) 20–26.

[27] G. 't Hooft and M. J. G. Veltman, "Regularization and renormalization of gauge fields," *Nucl. Phys. B* **44** (1972) 189–213.

[28] W. E. Caswell, "Asymptotic Behavior of Nonabelian Gauge Theories to Two Loop Order," *Phys. Rev. Lett.* **33** (1974) 244.

[29] D. R. T. Jones, "Two Loop Diagrams in Yang-Mills Theory," *Nucl. Phys. B* **75** (1974) 531.

[30] D. R. T. Jones, "Asymptotic Behavior of Supersymmetric Yang-Mills Theories in the Two Loop Approximation," *Nucl. Phys. B* **87** (1975) 127.

[31] E. Egorian and O. V. Tarasov, "Two Loop Renormalization of the QCD in an Arbitrary Gauge," *Teor. Mat. Fiz.* **41** (1979) 26–32.

[32] W. Celmaster and R. J. Gonsalves, "The Renormalization Prescription Dependence of the QCD Coupling Constant," *Phys. Rev. D* **20** (1979) 1420.

[33] W. Celmaster and R. J. Gonsalves, "QCD Perturbation Expansions in a Coupling Constant Renormalized by Momentum Space Subtraction," *Phys. Rev. Lett.* **42** (1979) 1435.

[34] R. Barbieri, L. Caneschi, G. Curci, and E. d'Emilio, "Scaling Violations and Perturbative Quantum Chromodynamics," *Phys. Lett. B* **81** (1979) 207–210.

[35] P. Boucaud, F. de Soto, J. P. Leroy, A. Le Yaouanc, J. Micheli, H. Moutarde, O. Pene, and J. Rodriguez-Quintero, "Artefacts and < A**2 > power corrections: Revisiting the MOM Z psi (p**2) and Z(V)," *Phys. Rev. D* **74** (2006) 034505, arXiv:hep-lat/0504017.

[36] P. Boucaud, F. De Soto, J. P. Leroy, A. Le Yaouanc, J. Micheli, O. Pene, and J. Rodriguez-Quintero, "Ghost-gluon running coupling, power corrections and the determination of Lambda(MS-bar)," *Phys. Rev. D* **79** (2009) 014508, arXiv:0811.2059 [hep-ph].

[37] T. van Ritbergen, J. A. M. Vermaseren, and S. A. Larin, "The Four loop beta function in quantum chromodynamics," *Phys. Lett. B* **400** (1997) 379–384, arXiv:hep-ph/9701390.

[38] M. Czakon, "The Four-loop QCD beta-function and anomalous dimensions," *Nucl. Phys. B* **710** (2005) 485–498, arXiv:hep-ph/0411261.

[39] P. A. Baikov, K. G. Chetyrkin, and J. H. Kühn, "Five-Loop Running of the QCD coupling constant," *Phys. Rev. Lett.* **118** no. 8, (2017) 082002, arXiv:1606.08659 [hep-ph].

[40] J. A. M. Vermaseren, S. A. Larin, and T. van Ritbergen, "The four loop quark mass anomalous dimension and the invariant quark mass," *Phys. Lett. B* **405** (1997) 327–333, arXiv:hep-ph/9703284.

[41] G. Grunberg, "Renormalization Group Improved Perturbative QCD," *Phys. Lett. B* **95** (1980) 70. [Erratum: Phys.Lett.B 110, 501 (1982)].

[42] G. Grunberg, "Renormalization Scheme Independent QCD and QED: The Method of Effective Charges," *Phys. Rev. D* **29** (1984) 2315–2338.

[43] G. Grunberg, "On Some Ambiguities in the Method of Effective Charges," *Phys. Rev. D* **40** (1989) 680.

[44] P. M. Stevenson, "Resolution of the Renormalization Scheme Ambiguity in Perturbative QCD," *Phys. Lett. B* **100** (1981) 61–64.

[45] P. M. Stevenson, "Optimized perturbation theory," *Phys. Rev. D* **23** (1981) 2916.

[46] P. Stevenson, "Sense and Nonsense in the Renormalization Scheme Dependence Problem," *Nucl. Phys. B* **203** (1982) 472–492.

[47] P. M. Stevenson, "Optimization and the Ultimate Convergence of QCD Perturbation Theory," *Nucl. Phys. B* **231** (1984) 65–90.

[48] S. J. Brodsky, G. P. Lepage, and P. B. Mackenzie, "On the Elimination of Scale Ambiguities in Perturbative Quantum Chromodynamics," *Phys. Rev. D* **28** (1983) 228.

[49] X.-G. Wu, S. J. Brodsky, and M. Mojaza, "The Renormalization Scale-Setting Problem in QCD," *Prog. Part. Nucl. Phys.* **72** (2013) 44–98, arXiv:1302.0599 [hep-ph].

[50] H. J. Lu and C. A. R. Sa de Melo, "Dressed skeleton expansion and the coupling scale ambiguity problem," *Phys. Lett. B* **273** (1991) 260–267. [Erratum: Phys.Lett.B 285, 399 (1992)].

[51] H. J. Lu, "Dressed skeleton expansion in (1+1)-dimensional field theory models," *Phys. Rev. D* **45** (1992) 1217–1232.

[52] S. J. Brodsky, A. H. Hoang, J. H. Kuhn, and T. Teubner, "Angular distributions of massive quarks and leptons close to threshold," *Phys. Lett. B* **359** (1995) 355–361, arXiv:hep-ph/9508274.

[53] S. J. Brodsky and H. J. Lu, "Commensurate scale relations in quantum chromodynamics," *Phys. Rev. D* **51** (1995) 3652–3668, arXiv:hep-ph/9405218.

[54] S. J. Brodsky, "Commensurate scale relations and the Abelian correspondence principle," in *Workshop on Future Directions in Quark Nuclear Physics*, pp. 97–110. 6, 1998. arXiv:hep-ph/9806445.

[55] M. Dine and J. R. Sapirstein, "Higher Order QCD Corrections in e+ e- Annihilation," *Phys. Rev. Lett.* **43** (1979) 668.

[56] K. G. Chetyrkin, A. L. Kataev, and F. V. Tkachov, "Higher Order Corrections to $\sigma_{\rm tot}(e^+e^- \to$ Hadrons in Quantum Chromodynamics," *Phys. Lett. B* **85** (1979) 277–279.

[57] K. G. Chetyrkin, J. H. Kuhn, and A. Kwiatkowski, "QCD corrections to the e^+e^- cross-section and the Z boson decay rate," *Phys. Rept.* **277** (1996) 189–281, arXiv:hep-ph/9503396.

[58] Y. Kiyo, A. Maier, P. Maierhofer, and P. Marquard, "Reconstruction of heavy quark current correlators at O(alpha(s)**3)," *Nucl. Phys. B* **823** (2009) 269–287, arXiv:0907.2120 [hep-ph].

[59] P. A. Baikov, K. G. Chetyrkin, J. H. Kuhn, and J. Rittinger, "Complete $\mathcal{O}(\alpha_s^4)$ QCD Corrections to Hadronic Z-Decays," *Phys. Rev. Lett.* **108** (2012) 222003, arXiv:1201.5804 [hep-ph].

[60] P. A. Baikov, K. G. Chetyrkin, and J. H. Kuhn, "Order alpha**4(s) QCD Corrections to Z and tau Decays," *Phys. Rev. Lett.* **101** (2008) 012002, arXiv:0801.1821 [hep-ph].

[61] S. J. Brodsky and X.-G. Wu, "Scale Setting Using the Extended Renormalization Group and the Principle of Maximum Conformality: the QCD Coupling Constant at Four Loops," *Phys. Rev. D* **85** (2012) 034038, arXiv:1111.6175 [hep-ph]. [Erratum: Phys.Rev.D 86, 079903 (2012)].

[62] S. J. Brodsky and L. Di Giustino, "Setting the Renormalization Scale in QCD: The Principle of Maximum Conformality," *Phys. Rev. D* **86** (2012) 085026, arXiv:1107.0338 [hep-ph].

[63] S. J. Brodsky and X.-G. Wu, "Eliminating the Renormalization Scale Ambiguity for Top-Pair Production Using the Principle of Maximum Conformality," *Phys. Rev. Lett.* **109** (2012) 042002, arXiv:1203.5312 [hep-ph].

[64] M. Mojaza, S. J. Brodsky, and X.-G. Wu, "Systematic All-Orders Method to Eliminate Renormalization-Scale and Scheme Ambiguities in Perturbative QCD," *Phys. Rev. Lett.* **110** (2013) 192001, arXiv:1212.0049 [hep-ph].

[65] S. J. Brodsky, M. Mojaza, and X.-G. Wu, "Systematic Scale-Setting to All Orders: The Principle of Maximum Conformality and Commensurate Scale Relations," *Phys. Rev. D* **89** (2014) 014027, arXiv:1304.4631 [hep-ph].

[66] G. Grunberg and A. L. Kataev, "On Some possible extensions of the Brodsky-Lepage-MacKenzie approach beyond the next-to-leading order," *Phys. Lett. B* **279** (1992) 352–358.

[67] S. V. Mikhailov, "Generalization of BLM procedure and its scales in any order of pQCD: A Practical approach," *JHEP* **06** (2007) 009, arXiv:hep-ph/0411397.

[68] A. L. Kataev and S. V. Mikhailov, "The $\{\beta\}$-expansion formalism in perturbative QCD and its extension," *JHEP* **11** (2016) 079, arXiv:1607.08698 [hep-th].

[69] P. A. Baikov, K. G. Chetyrkin, J. H. Kuhn, and J. Rittinger, "Adler Function, Sum Rules and Crewther Relation of Order $\mathcal{O}(\alpha_s^4)$: the Singlet Case," *Phys. Lett. B* **714** (2012) 62–65, arXiv:1206.1288 [hep-ph].

[70] M. Mojaza, S. J. Brodsky, and X.-G. Wu, "Systematic All-Orders Method to Eliminate Renormalization-Scale and Scheme Ambiguities in Perturbative QCD," *Phys. Rev. Lett.* **110** (2013) 192001, arXiv:1212.0049 [hep-ph].

[71] S. J. Brodsky, M. Mojaza, and X.-G. Wu, "Systematic Scale-Setting to All Orders: The Principle of Maximum Conformality and Commensurate Scale Relations," *Phys. Rev. D* **89** (2014) 014027, arXiv:1304.4631 [hep-ph].

[72] S. J. Brodsky and X.-G. Wu, "Self-Consistency Requirements of the Renormalization Group for Setting the Renormalization Scale," *Phys. Rev. D* **86** no. 5, (2012) 054018, arXiv:1208.0700 [hep-ph].

[73] H. J. Lu and S. J. Brodsky, "Commensurate scale relations in quantum chromodynamics," *Nucl. Phys. B Proc. Suppl.* **39BC** (1995) 309–311.

[74] N. Gray, D. J. Broadhurst, W. Grafe, and K. Schilcher, "Three Loop Relation of Quark (Modified) Ms and Pole Masses," *Z. Phys. C* **48** (1990) 673–680.

[75] K. Melnikov and T. v. Ritbergen, "The Three loop relation between the MS-bar and the pole quark masses," *Phys. Lett. B* **482** (2000) 99–108, arXiv:hep-ph/9912391.

[76] P. Marquard, A. V. Smirnov, V. A. Smirnov, and M. Steinhauser, "Quark Mass Relations to Four-Loop Order in Perturbative QCD," *Phys. Rev. Lett.* **114** no. 14, (2015) 142002, arXiv:1502.01030 [hep-ph].

[77] M. Steinhauser, "Relation between the pole and $\overline{MS}$ quark mass in QCD," in *PoS DIS2016*, p. 148. 2016.

[78] A. L. Kataev and V. S. Molokoedov, "Multiloop contributions to the on-shell-$\overline{\text{MS}}$ heavy quark mass relation in QCD and the asymptotic structure of the corresponding series: the updated consideration," *Eur. Phys. J. C* **80** no. 12, (2020) 1160, arXiv:1807.05406 [hep-ph].

[79] P. Marquard, A. V. Smirnov, V. A. Smirnov, M. Steinhauser, and D. Wellmann, "$\overline{\text{MS}}$-on-shell quark mass relation up to four loops in QCD and a general SU(N) gauge group," *Phys. Rev. D* **94** no. 7, (2016) 074025, arXiv:1606.06754 [hep-ph].

[80] A. L. Kataev and V. S. Molokoedov, "From perturbative calculations of the QCD static potential towards four-loop pole-running heavy quarks masses relation," *J. Phys. Conf. Ser.* **762** no. 1, (2016) 012078, arXiv:1604.03485 [hep-ph].

[81] A. L. Kataev and V. S. Molokoedov, "On the flavour dependence of the $\mathcal{O}(\alpha_s^4)$ correction to the relation between running and pole heavy quark masses," *Eur. Phys. J. Plus* **131** no. 8, (2016) 271, arXiv:1511.06898 [hep-ph].

[82] A. H. Hoang and A. V. Manohar, "Charm quark mass from inclusive semileptonic B decays," *Phys. Lett. B* **633** (2006) 526–532, arXiv:hep-ph/0509195 [hep-ph].

[83] K. G. Chetyrkin and M. Steinhauser, "The Relation between the $\overline{\rm MS}$ and the on-shell quark mass at order α_s^3," *Nucl. Phys. B* **573** (2000) 617–651, arXiv:hep-ph/9911434 [hep-ph].

[84] R. L. P. D. G. Workman, "Review of Particle Physics," *PTEP* **2022** (2022) 083C01.

[85] A. H. Hoang, "What is the Top Quark Mass?," *Ann. Rev. Nucl. Part. Sci.* **70** (2020) 225–255, arXiv:2004.12915 [hep-ph].

[86] F. Jegerlehner and M. Y. Kalmykov, "$\mathcal{O}(\alpha\alpha_s)$ relation between pole- and $\overline{\rm MS}$- mass of the t quark," *Acta Phys. Polon. B* **34** (2003) 5335–5344, arXiv:hep-ph/0310361 [hep-ph].

[87] A. L. Kataev and V. S. Molokoedov, "Notes on Interplay between the QCD and EW Perturbative Corrections to the Pole-Running-to-Top-Quark Mass Ratio," *JETP Lett.* **115** no. 12, (2022) 704–712, arXiv:2201.12073 [hep-ph].

[88] S. Q. Wang, X. G. Wu, Z. G. Si, and S. J. Brodsky, "A precise determination of the top-quark pole mass," *Eur. Phys. J. C* **78** no. 3, (2018) 237, arXiv:1703.03583 [hep-ph].

[89] A. I. Bochkarev and R. S. Willey, "On the scheme dependence of the electroweak radiative corrections," *Phys. Rev. D* **51** (1995) 2049–2052, arXiv:hep-ph/9407261 [hep-ph].

[90] Q. Yu, H. Zhou, J. Yan, X. D. Huang, and X. G. Wu, "A new analysis of the pQCD contributions to the electroweak parameter ρ using the single-scale approach of principle of maximum conformality," *Phys. Lett. B* **820** (2021) 136574, arXiv:2105.07230 [hep-ph].

[91] A. A. Penin and A. A. Pivovarov, "Top quark threshold production in gamma gamma collision in the next-to-leading order," *Nucl. Phys. B* **550** (1999) 375–396, arXiv:hep-ph/9810496 [hep-ph].

[92] A. H. Hoang, M. Beneke, K. Melnikov, T. Nagano, A. Ota, A. A. Penin, A. A. Pivovarov, A. Signer, V. A. Smirnov, and Y. Sumino, "Top - anti-top pair production close to threshold: Synopsis of recent NNLO results," *Eur. Phys. J. direct* **2** no. 1, (2000) 3, arXiv:hep-ph/0001286 [hep-ph].

[93] M. J. G. Veltman, "Limit on Mass Differences in the Weinberg Model," *Nucl. Phys. B* **123** (1977) 89–99.

[94] F. Halzen, B. A. Kniehl, and M. L. Stong, "Two loop electroweak parameters," *Z. Phys. C* **58** (1993) 119–132.

[95] K. G. Chetyrkin, J. H. Kuhn, and M. Steinhauser, "Corrections of order $\mathcal{O}(G_F M_t^2 \alpha_s^2)$ to the ρ parameter," *Phys. Lett. B* **351** (1995) 331–338, arXiv:hep-ph/9502291.

[96] Y. Schroder and M. Steinhauser, "Four-loop singlet contribution to the rho parameter," *Phys. Lett. B* **622** (2005) 124–130, arXiv:hep-ph/0504055.

[97] R. Boughezal and M. Czakon, "Single scale tadpoles and $\mathcal{O}(G_F M_t^2 \alpha_s^2)$ corrections to the ρ parameter," *Nucl. Phys. B* **755** (2006) 221–238, arXiv:hep-ph/0606232.

[98] K. G. Chetyrkin, M. Faisst, J. H. Kuhn, P. Maierhofer, and C. Sturm, "Four-Loop QCD Corrections to the Rho Parameter," *Phys. Rev. Lett.* **97** (2006) 102003, arXiv:hep-ph/0605201.

[99] M. Faisst, P. Maierhoefer, and C. Sturm, "Standard and epsilon-finite Master Integrals for the rho-Parameter," *Nucl. Phys. B* **766** (2007) 246–268, arXiv:hep-ph/0611244.

[100] S. A. et al. [D0], "W and Z boson production in $p\bar{p}$ collisions at $\sqrt{s} = 1.8$ TeV," *Phys. Rev. Lett.* **75** (1995) 1456–1461, arXiv:hep-ex/9505013 [hep-ex].

[101] **ATLAS** Collaboration, M. Aaboud *et al.*, "Precision measurement and interpretation of inclusive W^+ , W^- and Z/γ^* production cross sections with the ATLAS detector," *Eur. Phys. J. C* **77** no. 6, (2017) 367, arXiv:1612.03016 [hep-ex].

[102] **LHCb** Collaboration, R. Aaij *et al.*, "Measurement of forward $W \to e\nu$ production in pp collisions at $\sqrt{s} = 8$ TeV," *JHEP* **10** (2016) 030, arXiv:1608.01484 [hep-ex].

[103] A. T. et al. [CMS], "Precision measurement of the W boson decay branching fractions in proton-proton collisions at $\sqrt{s} = 13$ TeV," *Phys. Rev. D* **105** no. 7, (2022) 072008, arXiv:2201.07861 [hep-ex].

[104] X.-G. Wu, Y. Ma, S.-Q. Wang, H.-B. Fu, H.-H. Ma, S. J. Brodsky, and M. Mojaza, "Renormalization Group Invariance and Optimal QCD Renormalization Scale-Setting," *Rept. Prog. Phys.* **78** (2015) 126201, arXiv:1405.3196 [hep-ph].

[105] D. Y. Bardin, S. Riemann, and T. Riemann, "Electroweak one loop corrections to the decay of the charged vector boson," *Z. Phys. C* **32** (1986) 121–125.

[106] A. Denner and T. Sack, "The w boson width," *Z. Phys. C* **46** (1990) 653–663.

[107] A. Denner, "Techniques for calculation of electroweak radiative corrections at the one loop level and results for W physics at LEP-200," *Fortsch. Phys.* **41** (1993) 307–420, arXiv:0709.1075 [hep-ph].

[108] B. A. Kniehl, F. Madricardo, and M. Steinhauser, "Gauge independent w boson partial decay widths," *Phys. Rev. D* **62** (2000) 073010, arXiv:hep-ph/0005060 [hep-ph].

[109] D. Kara, "Corrections of Order $\alpha\alpha_s$ to W Boson Decays," *Nucl. Phys. B* **877** (2013) 683–718, arXiv:1307.7190 [hep-ph].

[110] D. d'Enterria and M. Srebre, "α_s and V_{cs} determination, and CKM unitarity test, from W decays at NNLO," *Phys. Lett. B* **763** (2016) 465–471, arXiv:1603.06501 [hep-ph].

[111] D. d'Enterria and V. Jacobsen, "Improved strong coupling determinations from hadronic decays of electroweak bosons at N^{3}LO accuracy," arXiv:2005.04545 [hep-ph].

[112] D. Salinas-Arizmendi and I. Schmidt, "Relation between pole and running masses of heavy quarks using the principle of maximum conformality," *Progress of Theoretical and Experimental Physics* (02, 2024) ptae020, arXiv:2209.06881 [hep-ph]. https://doi.org/10.1093/ptep/ptae020.

[113] S.-Q. Wang, X.-G. Wu, S. J. Brodsky, and M. Mojaza, "Application of the Principle of Maximum Conformality to the Hadroproduction of the Higgs Boson at the LHC," *Phys. Rev. D* **94** no. 5, (2016) 053003, arXiv:1605.02572 [hep-ph].

[114] H. A. Chawdhry and A. Mitov, "Ambiguities of the principle of maximum conformality procedure for hadron collider processes," *Phys. Rev. D* **100** no. 7, (2019) 074013, arXiv:1907.06610 [hep-ph].

[115] S. G. Gorishnii, A. L. Kataev, and S. A. Larin, "The $O(\alpha_s^3)$-corrections to $\sigma_{tot}(e^+e^- \to hadrons)$ and $\Gamma(\tau^- \to \nu_\tau + hadrons)$ in QCD," *Phys. Lett. B* **259** (1991) 144–150.

[116] K. G. Chetyrkin, "Corrections of order α_s^3 to R(had) in pQCD with light gluinos," *Phys. Lett. B* **391** (1997) 402–412, arXiv:hep-ph/9608480.

[117] P. A. Baikov, K. G. Chetyrkin, and J. H. Kuhn, "Adler function, bjorken sum rule, and the crewther relation to order α_s^4 in a general gauge theory," *Phys. Rev. Lett.* **104** (2010) 132004, arXiv:1001.3606 [hep-ph].

[118] M. R. Pennington and G. G. Ross, "Perturbative qcd for timelike processes: What is the best expansion parameter?," *Phys. Lett. B* **102** (1981) 167–171.